

Title: Single-Component, Photocatalytic H₂ Production Through Acceptorless Alcohol Dehydrogenation: Atypical Metal-Ligand Cooperativity in a Ruthenium(II)-PN/P Complex

Authors: Paul M. Fanara¹, Vipulan Vigneswaran¹, Parami S. Gunasekera¹, Samantha N. MacMillan², and David C. Lacy^{1*}

Affiliations:

¹Department of Chemistry, University at Buffalo, State University of New York; Buffalo, New York 14260, United States.

²Department of Chemistry and Chemical Biology, Cornell University; Ithaca, New York 14853, United States.

*Corresponding author. Email: DCLacy@Buffalo.edu

Abstract: Metal-ligand cooperativity (MLC) involving reversible aromatization/dearomatization of pyridine-derived pincer ligands is considered important in acceptorless (de)hydrogenation for dihydrogen generation and storage. Dehydrohalogenation of pyridine-derived pincer ruthenium complexes often leads to dearomatized moieties. Thus, we were surprised to find an aromatized *kappa*-3-NCP binding mode in [$\{\text{LutP}\}\text{Ru}(\text{CO})(\text{H})(\text{PPh}_3)$] (**2**) upon dehydrohalogenation of the lutidine-derived PN/P complex [$\{\text{LutP}\}\text{Ru}(\text{CO})(\text{Cl})(\text{H})(\text{PPh}_3)$] (**1**) with KO^tBu. The reaction of H₂ with **2** results in formation of a *cis*-dihydride [$\{\text{LutP}\}\text{Ru}(\text{CO})(\text{H})_2(\text{PPh}_3)$] (**3**) and labeling studies confirm cooperative metal-ligand activation. **3** exhibits reversible photochemistry that we leveraged to demonstrate a unique strategy for unsensitized single-component photocatalytic H₂ production *via* acceptorless alcohol dehydrogenation. Although labeling studies implicate MLC processes during the photocatalytic reaction, they may be off-path intermediates, emphasizing that aromatization/dearomatization may not be necessary for acceptorless transformations.

One-Sentence Summary: Novel ruthenium coordination chemistry enables H₂ production from alcohols and light without any additives.

Main Text: Acceptorless metal-ligand cooperative (MLC) alcohol dehydrogenation using aromatization/dearomatization is a strategy for hydrogen storage and recovery (1–4). Typically, high temperatures are needed to drive the uphill alcohol dehydrogenation (1, 5), and low-temperature methods involve co-liberation of CO₂ or use photosensitizers (6, 7). An alternative, green method is unsensitized photochemical dehydrogenation, which is possible if the catalyst reversibly interacts with light (8). To this end, we were interested in capitalizing on photoactive ruthenium *cis*-dihydrides to generate dehydrogenation catalysts toward applications in dihydrogen production from alcohols under mild conditions (9). During the course of our studies (10), we discovered a Ru alcohol dehydrogenation catalyst (1) and expound herein a nominally on-path *cis*-dihydride complex (3) with reversible photochemistry allowing for single-component photocatalysis. Furthermore, coordination and mechanistic studies reported herein reveal unique insight into the MLC paradigm where there has been, as of late, new developments that suggest aromatization/dearomatization steps may have diminished importance in catalysis.

For instance, it is possible to envision MLC catalytic processes that do not involve any aromatization/dearomatization steps (11). Furthermore, Keith and Chianese and coworkers showed that Milstein's catalyst (2Py) undergoes dehydroalkylation into active ester hydrogenation catalysts (12), and Khaskin and Gusev and coworkers showed that a bipyridyl-derived Ru-PNN catalyst self-hydrogenates into a piperidine-based Ru-PNN catalyst (13). Both of these recent developments show that pyridine-derived pincer Ru catalysts have pathways to highly active Noyori-type catalysts. While these discoveries do not rule out reversible aromatization/dearomatization steps, they add more evidence to the contrary. In this report, we present another piece of the puzzle of aromatization/dearomatization chemistry that further deemphasizes the importance of the dearomatized form. Notwithstanding, our findings provide new insight into possible MLC activation modes that prior to our report has not been observed in Ru-based catalysts. Moreover, the unique coordination chemistry and reversible photochemistry from 3 enabled single-component photo-assisted H₂ production (14–17) and uses some of the mildest reagents and conditions reported for acceptorless alcohol dehydrogenation.

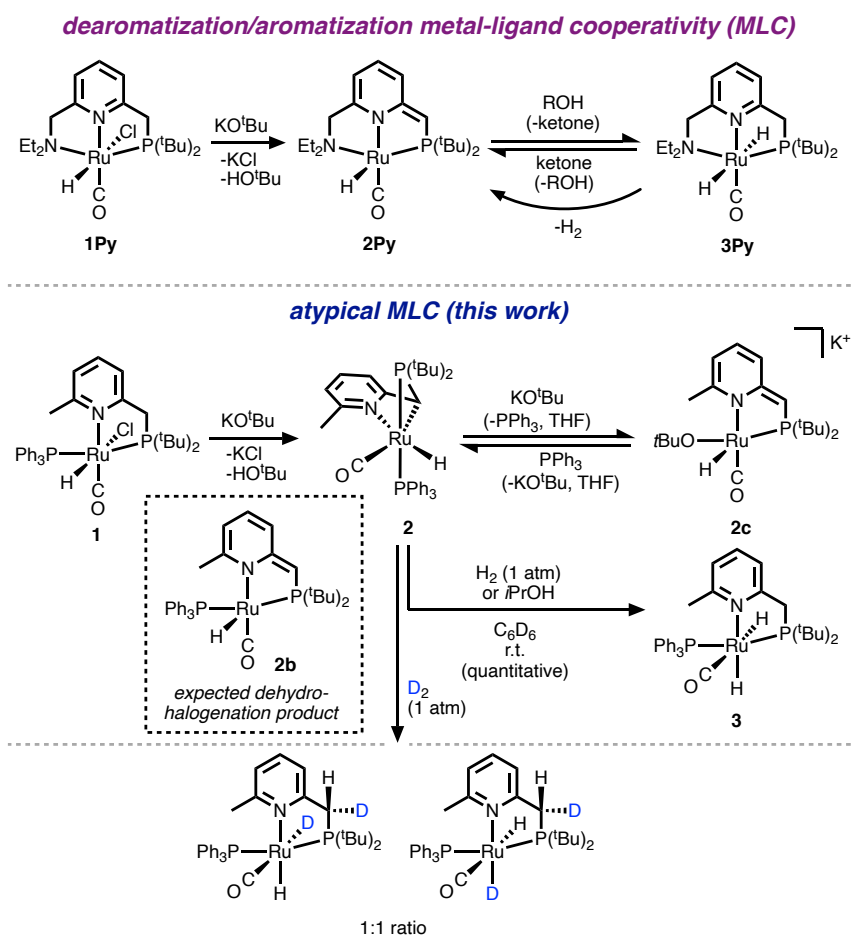


Fig. 1. (top) Conventional metal-ligand cooperativity (MLC) with non-Noyori type pyridine-based Ru(II) catalysts. (middle) Atypical MLC described in this study. (bottom) Ratio of deuterated isotopomers of **3** when **2** was treated with D_2 ; when light was rigorously excluded, only the first two species on the right were obtained.

In an earlier report detailing the synthesis and characterization of $[\{LutP\}Ru(CO)(H)(Cl)(PPh_3)]$ (**1**), we briefly investigated its reaction with $KOtBu$ and initially hypothesized a prototypical dearomatized bidentate binding mode for the product **2b** (Fig. 1) (10). However, the product exhibited unusual sensitivity to water and we did not pursue it further at the time. Since this initial study, we discovered that activation of **1** with 1 eq. $K[N(SiMe_3)_2]$ in cold ($-35\text{ }^\circ\text{C}$) THF (or $KOtBu$ in benzene, r.t.) results in formation of a highly moisture-sensitive amber-colored species (**2**) (Fig. 1) whose X-ray crystal structure reveals a unique NCP κ -3 binding mode (Fig. 2). Importantly, the atypical κ -3 binding mode remains intact in solution as evidenced from 1H - 1H ROESY NMR correlations and 1H / ^{13}C coupled HSQC NMR spectroscopy (Figs. S1–8). Analogous atypical binding modes and spectroscopic features have been observed in other systems (18–21), but not for ruthenium pincer complexes with pyridine-derived ligands that instead have dearomatized modes (22).

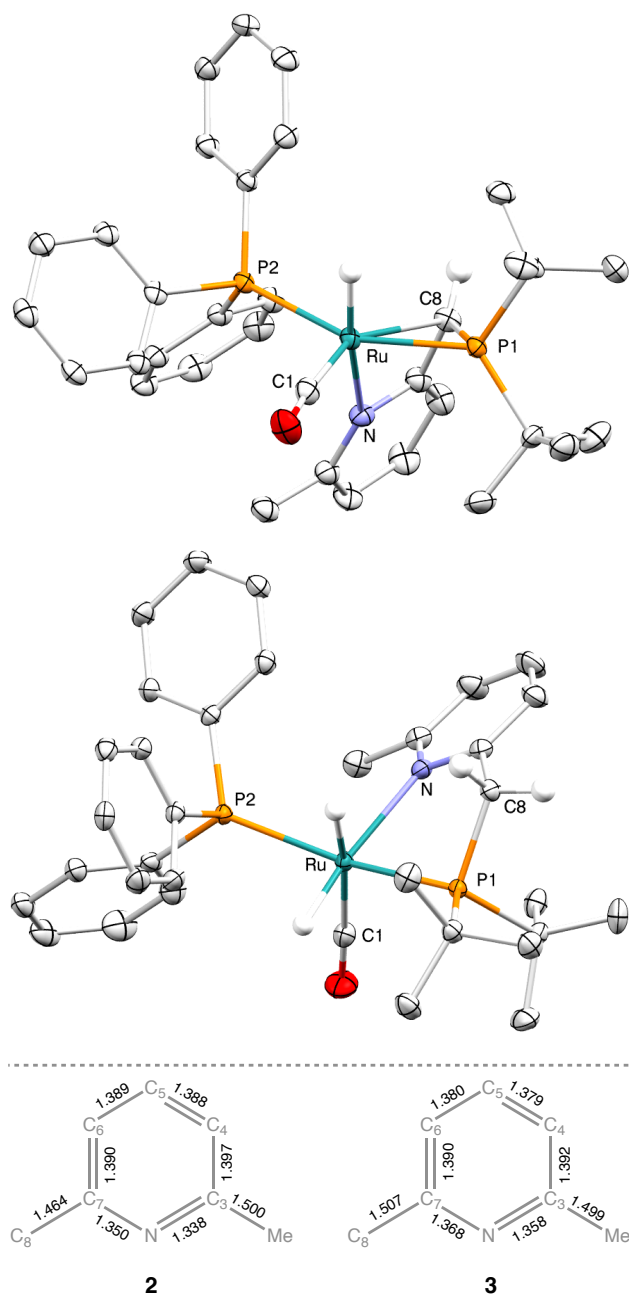


Fig. 2. XRD molecular structure of **2** (top) and **3** (middle) with ellipsoids 50% probability. Except for the RuH and methine/methylene CH atoms, hydrogen atoms have been removed for clarity. (bottom) distances in pyridine ring for **2** and **3**.

A future study will explore the reactivity of **2** in more detail, but an observation pertinent to the current study is PPh₃ lability. When excess KO*t*Bu was used to prepare **2** from **1**, we noted that free PPh₃ was formed along with a new species whose ¹H and ³¹P{¹H} NMR characterization is consistent with a LutP-bound Ru-O*t*Bu anionic complex (**2c**) (Figs. S9–10). The ligand substitution is reversible, as removal of solvent from **2c** reforms **2** in essentially quantitative yield. The nature of the [Ru-O*t*Bu][−] complex (**2c**) is not explored in detail here, but the lability of PPh₃ is an important factor for the catalytic studies (see below).

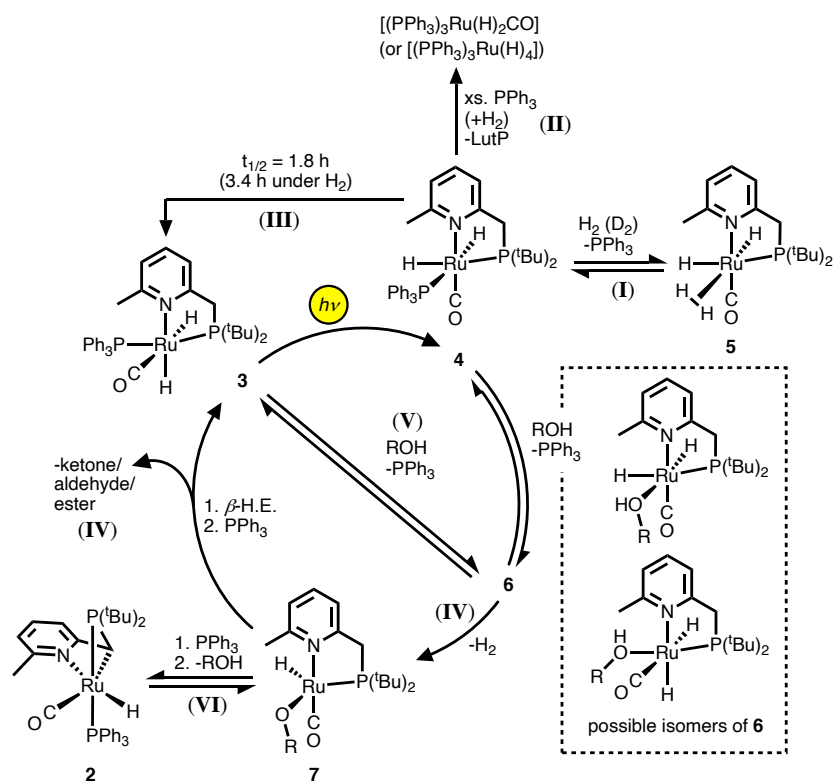
The reactivity of **2** in the presence of H₂ and 2-propanol were also explored. When a benzene solution of **2** was exposed to an atmosphere of H₂, an immediate color change from amber to light

yellow occurred and NMR analysis demonstrated the quantitative formation of dihydride **3**. Similarly, **2** reacts quantitatively with 2-propanol to form **3** and equimolar acetone. X-ray crystallographic characterization revealed the *cis*-dihydride motif and 2D NMR and ¹H-¹H ROESY spectroscopic characterization confirms its solution-state structure is identical (Figs. S11–S15). The reactions with H₂ and 2-propanol are not reversible. Subjecting **3** to vacuum (60 °C) or excess acetone (r.t.) resulted in no conversion to **2**. More forcing conditions (110 °C) resulted in trace formation of **2** along with other identified byproducts (Fig. S16) (23). This lack of reactivity is in contrast to previous reports with Milstein's dihydride complex, **3Py**, which spontaneously converts to **2Py** at r.t. (10, 11, 22).

When D₂ was used to prepare **3**, deuterium incorporation occurs at both ruthenium and the ligand. The mixture of isotopomers is best represented pictorially in Fig. 1 (²H NMR, Fig. S17) and is generally consistent with what others have observed (24). Interestingly, the ¹H NMR spectrum of the reaction mixture contained H₂ and HD indicating exchange of free dihydrogen with **3** (Fig. S18). While not completely eliminated, the presence of H₂ and HD is significantly reduced when light is rigorously excluded and we hypothesized light-induced exchange (Figs. S19–S20).

We tested this hypothesis with broad-band irradiation of **3** with a Xe-arc lamp (100 W) which caused a color change of the solution to orange/red, and the major species is consistent with a new *cis*-dihydride (**4**). The stability of **4** was monitored with ¹H NMR spectroscopy and it quantitatively decayed with $t_{1/2} = 1.9 \pm 0.04$ h (r.t.) back to **3** under N₂ (Figs. S21–S22), and was unaffected by static vacuum $t_{1/2} = 1.8 \pm 0.14$ h (r.t.) (Figs. S23–S24). The spectral features of **4** include two hydride resonances in the ¹H NMR spectrum at -5.13 ppm (dd, $J = 101, 25$ Hz) and -6.09 (dd, $J = 92, 17$ Hz), consistent with a phosphine *trans* and *cis* to each hydride (Fig. S25). The ³¹P{¹H} NMR spectrum indicates a *cis* conformation of the PtBu₂ and PPh₃ ligands, as the resonances at 77.3 ppm and 42.7 ppm are doublets with $J_{PP} = 10$ Hz and 11 Hz, respectively (Fig. S26). A ¹H-¹H ROESY NMR of **4** shows exchange coupling between the two hydride resonances, explaining the observed lack of through-bond coupling and the two isomers of deuterated **3** shown in Figure 1. Additionally, the hydride resonance at -6.09 ppm exhibits through-space coupling to one of the PtBu₂ resonances at 1.30 ppm. The hydride resonance at -5.13 ppm has through-space coupling to the PPh₃ and methyl resonances at 7.72 ppm and 2.56 ppm, respectively (Fig. S27). Together with FTIR-ATR spectroscopy (Fig. S28), the NMR data enables confident assignment of the structure of **4** as shown in Figure 3.

When irradiation of **3** was carried out under an atmosphere of H₂, the same process occurred, except that the decay of **4** to **3** was slower ($t_{1/2} = 3.38 \pm 0.08$ h) (Figs. S29–S30). When D₂ was used, the hydride resonances wash out in the ¹H NMR spectrum and reappear in the ²H NMR spectrum, but D-incorporation into the ligand was not observed (Figs. S31–S32). Thermal ligand exchange between PPh₃ and H₂ in **3** is also suspected because a solution of **3** and D₂ allowed to stand in the dark for several days resulted in washing out of the hydride resonances in the ¹H NMR spectrum (Figs. S33). The hydrides of complex **4** exchange with free H₂, confirmed using ¹H-¹H ROESY NMR showing exchange coupling between both hydride resonances and free dihydrogen (Fig. S27). Variable temperature NMR and line broadening analysis furnished activation parameters $\Delta H^\ddagger = 25.3$ kcal·mol⁻¹ and $\Delta S^\ddagger = 26.7$ cal·K⁻¹·mol⁻¹ (Figs. S34–S35), consistent with a ligand interchange substitution process between H₂ and PPh₃ to form proposed complex **5** (Fig. 3) accounting for the isotope scrambling (25).



alcohol	catalyst	other products	H_2 relative to cat^\ddagger (after 12 h)
MeOH	3	H_2CO^{fl}	270% (400%)
EtOH	3	ethyl acetate ^{fl}	640% (1000%)
1PhEtOH	3	acetophenone	640% (1100%)
<i>i</i> PrOH	3	acetone	300% (510%)
<i>i</i> PrOH	1	–	78%
<i>i</i> PrOH	$(CO)(PPh_3)_3Ru(H)_2$	–	33%
<i>i</i> PrOH	$(Cl)(CO)(PPh_3)_3Ru(H)$	–	28%

^{fl} trace CO observed, [‡] average of three runs

Fig. 3. (top) Photochemistry and proposed mechanism of photocatalytic alcohol dehydrogenation. The steps with roman numerals are supported by the following observations: **I**, **4** exhibits exchange coupling with free H_2 and species **5** is consistent with observed H_2/D_2 scrambling; **II**, impurities are observed with excess PPh_3 and/or extensive irradiations (Fig. S36); **III**, prolonged $t_{1/2}$ for **4** to **3** conversion under H_2 explained by **4** to **5** equilibrium; **IV**, catalytic alcohol dehydrogenation products observed; **V**, when light was excluded, H_2 production is sub-stoichiometric relative to **3**; **VI**, *d*-incorporation into ligand occurs; **finally**, complexes **3** and **4** are two of many species present in solution after photocatalysis in alcohol. (bottom) Summarized results of photocatalysis (Fig. S37-S43).

Our previous investigation with **1** involved testing role of ligand structure variation in alcohol dehydrogenation (10). Typically, catalytic behavior is not achieved unless reactions are carried out at elevated temperatures (6). However, we intuited that complexes like **3** having reversible photochemistry might be amenable to r.t. photocatalytic alcohol dehydrogenation akin to what has been observed for $[Rh(PPh_3)_3Cl]$ (26). We tested several simple alcohols using **3** with irradiation from a Xe arc lamp (100 W, 345 nm cutoff filter) achieving catalytic turnover at r.t. (Fig. 3). Under

the same conditions but with the exclusion of light, only sub-stoichiometric H₂ was formed (e.g., 27% H₂ relative to **3** from 2-propanol). Control reactions with known active alcohol dehydrogenation catalysts like [CO(PPh₃)₃Ru^{II}(H)₂] gave 10% H₂ in the dark, and 33% when irradiated. When **3** was irradiated in C₆D₆ in the presence of *d*₈-isopropanol, deuteration occurred on the ligand (Figs. S44–S45).

The current system is not optimized, and a future investigation is required for a detailed mechanistic scheme. Nevertheless, the collective information allows for a proposed mechanism and is provided in Figure 3. The salient component is the enhanced lability of PPh₃ upon irradiation because of the *trans*-effect of the hydride ligand, and potentially steric crowding from the *cis*-diphosphine motif, in **4**. The wavelength requirements for photocatalysis are the same as those required for isomerization, so it is reasonable that the process is at least photo-assisted in nature (Fig. S46–47). The lability enhancement allows for alcohol coordination and subsequent liberation of H₂, which is observed, from proposed intermediate **6**. Loss of H₂ forms proposed coordinatively unsaturated species **7**, which is predisposed to undergo beta-hydride elimination and concomitant PPh₃ coordination reforming **3**; thus, the dehydrogenation is an inner sphere mechanism. Notably, post-irradiated solutions contain **3** and **4** as the major species, in addition to what we believe to be a carbonylated byproduct (**8**) and alkoxide coordinated species (Fig. S48–S51). To explain the deuteration of the ligand when **3** was irradiated with *d*₈-isopropanol, we propose that **6** may also be deprotonated by the (weakly) coordinated alkoxide to afford **2** (or a species like it), which undergoes MLC activation of alcohol. Finally, we found that sub-stoichiometric H₂ formed when light was excluded in reactions between **3** and 2-propanol, indicating thermal pathways are also possible when the net reaction is favored. All of these steps are consistent with the reported chemistry of **2** and **3** (*vide supra*) in addition to our previous considerations of analogous Ru-PNN 1PhEtOH dehydrogenation catalysis (10).

The *cis*-dihydride motif of **3** enabled light-induced isomerization, something that is not likely on analogous *trans*-dihydride catalysts (e.g., **2Py**), giving rise to labile PPh₃. Phosphine lability is critical since this will enhance inner sphere dehydrogenation paths. The data supports an inner sphere non-MLC catalytic cycle, coherent with a growing body of literature that indicates diminished importance of aromatization/dearomatization MLC steps. Although intermediates involved in MLC were produced through photochemical means, they are probably not catalytically relevant. These off-path intermediates may be dearomatized, but our work with **2** provides another possible mode to consider when invoking MLC on pyridine-derived ligands. Overall this work provides a new strategy to access H₂ formation by direct photochemical dehydrogenation of alcohols and is under further investigation in our laboratory.

References

1. K. Sordakis, C. Tang, L. K. Vogt, *et. al. Chem. Rev.* **118**, 372–433 (2018).
2. C. Gunanathan, D. Milstein, *Acc. Chem. Res.* **44**, 588–602 (2011).
3. R. H. Crabtree, *Chem. Rev.* **117**, 9228–9246 (2017).
4. H. Grützmacher, *Angew. Chem. Int. Ed.* **47**, 1814–1818 (2008).
5. E. Alberico, M. Nielsen, *Chem. Commun.* **51**, 6714–6725 (2015).
6. M. Trincado, D. Banerjee, H. Grutzmacher, *Energy Environ. Sci.* **7**, 2464–2503 (2014).
7. H. Fuse, H. Mitsunuma, M. Kanai, M. *J. Am. Chem. Soc.* **142**, 4493–4499 (2020).
8. J.-J. Zhong, W.-P. To, Y. Liu, W. Lu, C.-M. Che, *Chem. Sci.* **10**, 4883–4889 (2019).
9. R. N. Perutz, B. Procacci, *Chem. Rev.* **116**, 8506–8544 (2016).

10. P. M. Fanara, S. N. MacMillan, D. C. Lacy, *Organometallics* **39**, 3628–3644 (2020).
11. D. Gusev, *Organometallics* **39**, 258–270 (2020).
12. J. M. Keith, A. R. Chianese, *et. al. J. Am. Chem. Soc.* **141**, 17404–17413 (2019).
13. L. N. Dawe, M. Karimzadeh-Younjali, Z. Dai, E. Khaskin, D. G. Gusev, *J. Am. Chem. Soc.* **142**, 19510–19522 (2020).
14. K. R. Brereton, A. G. Bonn, A. J. M. Miller, *ACS Energy Lett.* **3**, 1128–1136 (2018).
15. W. Wang, T. B. Rauchfuss, L. Bertini, G. Zampella, *J. Am. Chem. Soc.* **134**, 4525–4528 (2012).
16. T. J. Whittemore, C. Xue, J. Huang, J.C. Gallucci, C. Turro, *Nat. Chem.* **12**, 180–185 (2020).
17. R. H. Schmehl, C. E. Webster, J. H. Delcamp, *et. al. ACS Catal.* **8**, 4838–4847 (2018).
18. J.-B. Sortais, *et. al. Angew. Chem. Int. Ed.* **58**, 6727–6731 (2019).
19. D. Milstein, *et. al. Angew. Chem. Int. Ed.* **56**, 4229–4233 (2017).
20. J. I. van der Vlugt, *et. al. Chem. Eur. J.* **25**, 3875–3883 (2019).
21. H. Werner, R. J. Werner, *Organomet. Chem.* **209**, C60–C64 (1981).
22. J. Zhang, G. Leitus, Y. Ben-David, D. Milstein, *J. Am. Chem. Soc.* **127**, 10840–10841 (2005).
23. At 110 °C in toluene with static vacuum free ligand, (CO){PPh₃}₃Ru^{II}(H)₂, and **3** were observed in a nearly 1:1:1 ratio.
24. D. Milstein, *et. al. J. Am. Chem. Soc.* **128**, 15390–15391 (2006).
25. D. G. Gusev, A. B. Vymontis, V. I. Bakhmutov, *Inorganica Chim. Acta* **179**, 195–201 (1991).
26. See Table 2 in: A. J. Esswein, D. G. Nocera, *Chem. Rev.* **107**, 4022–4047 (2007).
27. (SI only) *CrysAlisPro*; Rigaku OD, The Woodlands, TX, 2015
28. (SI only) G. M. Sheldrick, *Acta Cryst.* **A71**, 3-8 (2015).
29. (SI only) G. M. Sheldrick, *Acta Cryst.* **A64**, 112-122 (2008).
30. (SI only) P. Müller, *Crystallography Reviews* **15**, 57-83 (2009).

5

Acknowledgments: University at Buffalo Chemistry Department Magnetic Resonance Center and Chemistry Instrument Center is acknowledged.

10

Funding: National Science Foundation (NSF) CAREER award 1847933. Orbitrap mass spectrometer: NSF MRI award 1919594. FTICR mass spectrometer: NIH award S10RR029517.

15

Author contributions: P.M.F. performed most of the experiments, data interpretation and analysis. V.V. and P.S.G. provided experimental support. D.C.L. conceived the project and wrote the manuscript and worked in consultation with P.M.F, P.S.G, and V.V throughout the project. S.N.M. performed the X-ray crystallographic characterization of **2** and **3**. All authors aided in manuscript preparation.

Competing interests: Authors declare that they have no competing interests.

Data and materials availability: All data are available in the main text or supplementary materials.

20

Supplementary Materials

Materials and Methods

Supplementary Text

Figs. S1 to S51

Tables S1 to S2

References (*S27–30*)

Supplementary Materials for
**Single-Component, Photocatalytic H₂ Production Through Acceptorless
Alcohol Dehydrogenation: Atypical Metal-Ligand Cooperativity in a
Ruthenium(II)-PN/P Complex**

Paul M. Fanara, Vipulan Vigneswaran, Parami S. Gunasekera, Samantha N. MacMillan, and
David C. Lacy*

Correspondence to: dclacy@Buffalo.edu

This PDF file includes:

Methods and Materials
Supplementary Text
Figs. S1 to S51
Tables S1 to S2

METHODS AND MATERIALS

General Methods

Chemicals were obtained from commercial vendors unless noted. All manipulations of oxygen sensitive compounds were performed under an argon atmosphere with standard Schlenk techniques or under nitrogen in a VAC Atmosphere Genesis Glovebox. Complex **1** was prepared from a previously reported procedure (10). Anhydrous organic solvents were sparged with argon and purified using a Pure Process Technology solvent purification system and were stored over 3 Å molecular sieves before use. Molecular sieves were activated at 200 °C under vacuum (< 100 mTorr) for 3-4 days prior to use. Deuterated solvents were degassed via three freeze-pump-thaw cycles and stored over sieves in a glovebox. In addition, manipulations towards the synthesis of **2** or in syntheses featuring **2** as a starting material, all solvents were dried additionally by passing over a plug of dry basic alumina on a medium fritted glass funnel in a glovebox. Basic alumina was dried at 200 °C under vacuum (< 100 mTorr) for 2-3 days prior to use. NMR spectra were collected on a Varian Mercury-300 MHz, Inova-400 MHz, or Inova-500 MHz spectrometer. FTIR-ATR spectra were collected inside of a VAC Atmospheres Genesis glovebox using a Bruker Alpha IR spectrometer with the “ATR Platinum” insert adapter (diamond crystal). Headspace analysis was obtained using a PerkinElmer Clarus 580 GC. High resolution mass spectrometry of **3** was conducted in MeOH using an FTICR Bruker 12 T mass spectrometer. Headspace GC-MS analysis for MeOH dehydrogenation product identification was performed on a Thermo Scientific Q-Exactive Gas Chromatographic Orbitrap Mass Spectrometer (QE-GCMSMS) equipped with a TG-5SILMS, 30m x 0.25 mm chromatographic column from Thermo Fisher Scientific. LC-MS analysis of reaction mixtures was performed on a Thermo Fisher Q-Exactive Liquid Chromatograph Orbitrap Tandem Mass Spectrometer (QE-LCMSMS).

Crystallographic Methods

Low-temperature X-ray diffraction data for Rlacy87 (**2**) (CCDC 2091357) and Rlacy86 (**3**) (CCDC 2091358) were collected on a Rigaku XtaLAB Synergy diffractometer coupled to a Rigaku HyPix detector with either Mo K α radiation ($\lambda = 0.71073$ Å) or Cu K α radiation ($\lambda = 1.54184$ Å), from a PhotonJet micro-focus X-ray source at 100 K and 104 K, respectively. The diffraction images were processed and scaled using the CrysAlisPro software (27). The structures were solved through intrinsic phasing using SHELXT (28) and refined against F^2 on all data by full-matrix least squares with SHELXL (29) following established refinement strategies (30). All non-hydrogen atoms were refined anisotropically. All hydrogen atoms bound to carbon were included in the model at geometrically calculated positions and refined using a riding model. Hydrogen atoms bound to ruthenium were located in the difference Fourier synthesis and subsequently refined freely. The isotropic displacement parameters of all hydrogen atoms were fixed to 1.2 times the U_{eq} value of the atoms they are linked to (1.5 times for methyl groups). Details of the data quality and a summary of the residual values of the refinements are listed in Table S2.

Photochemistry Methods

General

All photolysis experiments were carried out in sealed vessels, which were positioned 2” away from the aperture of a 100 W xenon-arc lamp (Newport INC.; APEX2). Various filters were employed with the xenon arc lamp: no filter (broadband), UV band pass filter (50% Abs Cutoff = 382 nm; % $T_{avg} \geq 70\%$ = 300 – 375 nm; % $T_{avg} \leq 1\%$ = 400 – 635 nm; % $T_{avg} \leq 10\%$ = 280 – 290

nm), a 345 nm cutoff filter ($\lambda \geq 345$ nm), a 420 nm cutoff filter ($\lambda \geq 420$ nm), and a 512 nm cutoff filter ($\lambda \geq 512$ nm). Temperature control was achieved using a water-cooling jacket set at the desired temperature.

Photocatalysis

In a N₂ filled glovebox, 200 μ L of a stock solution of complex **3** (0.04 M) in dry benzene was added to a 50 mL Schlenk tube along with a stir bar. The specified alcohol was dried over basic alumina (1-phenylethanol and isopropanol) or 3 Å molecular sieves for at least 2 days (methanol and ethanol) before 2.0 mL was added to the tube. The final concentration of catalysts was 0.004 M. The Schlenk tube was then sealed with a rubber septum, taken out of the glovebox, and irradiated at 23 °C. Each alcohol was done in triplicate except when H₂ yields were below 100%. The overnight experiments for each alcohol were sampled after 4 h and again after 12 h. **The yields are reported in Table S2.**

Note, **3** has poor solubility in neat alcohols. Irradiations of **3** in neat alcohols (except for MeOH) resulted in homogenous solutions during the course of irradiation, and the yields of H₂ for each alcohol were comparable (often slightly higher) to those that used benzene stock solutions of **3**.

H₂ Quantification from Photocatalysis

H₂ quantification was achieved by removing 3 mL of headspace with a gas-tight syringe and analyzed using gas chromatography. The area of the H₂ peak was compared to a calibration curve to determine the percent H₂ in the headspace (see Table S2 for results).

19 h photocatalysis in neat 2-propanol for bulk acetone quantification

3 mL of a 0.005 M 2-propanol solution of **3** was irradiated for 19 h (broadband). The apparatus was attached to a bubbler to vent H₂. To quantify acetone, the post-irradiated mixture was measured into a graduated cylinder and treated with standard (hexamethyldioxane) and an aliquot was dissolved in CDCl₃ and analyzed by ¹H NMR spectroscopy. The yield of acetone was 700% relative to **3**.

Characterization of the organic products from Photocatalysis with **3**

Organic products from the reaction were determined *via* separate NMR tube experiments.

*For the determination of organic products from the photolysis of **3** in methanol, ethanol, and 1-phenylethanol*

In a N₂-filled glovebox, a stock solution of **3** in C₆D₆ (0.0062 M) was prepared. Approximately 0.500 mL (0.00310 mmol, 1 equiv.) was transferred by glass syringe to an NMR tube equipped with J-Young valve. The alcohol (0.155 mmol, 50 equiv. for methanol and ethanol; 0.0931 mmol, 30 equiv. for 1-phenylethanol) was subsequently added by glass syringe. An initial ¹H NMR spectra was collected, and the tube was subsequently irradiated with a 100 W Xe arc lamp through a 345 nm cut off filter. ¹H NMR spectra were collected 2, 4.5 and 23 hours after initial photolysis for methanol and ethanol; for 1-phenylethanol photolysis was stopped after 7 hours and spectra was collected at this time. After 23 hours, compound **4** was still present in the

sample containing ethanol whereas in the sample containing methanol the only identifiable product was the carbonylated product **8**. In the ethanol experiment, ethyl acetate resonances were present after photolysis and were observed to grow in over time. The presence of ethyl acetate was confirmed by spiking this sample with 1 μL of dry ethyl acetate (Fig. S37). For 1-phenylethanol, peaks characteristic of acetophenone were observed and confirmed by spiking this sample with 1 μL of dry acetophenone (Fig. S38).

For the determination of organic products from the photolysis of **3** in 2-propanol

An NMR tube equipped with a J-Young valve was charged with 0.400 mL of a solution of **3** in C_6D_6 (0.012 M) in a N_2 -filled glovebox. Dry 2-propanol (0.097 mmol, 20 equiv.) was added via glass syringe to the tube. Initial spectra were collected before photolysis and then subsequently collected at 4, 6 and 12 hours after irradiation. After 12 hours, the single characteristic peak of acetone was observed to grow in and was confirmed by spiking this sample with 1 μL of acetone (Fig. S39).

Additional experiments for the determination of organic products from the photolysis of **3** in methanol

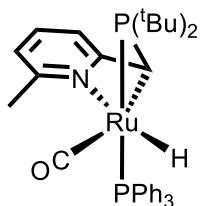
- 1) Neat CD_3OD : In a N_2 -filled glovebox, compound **3** (2.0 mg, 0.0031 mmol) was suspended in 0.500 mL of CD_3OD in a tared vial (Note: **3** is only partially soluble in methanol). This suspension was transferred to a J-Young NMR tube and ^1H and ^2H NMR spectra were obtained. The initial ^1H NMR spectrum shows the presence of HD and H_2 . After irradiation for a period of an hour, the hydridic resonances of **3** and **4** were not observed. Subsequent irradiation for 5 hours revealed a signal characteristic of carbonylated species **8** as determined by ^1H NMR (Fig. S40).
- 2) Mass spectrometric analysis: In a N_2 -filled glovebox, a 20 mL headspace GC vial was charged with 1.000 mL of methanol and 50 μL of a benzene solution of **3** (0.04 M). A stir bar was placed in the vial and was subsequently irradiated with a 100 W Xe arc lamp with a 345 nm cutoff filter for a period of 4 hours. Headspace GC-MS analysis using selective ion-monitoring showed the presence of formaldehyde (Fig. S41). Positive mode LC-MS analysis of the reaction mixture revealed the presence of signals consistent with $\{\text{LutP}\}\text{Ru}(\text{H})(\text{CO})$ and $\{\text{LutP}\}\text{Ru}(\text{H})(\text{CO})_2$ (Fig. S42).
- 3) Photolysis with paraformaldehyde: To test the effects of formaldehyde in irradiations of **3** we performed the following experiment. In a N_2 -filled glovebox, paraformaldehyde (1.7 mg, 0.057 mmol, 12 equiv.) was added to a solution of **3** (3.0 mg, 0.046 mmol, 1 equiv.) in 0.400 mL of C_6D_6 in a vial (Note: paraformaldehyde is not soluble in C_6D_6). The suspension was transferred to a J-Young NMR tube. Initial ^1H NMR spectrum, prior to photolysis, revealed the presence of H_2 indicating formaldehyde dehydrogenation. The tube was irradiated for 4 hours and a ^1H NMR spectrum was collected. The only hydridic signals observed were from carbonylated species **8**, the same product obtained when **3** was irradiated under CO in C_6D_6 . Additionally, other organic products, including methanol and some aldehydic species were observed (Fig. S43). Collectively, this indicates that **3** also dehydrogenates formaldehyde.

T₁ Measurements

T₁ measurements were recorded on a Inova-400 MHz instrument using the inversion recovery method according to D. G. Hamilton, R. H. Crabtree *J. Am. Chem. Soc.* **1988**, *110*, 4126. The reported T₁ (min) are the lowest T₁ observed between 298 K – 183K in THF-*d*₈ (**3**) or C₇D₈ (**4**).

Synthesis of Compounds

Synthesis of (CO)(H)(PPh₃)(κ³-*N,C,P*-LutP⁺)ruthenium(II) (**2**)



2

K[N(SiMe₃)₂] Method. A 20 mL scintillation vial was charged with a stir bar, 4 mL of freshly dried THF, and 50.0 mg (0.0736 mmol) of **1**. This mixture was stirred until homogenous. After which, the solution was cooled to -35 °C in a cold well before 14.6 mg (0.0736 mmol) of K[N(SiMe₃)₂] was added. Upon addition of K[N(SiMe₃)₂], the solution became an amber color. The solution was stirred for 5 minutes at -35 °C. After which, the amber solution was removed from the cold-well and was immediately concentrated *in vacuo* to dryness. The residue was treated with ~5 mL of dry diethyl ether. The resulting amber suspension was filtered and the solids were washed with diethyl ether until the filtrate was colorless. The filtrate was then concentrated *in vacuo* to dryness to yield an amber-brown solid: 43.0 mg (91%). Amber crystals suitable for diffraction were grown from Et₂O at -35 °C.

KOtBu Method. A 20 mL scintillation vial was charged with a stir bar, 2 mL of freshly dried benzene, and 20.0 mg (0.0294 mmol) of **1**. This mixture was stirred until homogenous. After which, 3.6 mg (0.0324 mmol) of KOtBu was added to the stirring pale-yellow solution at room temperature. Upon addition of KOtBu at room temperature, the solution became an amber color. The solution was stirred for a further hour at room temperature during which a white solid (KCl) formed. After an hour had passed the amber mixture was filtered and concentrated *in vacuo* leaving an amber-brown solid behind. To this residue was added ~5 mL of dry diethyl ether and the resulting amber suspension was filtered. The remaining solid residue was washed with diethyl ether until the filtrate was colorless. The amber filtrate was concentrated *in vacuo* to dryness to give an amber-brown solid: 18.0 mg (95%).

NOTE: Compound **2** is extremely water sensitive as well as thermally unstable and must be stored at -35 °C or used immediately after isolation. Thus, HRMS analyses was unsuccessful.

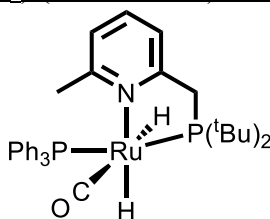
¹H NMR (300 MHz, C₆D₆) δ 7.75 (m, 6H), 7.01 (m, 9H), 6.60 (t, *J* = 8 Hz, 1H), 5.83 (t, *J* = 9 Hz, 2H) (overlapping doublets), 1.78 (d, *J* = 3 Hz, 1H), 1.70 (s, 3H), 1.40 (d, *J* = 14 Hz, 9H), 1.14 (d, *J* = 14 Hz, 9H), -14.16 (dd, *J* = 23, 19 Hz, 1H). **¹H NMR** (300 MHz, C₇D₈) δ 7.83 – 7.65 (m, 6H), 7.15 – 6.97 (m, 9H), 6.67 (t, *J* = 8 Hz, 1H), 5.92 (d, *J* = 8 Hz, 1H), 5.86 (d, *J* = 8 Hz, 1H), 1.79 (d, *J* = 3 Hz, 1H), 1.74 (s, 3H), 1.44 (d, *J* = 13 Hz, 9H), 1.19 (d, *J* = 13 Hz, 9H), -14.21 (dd, *J* = 23, 19 Hz, 1H).

$^{31}\text{P}\{^1\text{H}\}$ NMR (121 MHz, C_6D_6) δ 118.0 (d, $J = 234$ Hz), 54.7 (d, $J = 233$ Hz). ^{31}P NMR (121 MHz, C_7D_8) δ 118.3 (dd, $J = 235$, 5 Hz), 54.87 (dd, $J = 235$, 7 Hz).

$^{13}\text{C}\{^1\text{H}\}$ NMR (75 MHz, C_6D_6) δ 211.1, 168.1 (d, $J = 3$ Hz), 157.3, 138.6 (d, $J = 34$ Hz), 134.8, 133.6 (d, $J = 12$ Hz), 128.4, 128.2, 127.5, 116.6, 113.1 (d, $J = 3$ Hz), 35.7 (dd, $J = 13$, 9 Hz), 34.7 (d, $J = 26$ Hz), 31.2 (d, $J = 6$ Hz), 30.5 (d, $J = 4$ Hz), 21.8, 12.0 (dd, $J = 7$, 5 Hz).

FTIR-ATR: 1880 cm^{-1} (ν_{CO}).

Synthesis of (CO)-cis-(H)₂-trans-(PPh₃) (κ^2 -N,P-LutP)ruthenium(II) (**3**)



3

Dihydrogen Method. In a nitrogen filled glovebox, an oven-dried Schlenk flask equipped with a stir bar was loaded with **1** (80.0 mg, 0.118 mmol). Freshly dried THF (10 mL) was added, and the mixture was stirred until the solid was fully dissolved to yield a pale-yellow solution. To the Schlenk flask, a solid addition arm loaded with $\text{K}[\text{N}(\text{SiMe}_3)_2]$ (23.5 mg, 0.118 mmol) was equipped. The flask was sealed and brought out of the glovebox and attached to a Schlenk line. The solution was subjected to three freeze-pump-thaw cycles and then brought under an atmosphere of dihydrogen (1 atm) at room temperature and stirred for 10 minutes. $\text{K}[\text{N}(\text{SiMe}_3)_2]$ was then dispensed into the flask in one portion. Color changes were noted over a period of 10 minutes from pale-yellow to dark-yellow and finally to amber. The amber solution was allowed to stir for another one hour under the hydrogen atmosphere. Subsequently, solvent was removed *in vacuo* to yield an amber residue. The Schlenk flask was brought back into the glovebox and the residue was dissolved in dry benzene and filtered into a tared scintillation vial. The solution was placed in a freezer at $-35\text{ }^\circ\text{C}$ for a period of 20 minutes and then lyophilized over a period of 2 hours to yield a pale-yellow colored, fluffy solid that was identified as the title compound (66 mg, 87%). Pale-yellow crystals were grown from layering a solution of **3** under hexane at $-35\text{ }^\circ\text{C}$.

NOTE: Compound **2** can also be prepared independently and subjected to direct addition of H_2 . However, owing to the high-moisture sensitivity of **2**, it is advised to access **2** *in situ* to avoid decomposition products that are difficult to separate from the final product, **3**.

Isopropanol Method. A sealable NMR tube was charged with of a solution of 8.0 mg (0.0124 mmol) of **2** in ~ 0.75 mL of freshly dried C_6D_6 . To this solution was added $3.1\text{ }\mu\text{L}$ (0.0409 mmol) of degassed and alumina dried 2-propanol. An NMR of the resulting solution 15 min after the addition of 2-propanol revealed a mixture of **3**, excess 2-propanol, and acetone in a 1:2.3:1 ratio.

^1H NMR (300 MHz, C_6D_6) δ 7.93 – 7.75 (m, 6H), 7.13 – 6.91 (m, 9H), 6.78 (t, $J = 8$ Hz, 1H), 6.58 (d, $J = 8$ Hz, 1H), 6.29 (d, $J = 8$ Hz, 1H), 3.51 (dd, $J = 16$, 6 Hz, 1H), 3.23 (ddd, $J = 16$, 9, 4 Hz, 1H), 2.52 (s, 3H), 1.39 (d, $J = 13$ Hz, 9H), 1.11 (d, $J = 12$ Hz, 9H), -5.69 (dddd, $J = 38$, 22, 6, 4 Hz, 1H), -15.59 (ddd, $J = 31$, 17, 6 Hz, 1H).

$^{31}\text{P}\{^1\text{H}\}$ NMR (121 MHz, C_6D_6) δ 108.7 (d, $J = 251$ Hz), 59.4 (d, $J = 253$ Hz).

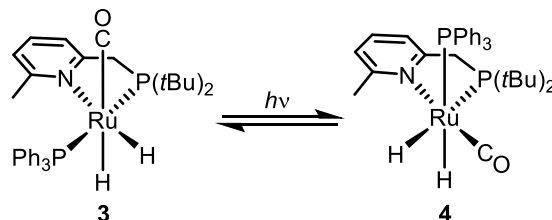
$^{13}\text{C}\{^1\text{H}\}$ NMR (101 MHz, C_6D_6) δ 210.5, 163.7 (dd, $J = 5, 2$ Hz), 163.0, 142.2, 141.8, 134.5, 134.1 (d, $J = 12$ Hz), 128.6, 128.5 (d, $J = 2$ Hz), 127.9, 127.7, 121.5, 119.3 (d, $J = 7$ Hz), 41.5 (d, $J = 16$ Hz), 36.6 (t, $J = 3$ Hz), 33.7 (d, $J = 3$ Hz), 33.5 (d, $J = 3$ Hz), 31.9 (d, $J = 6$ Hz), 31.7 (d, $J = 5$ Hz), 29.3 (d, $J = 6$ Hz).

FTIR-ATR: 1901 cm^{-1} (ν_{CO}).

HRMS (FT-ICR-MS): $[(\text{C}_{15}\text{H}_{26}\text{NP})(\text{PPh}_3)(\text{CO})(\text{H})_2\text{Ru}]^+$ ($[\text{M}-\text{H}]^+$); $m/z(\text{found}) = 644.176504$; $m/z(\text{calcd.}) = 644.177959$.

$T_1(\text{min@400 Hz})$: 315 ms (-5.69 ppm, 223 K) and 421 ms (-15.60 ppm, 213 K).

Characterization of (CO)-cis-(H)₂-cis-(PPh₃)(κ₂-N,P-LutP)ruthenium(II) (4)



Synthesis from 2: A J-Young tube was charged with a solution of 10 mg (0.0156 mmol) of **2** and ~0.5 mL of dry C_6D_6 to give a yellow solution. This tube was subjected to three freeze-pump-thawed cycles, after which the head space was charged with dihydrogen (1 atm) to give a yellow orange solution. After 15 min a ^1H NMR spectrum was taken to confirm complete conversion to **3**. Once the conversion was complete by NMR, the tube was irradiated with a 100 W xenon-arc lamp with no filter in a 23 °C water bath for 1 h. A ^1H NMR spectrum taken after irradiation was ceased (~5-10 min) indicates an ~80:20 ratio of **4**:**3**. Complex **4** converts cleanly back to **3** over the course of 12 h.

Synthesis from 3: A J-young tube was charged with a solution of 9.5 mg (0.0156 mmol) of **3** and ~0.5 mL of dry C_6D_6 in a glovebox with an $\text{N}_2(\text{g})$ atmosphere. This solution was irradiated at 23 °C with a 100 W xenon arc lamp with no filter for a period of 1 h. A ^1H NMR spectrum taken after irradiation was ceased (~5-10 min) indicates an ~80:20 ratio of **4**:**3**.

Note: Photolysis of **3** in $\text{THF}-d_8$ resulted in degradation products.

^1H NMR (300 MHz, C_6D_6) δ 7.77 – 7.64 (m, 6H), 7.12 – 6.98 (m, 9H), 6.59 (t, $J = 8$ Hz, 1H), 6.38 (d, $J = 8$ Hz, 1H), 6.16 (d, $J = 8$ Hz, 1H), 3.06 (dd, $J = 16, 8$ Hz, 1H), 2.76 (dd, $J = 17, 5$ Hz, 1H), 2.56 (s, 3H), 1.30 (d, $J = 12$ Hz, 9H), 1.11 (d, $J = 13$ Hz, 9H), -5.14 (dd, $J = 101, 25$ Hz, 1H), -6.10 (dd, $J = 92, 17$ Hz, 1H).

$^{31}\text{P}\{^1\text{H}\}$ NMR (202 MHz, C_6D_6) δ 75.5 (d, $J = 11$ Hz), 40.2 (d, $J = 11$ Hz).

FTIR-ATR: 1886 cm^{-1} (ν_{CO}).

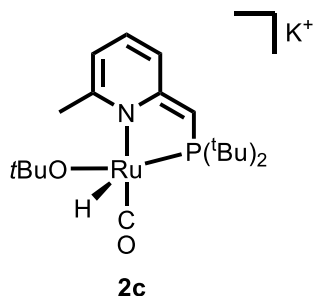
$T_1(\text{min@400 Hz})$: 349 ms (-5.14 ppm, 243 K) and 391 ms (-6.03 ppm, 243 K).

SUPPLEMENTARY TEXT

Reactivity of 2

Reaction of 2 with excess KOtBu (2c)

When more than one equivalent of KO t Bu was used in the synthesis of **2** from **1**, free PPh $_3$ and an anionic {LutP}Ru(O t Bu) complex (**2c**) was formed in addition to **2** (Figs. S9(top)–S10(top)). The reaction of **2** with one equiv. of KO t Bu and one equiv. of 18-crown-6 gave only **2c** (Figs. S9(bottom)–S10(bottom)). Further attempts to isolate **2c** were not performed at the time of preparing this manuscript.



Reaction of **2** with D $_2$

A solution of ~10 mg (0.0156 mmol) of **2** and ~0.5 mL of dry C $_6$ D $_6$ was added to a J-young tube under an N $_2$ atmosphere. This tube was sealed and freeze-pump-thawed three times before an atmosphere of D $_2$ (1 atm) was added using Schlenk line techniques. A 1 H NMR spectrum was taken before the tube was then brought back into the glovebox and concentrated *in vacuo*. The residue was dissolved ~0.5 mL C $_6$ H $_6$ and ~5 μ L of C $_6$ D $_6$ and transferred to a new J-young tube before a 2 H NMR spectrum was taken.

After 1 h under ambient light (Figs. S17–S18), the 1 H and 2 H NMR spectra indicate deuterium incorporation at both the ruthenium center and the methylene arm of the ligand. Two hydride/deuteride isotopomers are observed in a 1:1 ratio with minor shoulders which are suspected to be the diastereomers of these major complexes in which the methylene C–H/D stereochemistry is reversed. In the absence of light these minor peaks are not observed, indicating that light is involved in the isomerization process (Figs. S19–S20).

Note: H $_2$ and HD were observed in the 1 H NMR spectrum when **2** was treated with D $_2$ indicating exchange with free dihydrogen in the presence of light (Figs. S17–S18). In the absence of light only trace amounts of H $_2$ and HD were detected by NMR (Figs. S19–S20).

Reactivity of **3**

Reaction of **3** with D $_2$

A solution of ~10 mg (0.0156 mmol) of **3** and ~0.5 mL of dry C $_6$ D $_6$ was added to a J-young tube under an N $_2$ atmosphere. This tube was sealed and freeze-pump-thawed three times before an atmosphere of D $_2$ (1 atm) was added using Schlenk line techniques. A 1 H NMR spectrum was taken before the tube was then brought back into the glovebox and concentrated *in vacuo*. The residue was dissolved ~0.5 mL C $_6$ H $_6$ and ~5 μ L of C $_6$ D $_6$ and transferred to a new J-young tube before a 2 H NMR spectrum was taken.

With ~1 h of irradiation (Figs. S31–S32) or ~4 days in the dark (Fig. S33), 1 H and 2 H NMR spectra indicate nearly complete incorporation of deuterium into both hydride resonances. Importantly, no incorporation in the ligand was observed.

Note: H₂ and HD were observed in the ¹H NMR spectrum when **3** was treated with D₂ indicating exchange with free dihydrogen when irradiated (Figs. S31–S32). In the absence of light only trace amounts of H₂ and HD were detected by NMR (Fig. S33).

Reaction of **3** with 2-propanol-*d*₈

A solution of 9.25 mg (0.0143 mmol) of **3**, ~0.5 mL of dry C₆D₆, and 2.2 μL (0.0287 mmol) of 2-propanol-*d*₈ was added to a J-young tube under an N₂ atmosphere. This tube was sealed and irradiated for ~1.5 h with no filter. A ¹H NMR spectrum (Fig. S44) was taken before the tube was then brought back into the glovebox and concentrated *in vacuo*. The residue was dissolved ~0.5 mL C₆H₆ and ~5 μL of C₆D₆ and transferred to a new J-young tube before a ²H NMR spectrum was taken (Fig. S45).

With ~1.5 h of irradiation, ¹H and ²H NMR spectra clearly show incorporation of deuterium into the ligand methylene arm (Figs S44–S45).

Wavelength required for H₂ production from isopropanol and **3**

A solution of 10 mg of **3** in 2.0 mL of isopropanol was added to a 50 mL Schlenk flask in an N₂ filled glovebox. This tube was sealed with an unpunctured septa and secured with electrical tape before bringing out of the glovebox. The tube was irradiated for 1 h at 23 °C with a 520 nm cutoff filter before the head space was sampled and analyzed for H₂. This was repeated using 420 nm and 345 nm cutoff filters. The 512 nm and 420 nm filters gave very little H₂ while the 345 nm cutoff filter gave significantly more H₂ (Fig. S46).

Wavelength required for photoisomerization of **3** to **4**

To determine the wavelength of light required to isomerize **3** to **4**, a solution of 10 mg of **3** in ~0.5 mL of dry C₆D₆ was added to a J-young NMR tube in an N₂-filled glovebox. This tube as sealed, brought out of the glovebox, and photolyzed for 1 min at 23 °C using a filter before a ¹H NMR spectrum was taken to determine the ratio of **4** to **3**. A 515 nm cutoff filter, a 420 nm cutoff filter, a 345 nm cutoff filter, and a UV band pass filter were used. Very little conversion to **4** was observed for the 515 nm cutoff filter (~2%), 420 nm cutoff filter (~7 %), and UV band pass filter (~5%). Only with the 345 nm cutoff filter was significant conversion to **4** observed (~24%, 345 nm) (Fig. S47).

Other observed byproducts during photolysis of **3**

In some cases, when less than pristine samples of **3** were irradiated under H₂, {PPh₃}₃Ru^{II}(H)₄ and a byproduct (**8**) with a resonance at -7.30 ppm was observed. When excess (10 eq) PPh₃ was added to **3** prior to irradiation, no reaction occurred by ¹H and ³¹P {¹H} NMR. However, after 2 h of photolysis with a 100 W xenon-arc lamp with no filter, (CO)(PPh₃)₃Ru(H)₂ was observed as a major byproduct (Fig. S36).

Carbonylated product (**8**): Photolysis of **3** under CO

An NMR sample of **3** (6.7 mg, 0.010 mmol) in C₆D₆ (0.450 mL) was prepared in a nitrogen filled glovebox and quantitatively transferred to a J-Young tube. The tube was removed from the glovebox and then connected to a Schlenk line and subjected to three freeze-pump-thaw cycles to remove dissolved dinitrogen. After the tube had returned to room temperature, CO (10% in Ar_(g)),

1 atm) was introduced to the sample for a period of two minutes. The tube was inverted and shaken and subsequently irradiated with broadband light for one hour. The sample was then quickly analyzed by ^1H and $^{31}\text{P}\{^1\text{H}\}$ NMR spectroscopy with no further isolation or purification (Figs. S49–51). The major product (**8**) contains resonances consistent with a carbonylated product in which the pyridine ring has been substituted with a CO ligand. When **8** was prepared for an overnight ^{13}C NMR experiment, other products (from a multitude of ^{13}C signals) and free H_2 were observed in a subsequent ^1H NMR experiment suggesting that **8** is not indefinitely stable under an atmosphere of CO. Complex **8** is also observed when **3** is irradiated under N_2 , and is a commonly observed byproduct in post-irradiated.

^1H NMR (300 MHz, C_6D_6) δ 7.85 – 7.71 (m, 5H), 7.41 (d, $J = 8$ Hz, 1H), 6.62 (d, $J = 7$ Hz, 1H), 3.44 (dd, $J = 10, 2$ Hz, 2H), 2.39 (s, 3H), 1.45 (d, $J = 13$ Hz, 18H), -7.30 (dd, $J = 25, 21$ Hz, 2H).

$^{31}\text{P}\{^1\text{H}\}$ NMR (202 MHz, C_6D_6) δ 96.90 (d, $J = 212.0$ Hz), 58.58 (d, $J = 212.7$ Hz).

FTIR-ATR: (Major stretches) 2009 cm^{-1} , 1962 cm^{-1} , 1891 cm^{-1} , 1872 cm^{-1} .

Half-Life Determination of **4**

A J-Young tube was charged with a solution of 9.5 mg (0.0156 mmol) of **3** and 0.4 mg of hexamethylbenzene in ~ 0.5 mL of dry C_6D_6 in a glovebox with an $\text{N}_2(\text{g})$ atmosphere. This solution was used as it is (N_2 atmosphere), subjected to three freeze-pump-thaw cycles (static vacuum), or subjected to three freeze-pump-thaw cycles followed by addition of H_2 before being irradiated with a 100 W xenon arc lamp (broad band, no filter) for a period of 1 h. The samples were monitored by ^1H NMR after irradiation to measure the disappearance of **4** and reappearance of **3** by comparing the integrations of the δ_{CH_3} of **4** and **3**. All experiments were performed in triplicate and average $t_{1/2}$ is reported (Figs. S21–S24, S29–30).

Eyring plot of **4**

A solution of 10 mg of **3** in ~ 0.5 mL C_6D_6 was added to a J-Young tube in a N_2 filled glovebox. This tube was sealed and irradiated with a 100 W xenon arc lamp with a 345 nm cutoff filter for 1 h. ^1H NMR spectra were taken from 25 $^\circ\text{C}$ to 45 $^\circ\text{C}$ in 2.5 $^\circ\text{C}$ increments. Line fitting analysis was performed on the -5.14 ppm and -6.10 ppm resonances of **4** and the average width at half height (w_t) of each resonance was determined. The rate constant at each temperature (k_T) was calculated using the following equation:

$$k_t = \pi(w_t - w_0)$$

Where w_t is the width at half height of the resonance at a specific temperature and w_0 is the width at half height at 25 $^\circ\text{C}$. An Eyring plot ($\ln [k_T/T]$ vs $1/T$) was constructed from this data which furnished a straight line with an $R^2 = 0.993$ (Figs. S34–S35). This plot furnished a ΔH^\ddagger value of 25.3 $\text{kcal}\cdot\text{mol}^{-1}$ and ΔS^\ddagger value of 26.7 $\text{cal}\cdot\text{K}^{-1}\cdot\text{mol}^{-1}$. The ΔG^\ddagger at 293K was calculated to from these values as 17.4 $\text{kcal}\cdot\text{mol}^{-1}$.

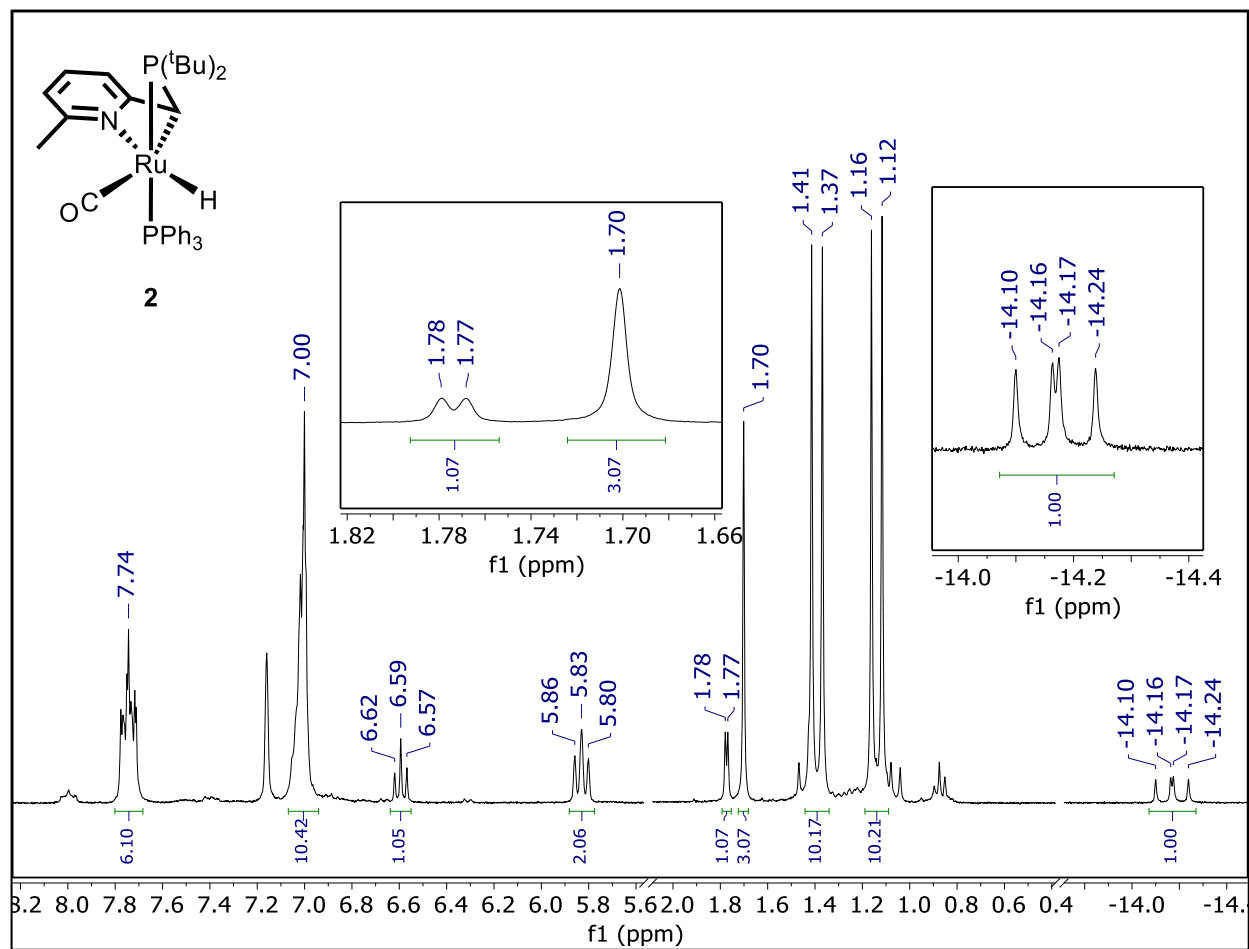


Fig. S1.
300 MHz ^1H NMR spectrum of **2** in C_6D_6 .

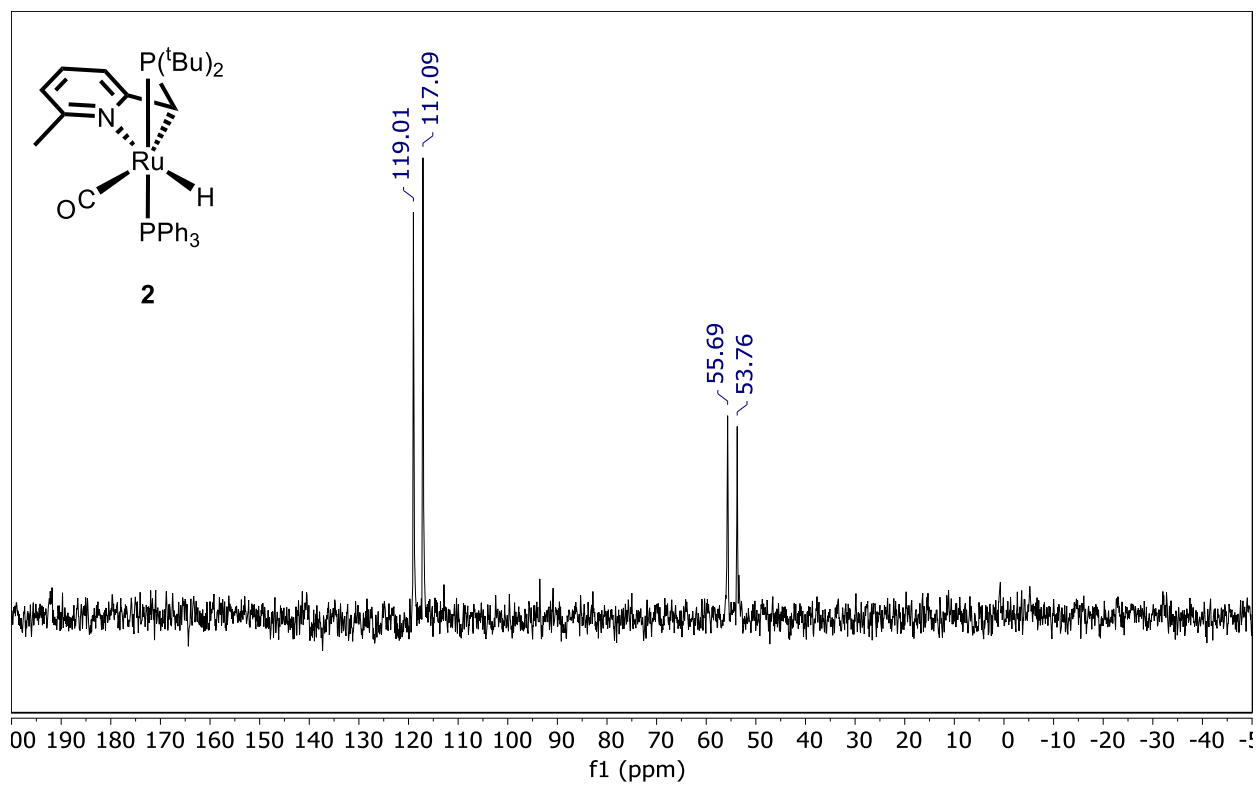


Fig. S2.
121 MHz $^{31}\text{P}\{^1\text{H}\}$ NMR spectrum of **2** in C_6D_6 .

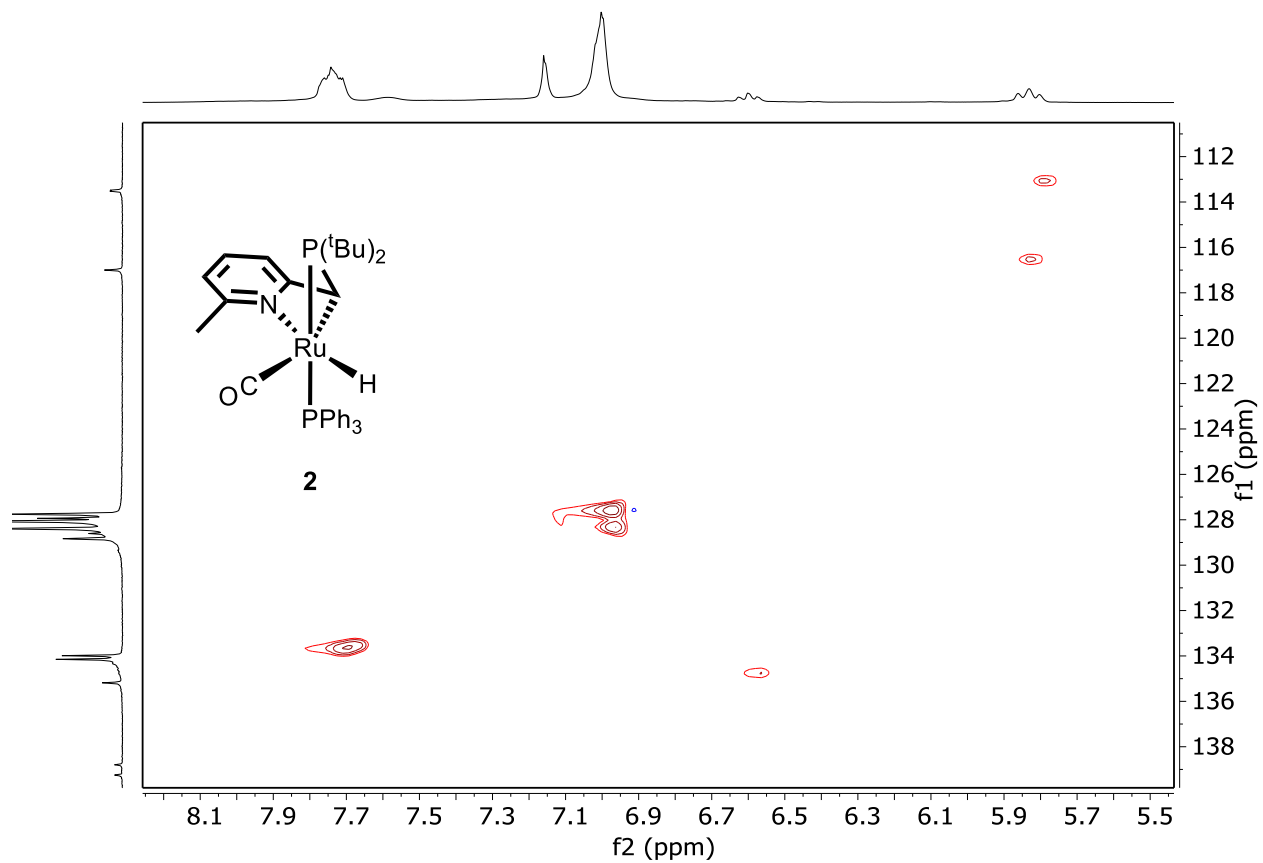


Fig. S4.

$^1\text{H}/^{13}\text{C}$ correlated HSQC spectrum of **2** in C_6D_6 zoomed in on the aromatic region.

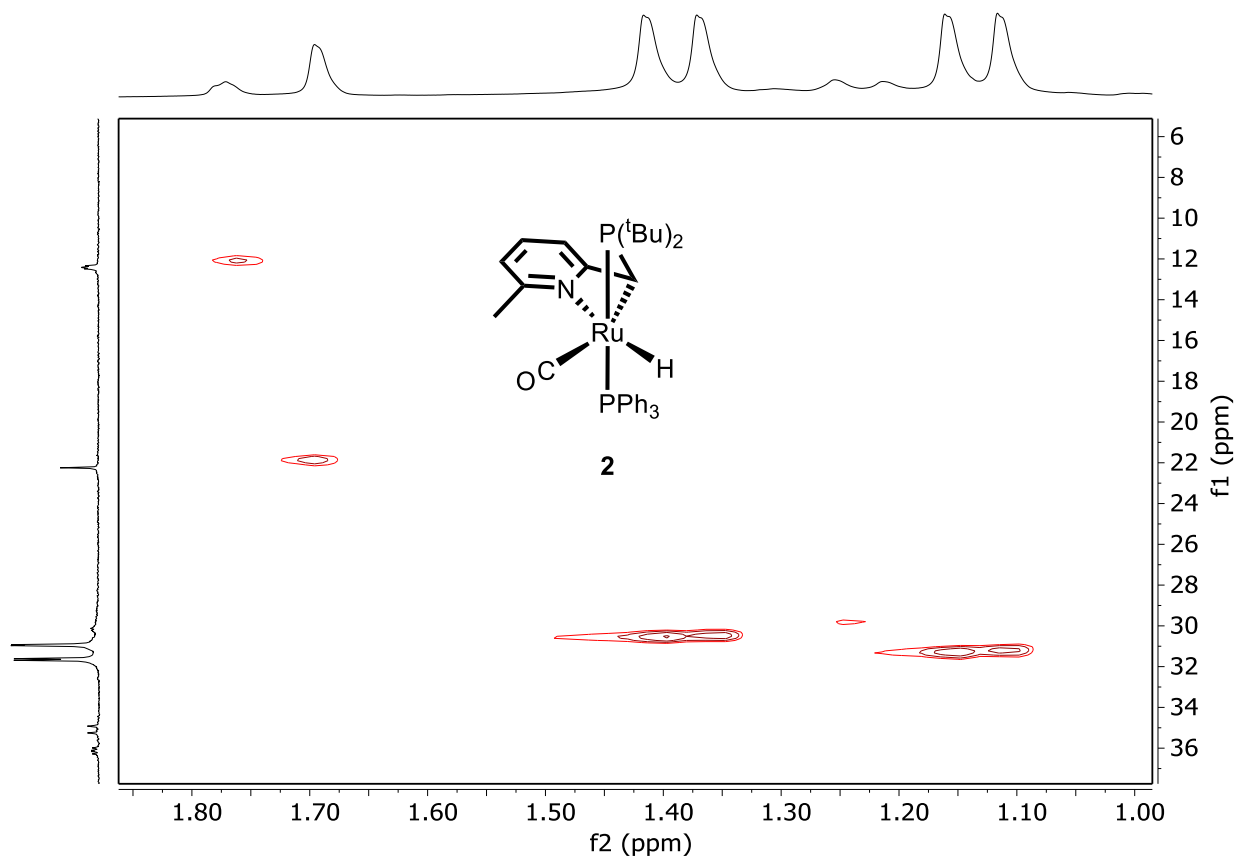


Fig. S5.

¹H/¹³C correlated HSQC spectrum of **2** in C₆D₆ zoomed in on the aliphatic region.

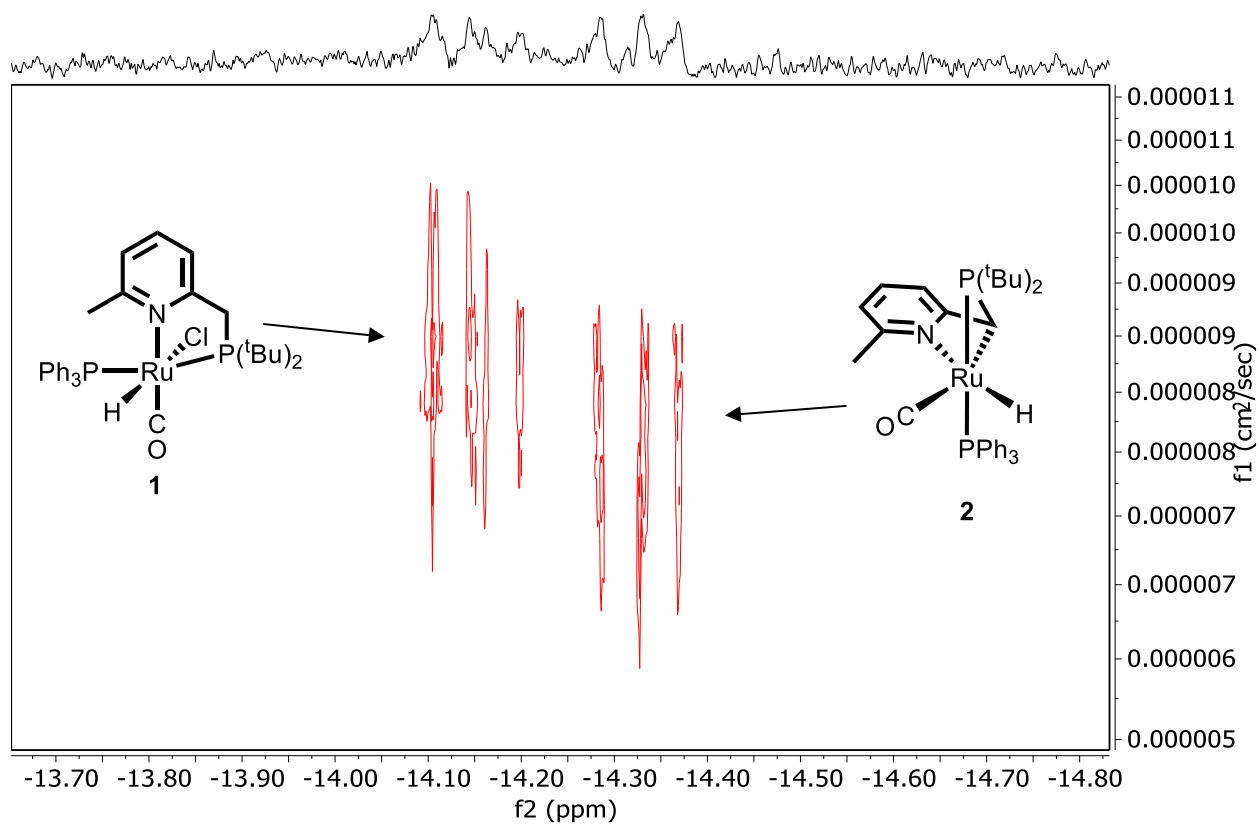


Fig. S6.

DOSY spectra of a 50:50 mixture of **1**:**2** in C_6D_6 zoomed in on the hydride region.

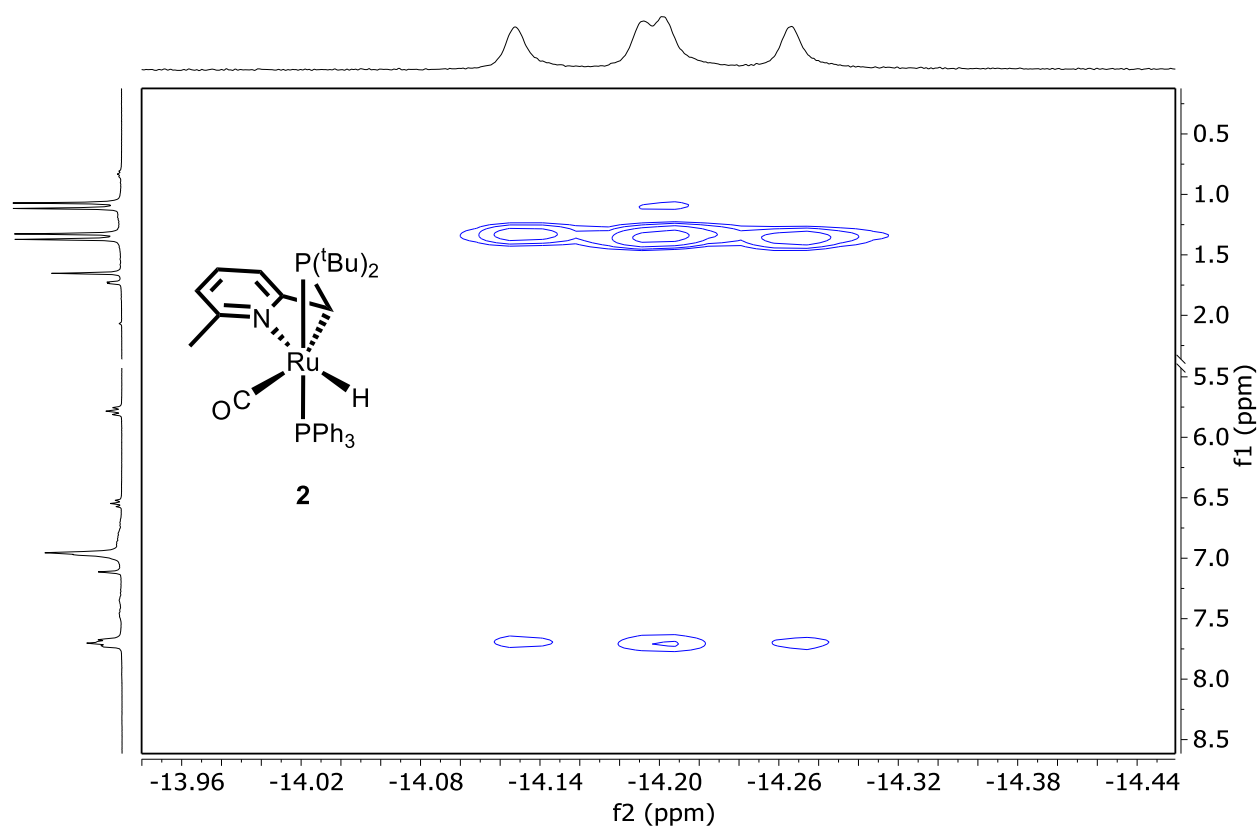


Fig. S7.

^1H - ^1H ROESY NMR spectrum of **2** in C_6D_6 zoomed in on the hydride region.

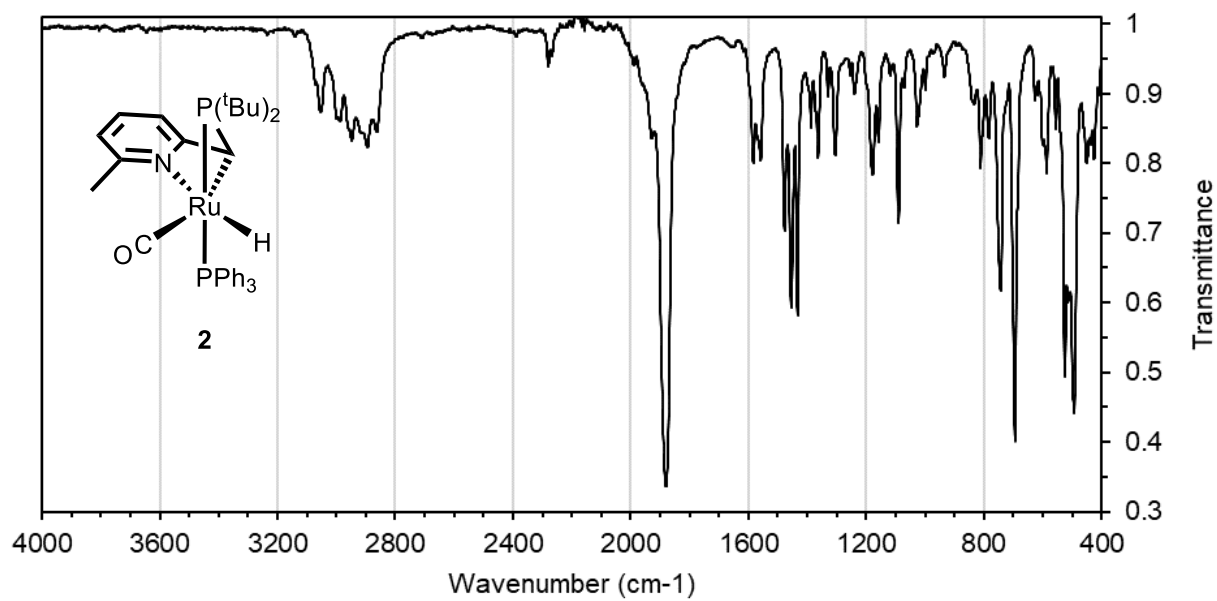


Fig. S8.
Drop-cast FTIR-ATR spectrum of **2**.

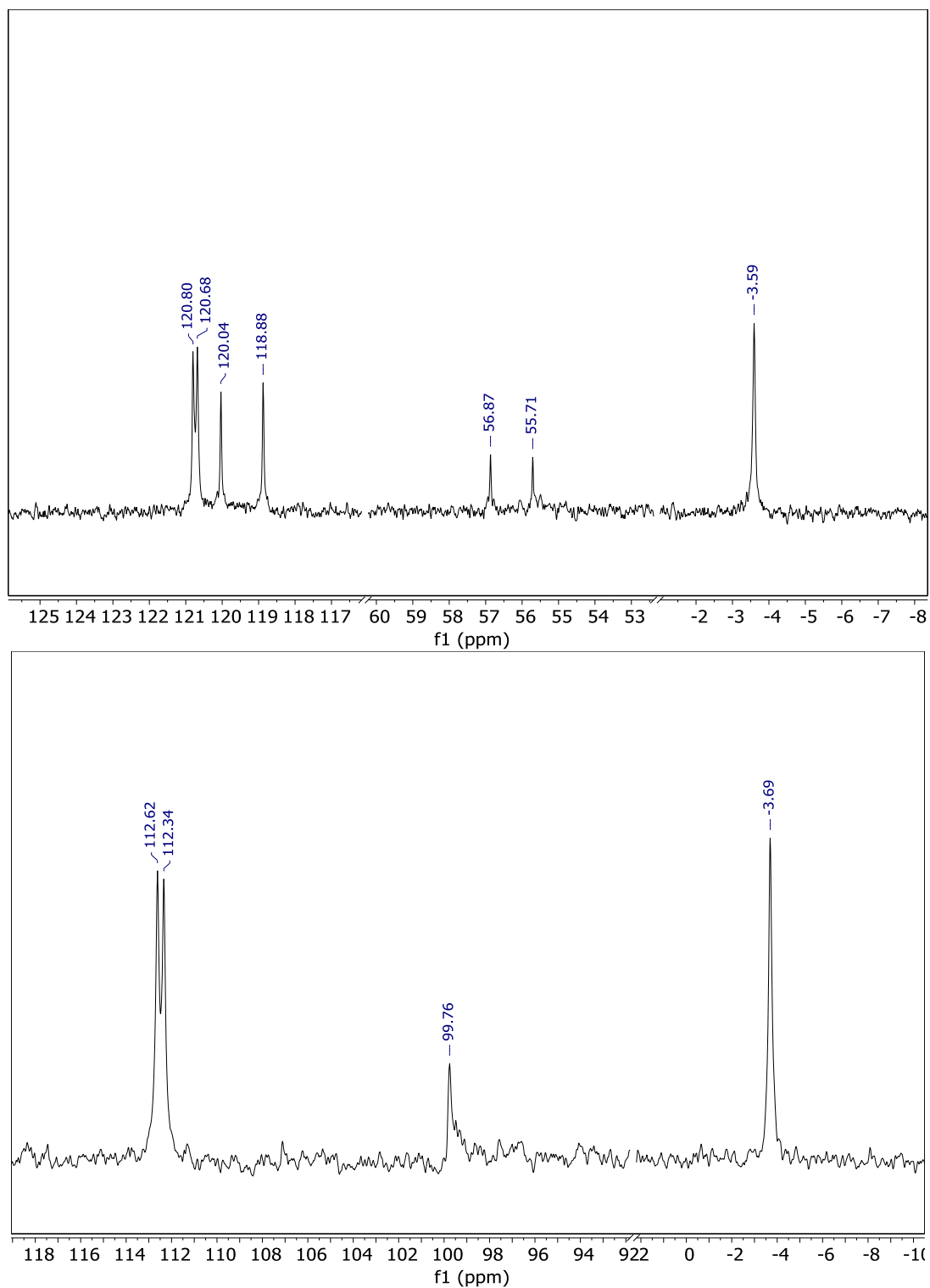


Fig. S10.

(top) 202 MHz $^{31}\text{P}\{^1\text{H}\}$ NMR spectrum of the reaction of **1** with 2 equiv. of KO t Bu in THF- d_8 .
 (bottom) 121 MHz $^{31}\text{P}\{^1\text{H}\}$ NMR spectrum of a solution of **2** in THF- d_8 treated with 1 equiv. of KO t Bu and 1 equiv. of 18-crown-6.

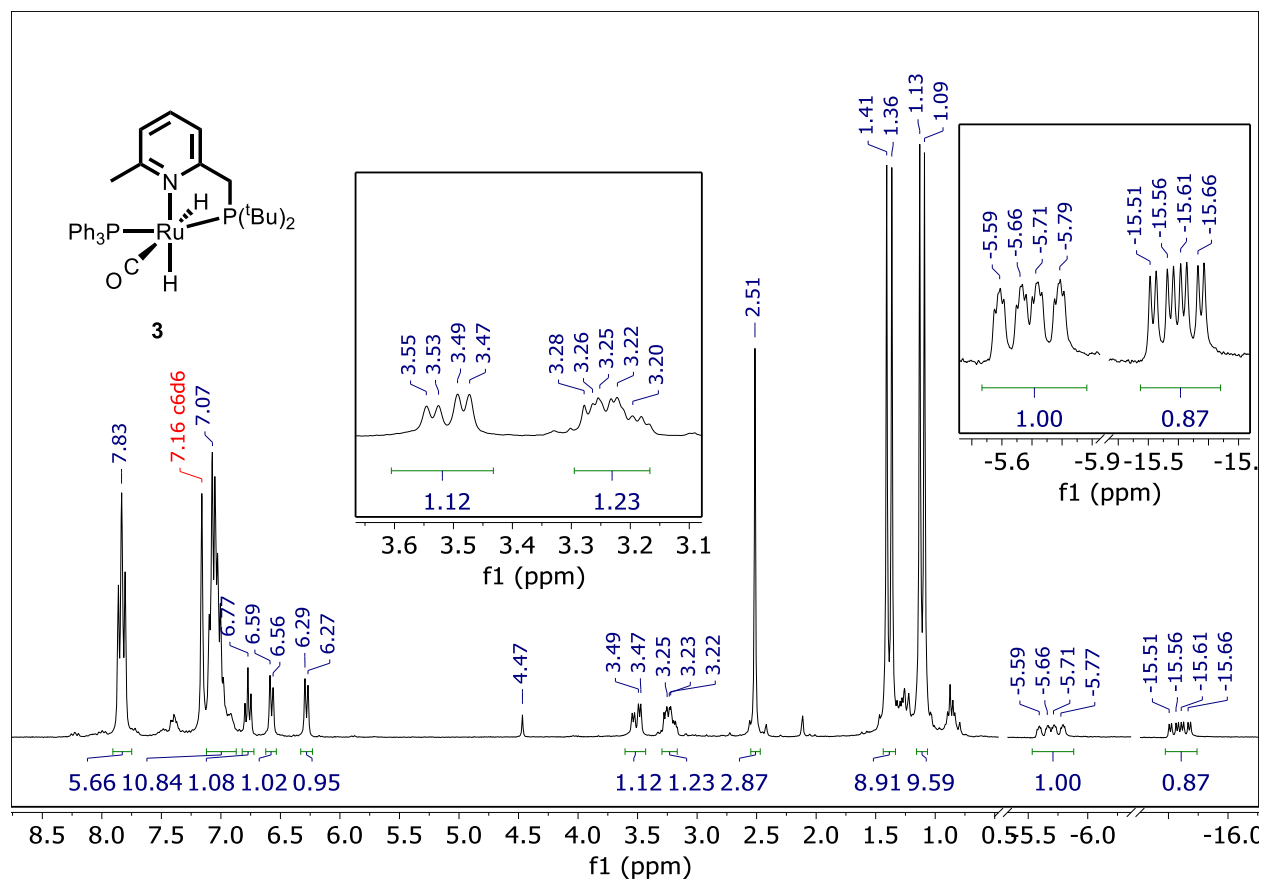


Fig. S11.
300 MHz ^1H NMR spectrum of **3** in C_6D_6 .

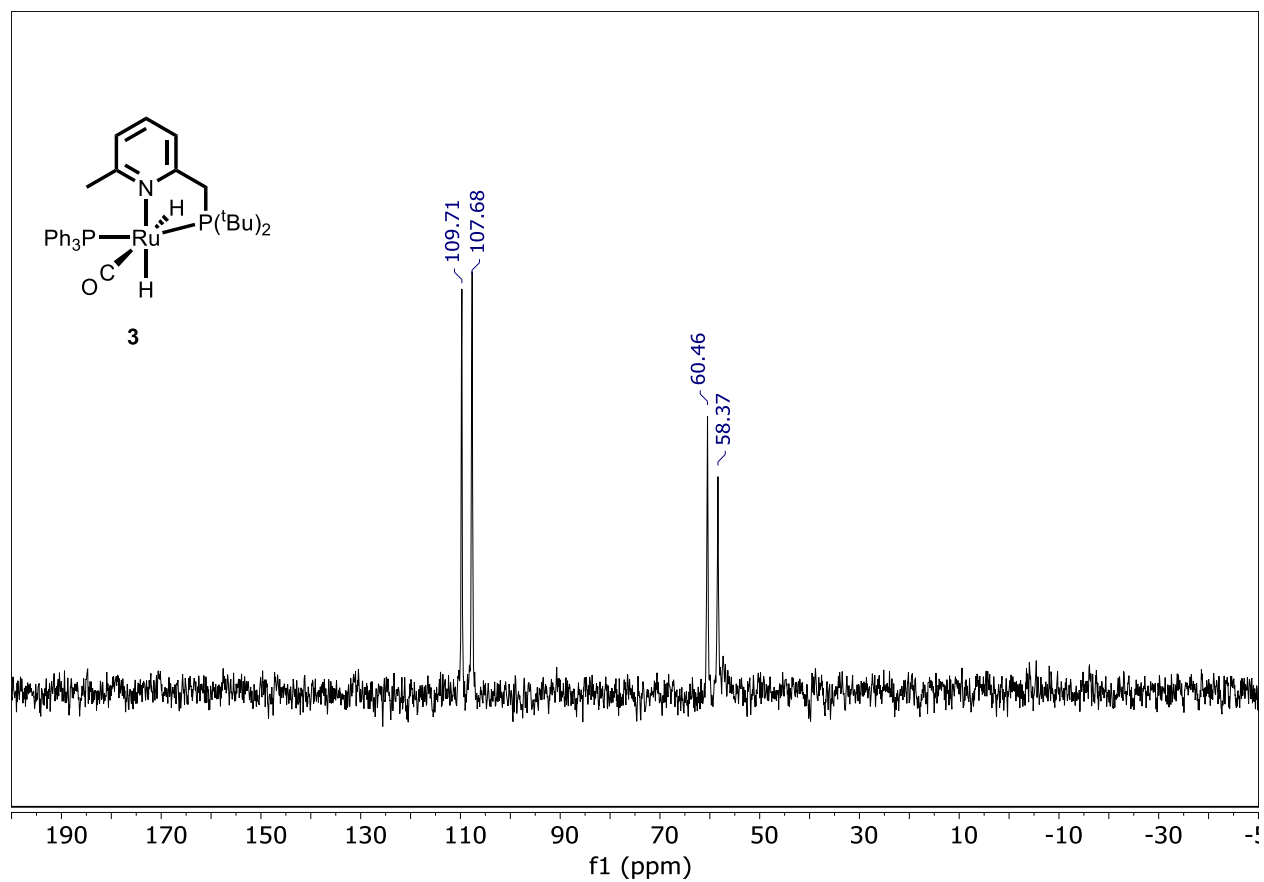


Fig. S12.
121 MHz $^{31}\text{P}\{^1\text{H}\}$ NMR spectrum of **3** in C_6D_6 .

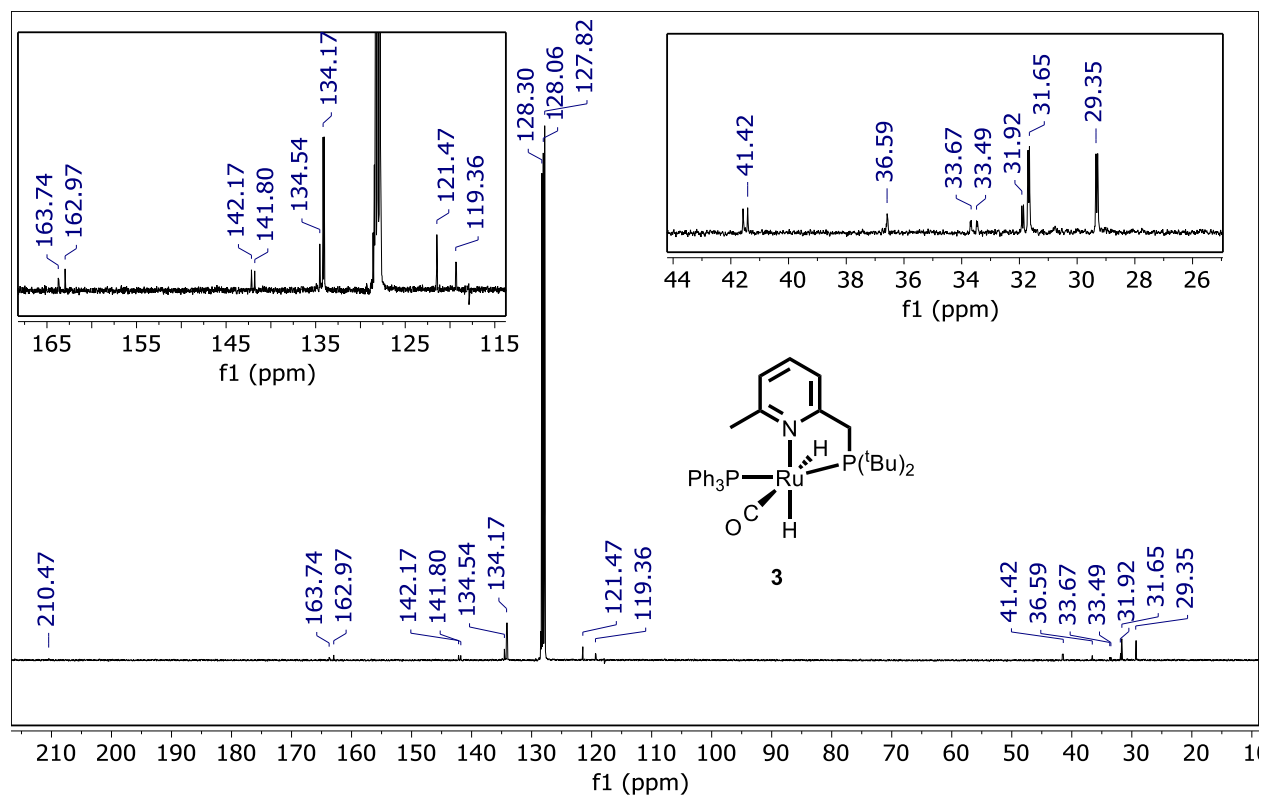


Fig. S13.
101 MHz $^{13}\text{C}\{^1\text{H}\}$ NMR spectrum of **3** in C_6D_6 .

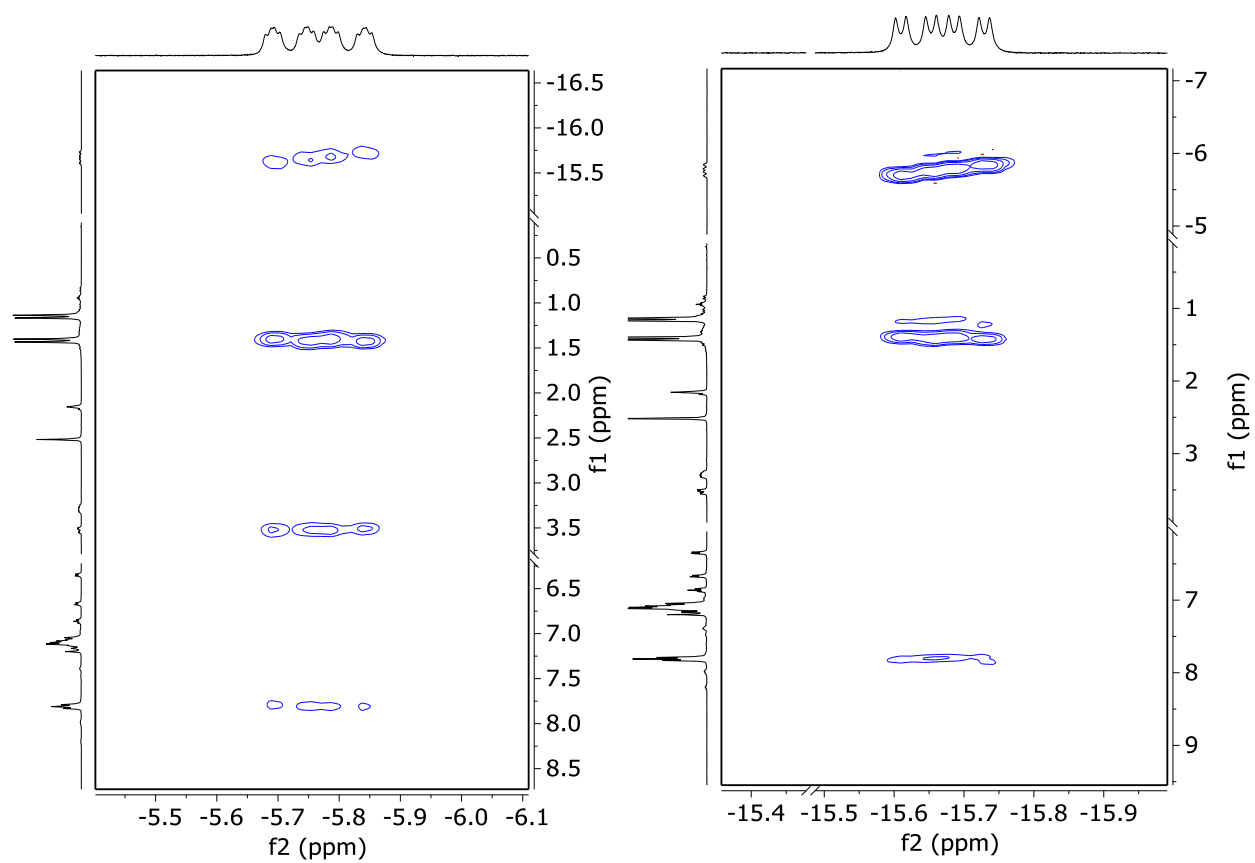


Fig. S14.

400 MHz ^1H - ^1H ROESY NMR spectrum of **3** in C_6D_6 zoomed in on the hydride region.

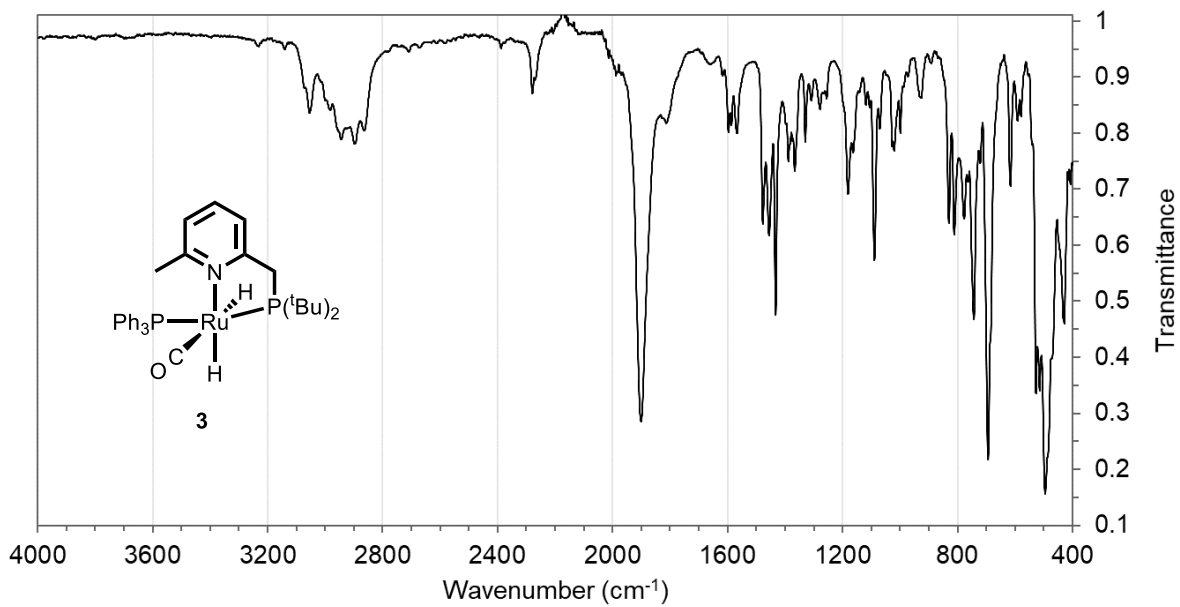


Fig. S15.
Drop-cast FTIR-ATR spectrum of **3**.

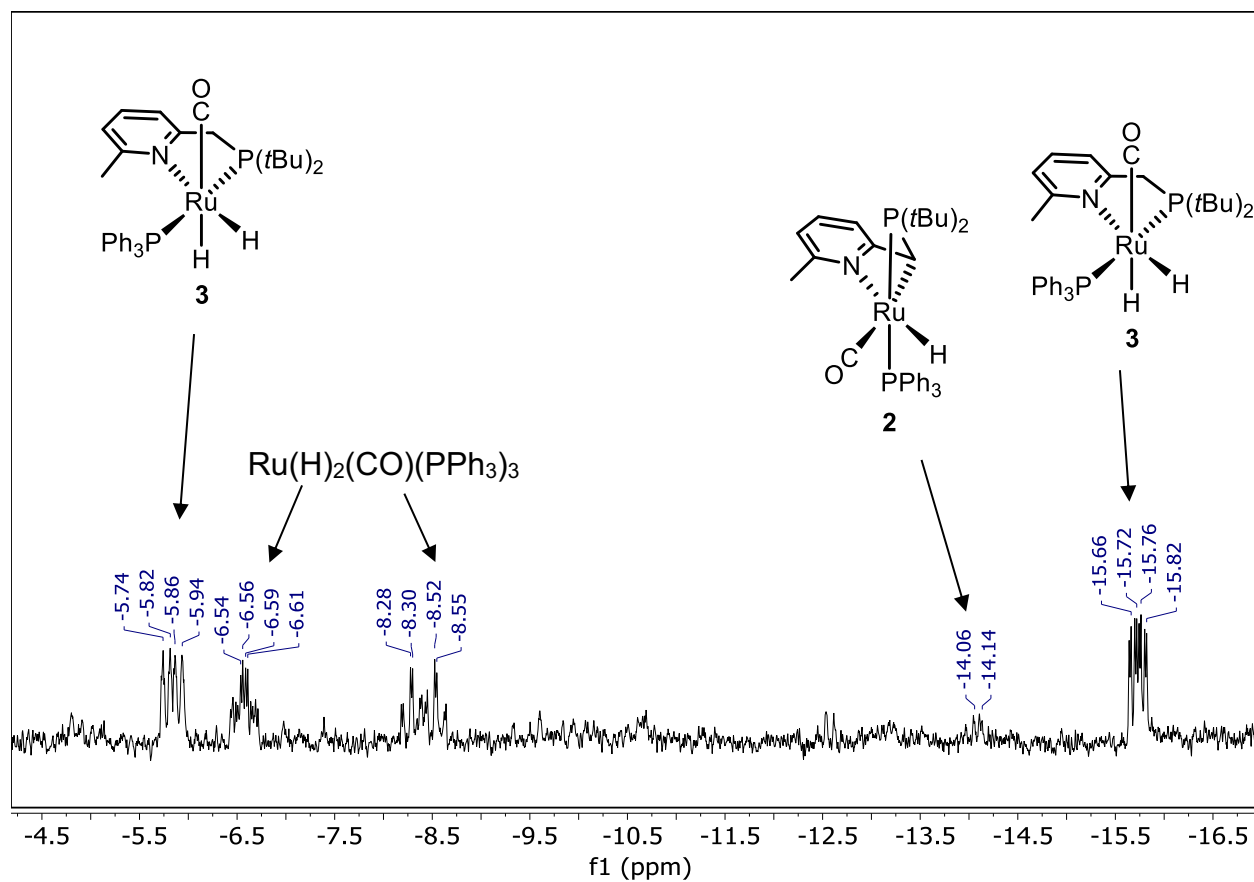


Fig. S16.

300 MHz ^1H NMR spectrum of the hydride region of complex **3** in C_7D_8 after heating to 110 $^\circ\text{C}$ for 4 h. The resonances at -5.6 ppm and -15.6 ppm are from **3**. Trace amounts of complex **2** can be observed at -14.1 ppm. $\text{Ru}(\text{H})_2(\text{CO})(\text{PPh}_3)_3$ can also be observed at -6.5 ppm and -8.5 ppm.

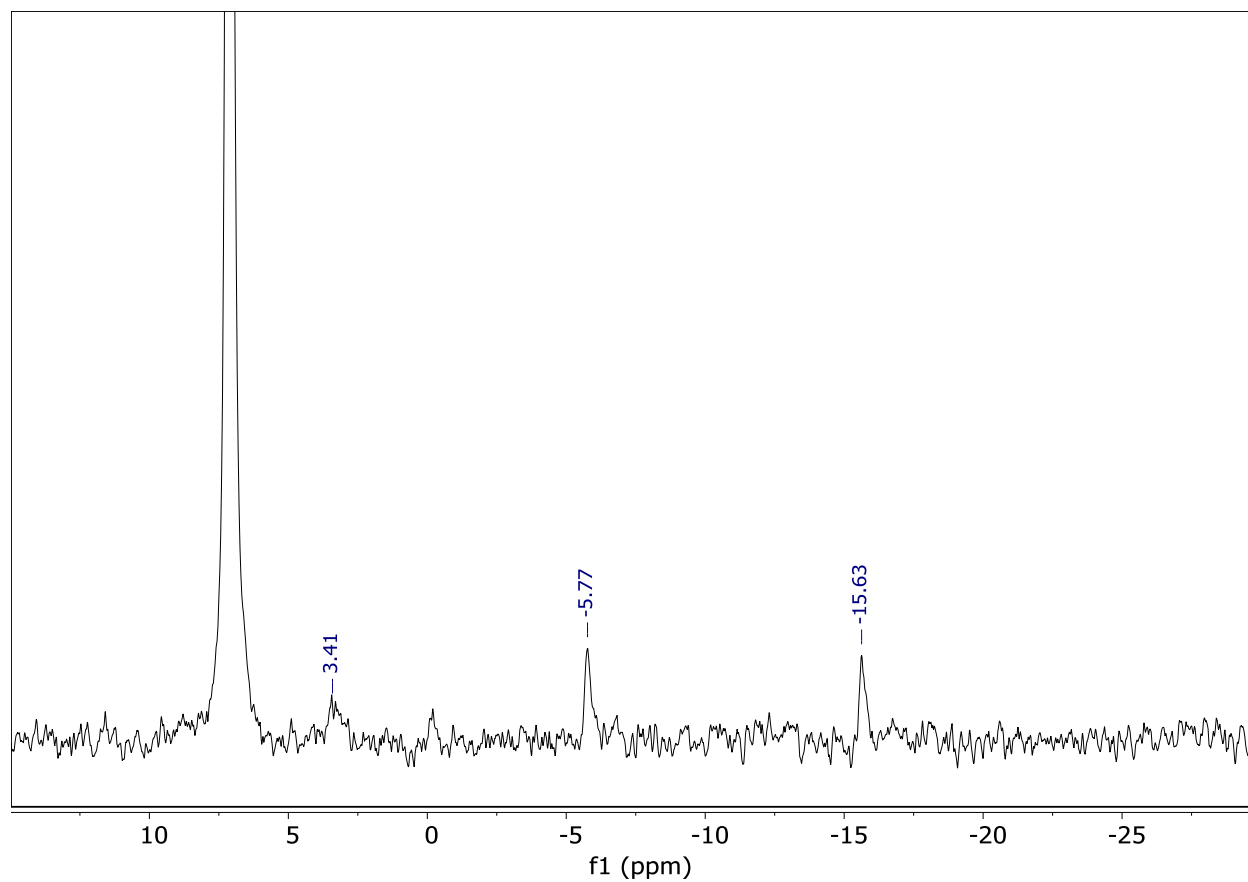


Fig. S17.
500 MHz ^2H NMR spectrum of the reaction of **2** with D_2 in C_6H_6 after ~ 1.5 h under ambient light.

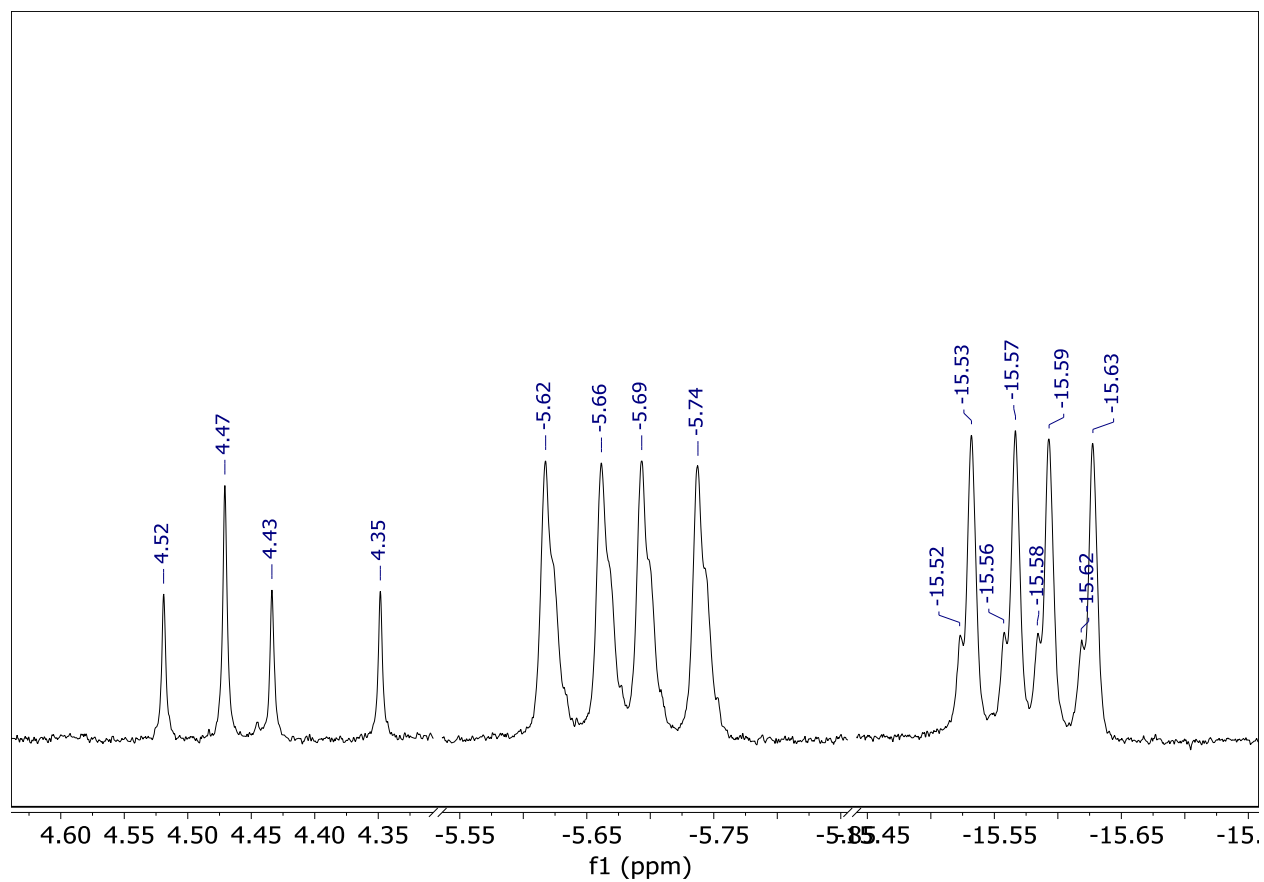


Fig. S18.

500 MHz ¹H NMR spectrum of the reaction of **2** with D₂ in C₆D₆ after ~1 h under ambient light. Zoomed in on the H₂ (4.47 ppm) and HD (t, 4.43 ppm) resonances observed (left) and the hydride resonances (right).

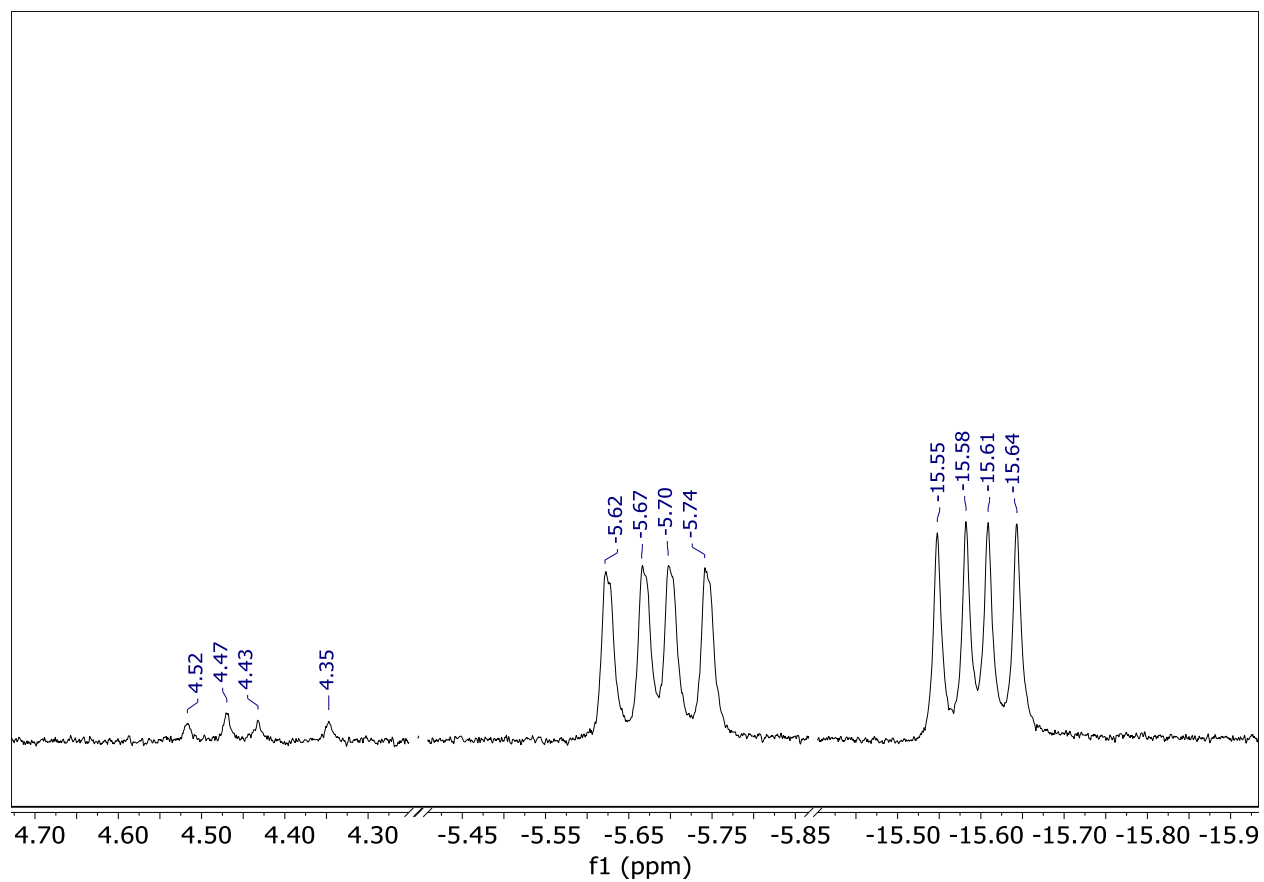


Fig. S19.

500 MHz ^1H NMR spectrum of a solution of **2** treated with D_2 in C_6D_6 after 15 min in the dark. Zoomed in on the H_2 (4.47 ppm) and HD (t, 4.43 ppm) resonances observed (left) and the hydride resonances (right).

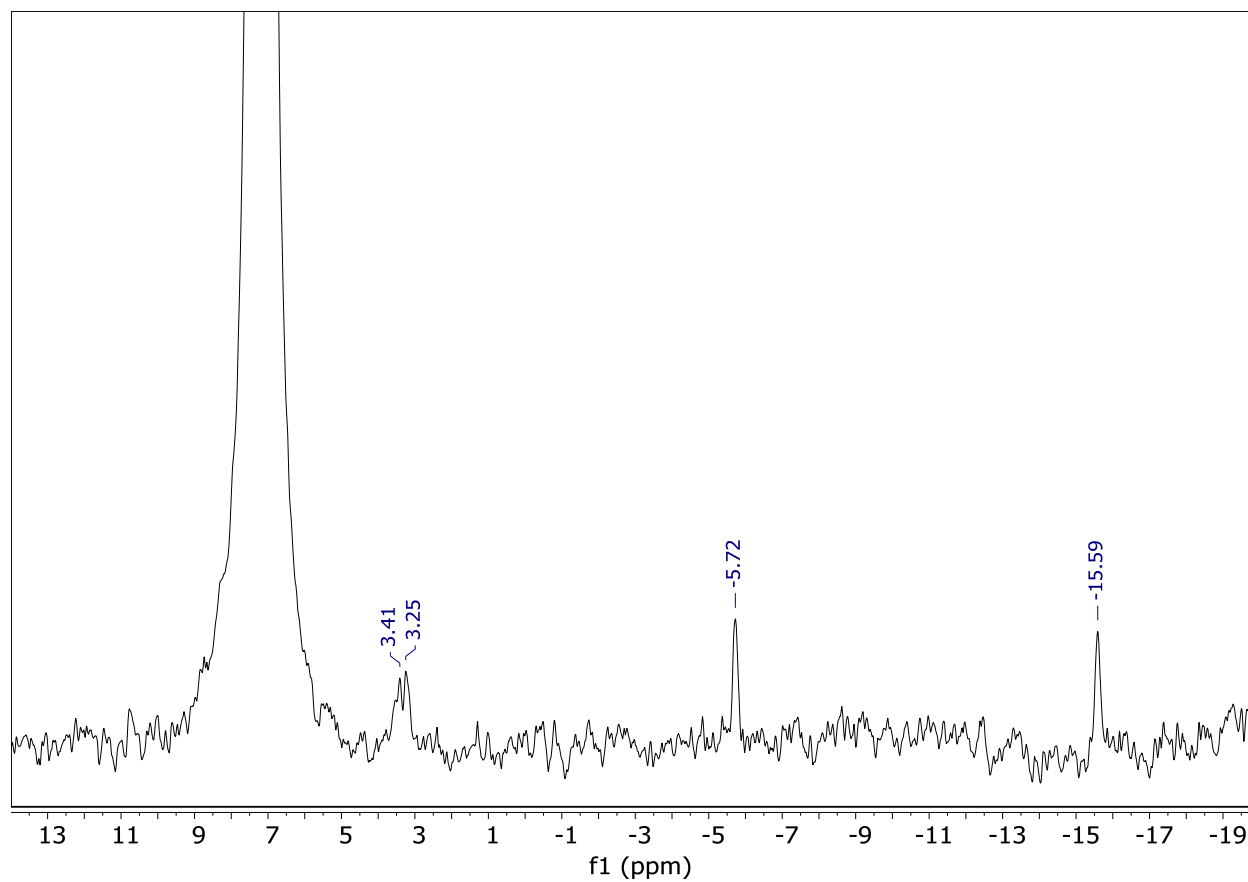


Fig. S20.

500 MHz ^2H NMR spectrum of a solution of **2** treated with D_2 in C_6H_6 spiked with C_6D_6 after 30 min in the dark.

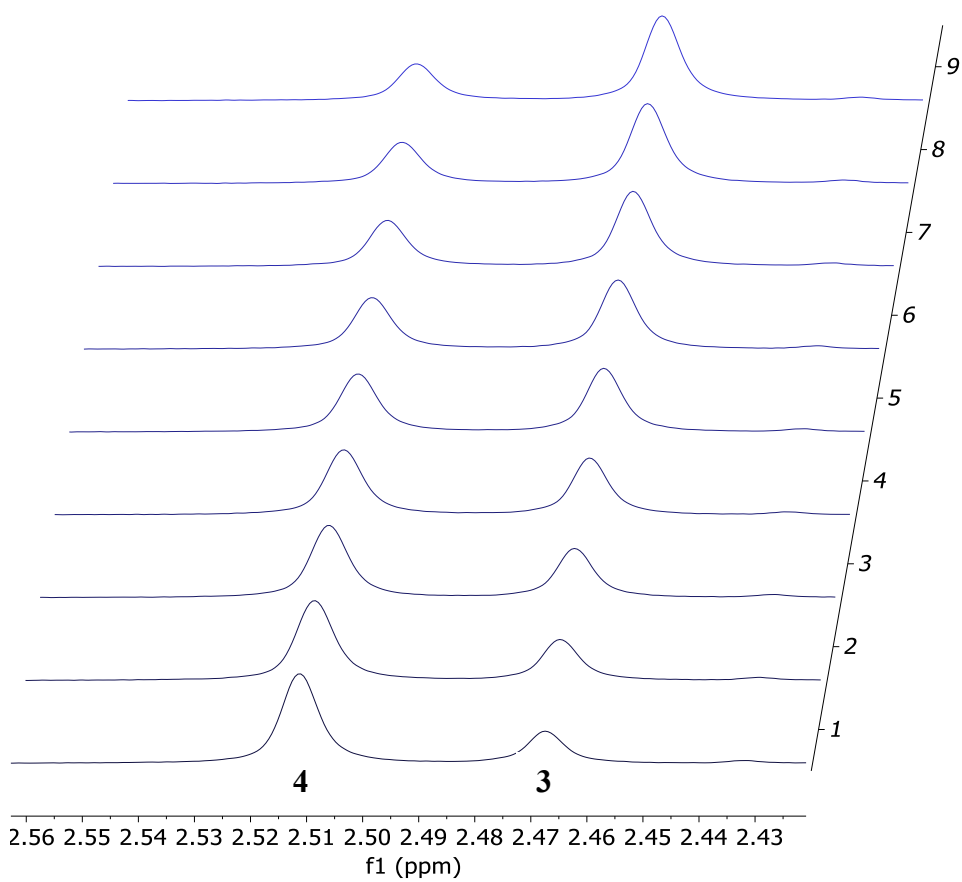


Fig. S21.

300 MHz ¹H NMR spectra of the δ_{CH_3} of **3** and **4** over the course of 2.5 h (bottom to top) after 1 h of irradiation of a solution of **3** in C₆D₆ with no filter at 23 °C under N₂(g).

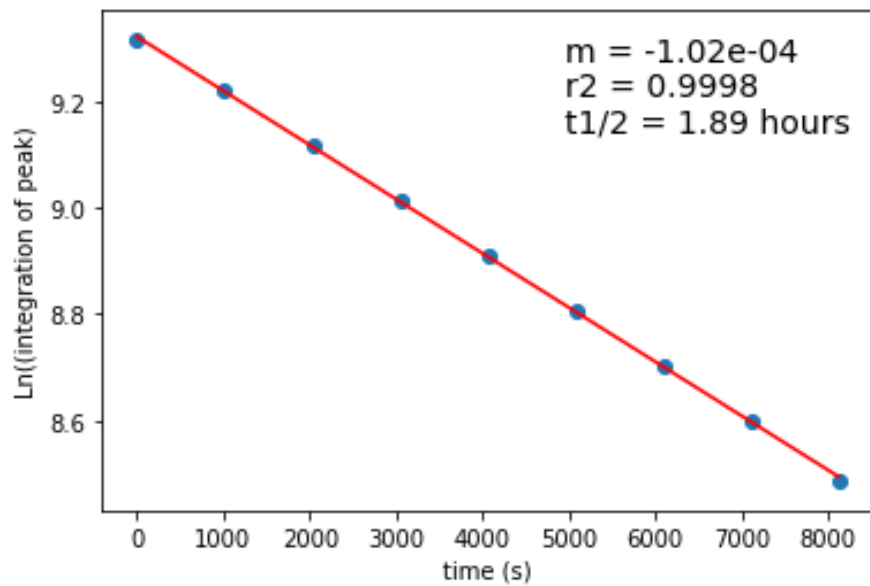


Fig. S22.

Plot of the ln of the peak area of the δ_{CH_3} of **4** versus time (s) under $\text{N}_2(\text{g})$.

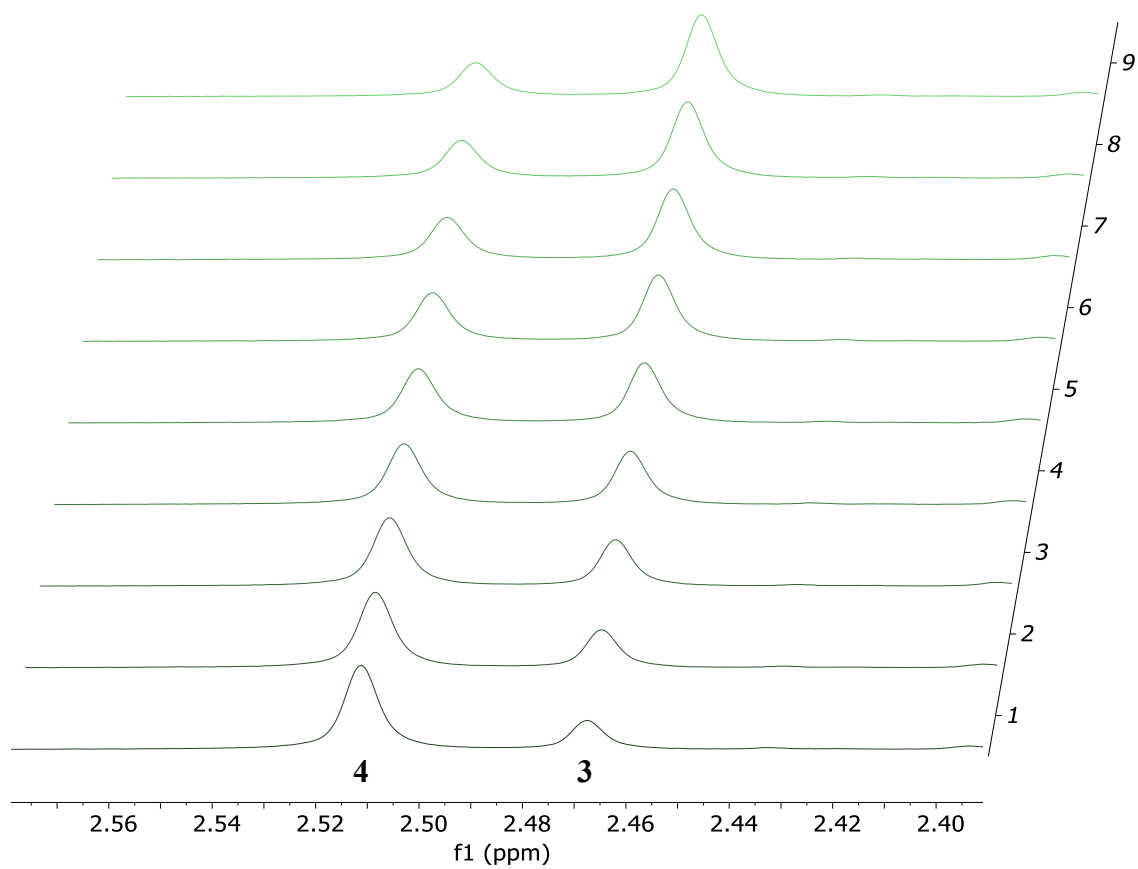


Fig. S23.

300 MHz ¹H NMR spectra of the δ_{CH_3} of **3** and **4** over the course of 2.5 h (bottom to top) after 1 h of irradiation of a solution of **3** in C₆D₆ with no filter at 23 °C under static-vacuum.

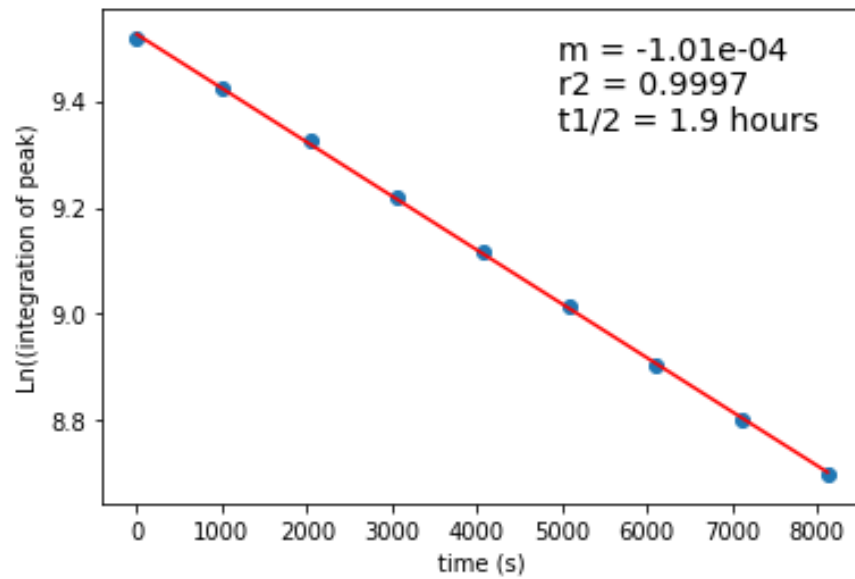


Fig. S24.

Plot of the ln of the peak area of the δ_{CH_3} of **4** versus time (s) under static-vacuum.

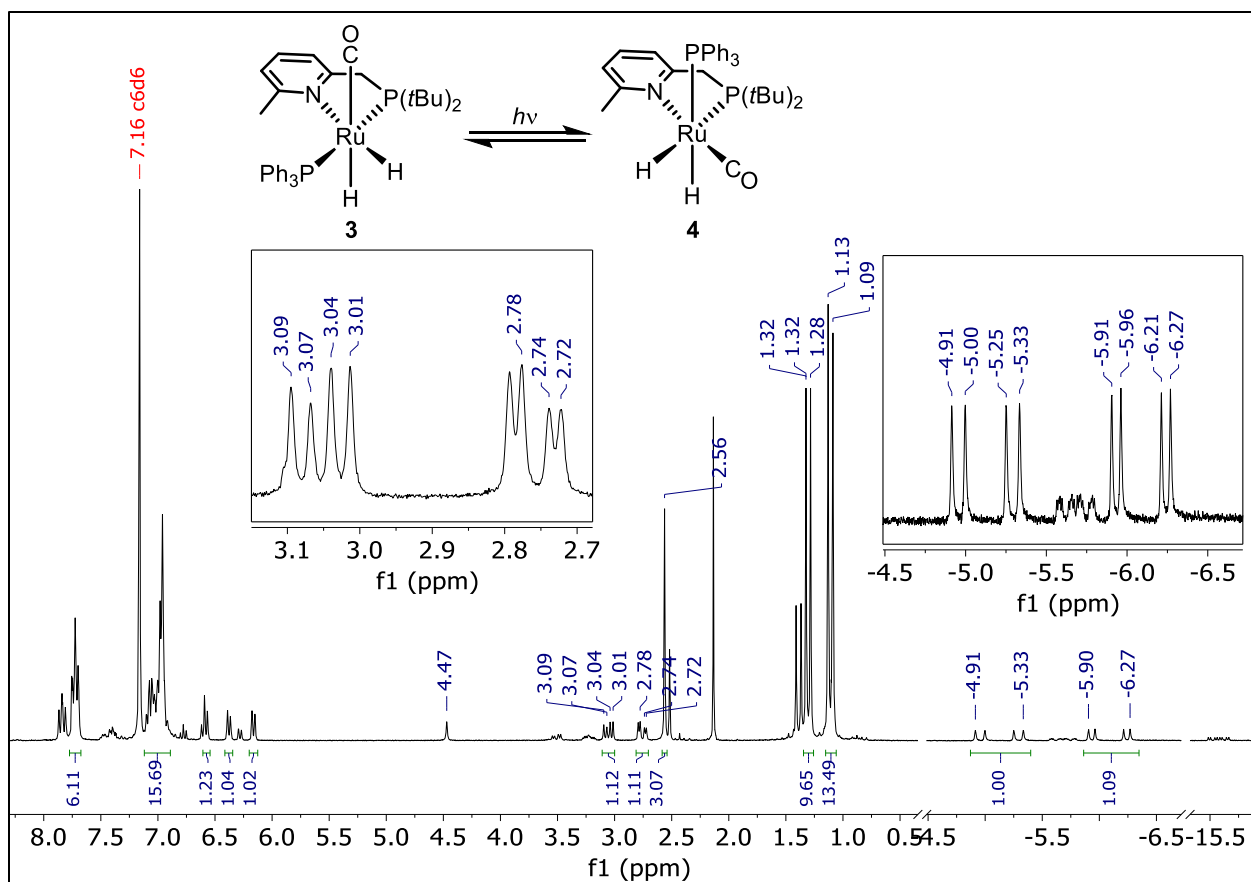


Fig. S25.

500 MHz ^1H NMR spectrum of a solution of **3** in C_6D_6 under H_2 after 1 h of irradiation with no filter at 23 °C. The integrated resonances are from complex **4**.

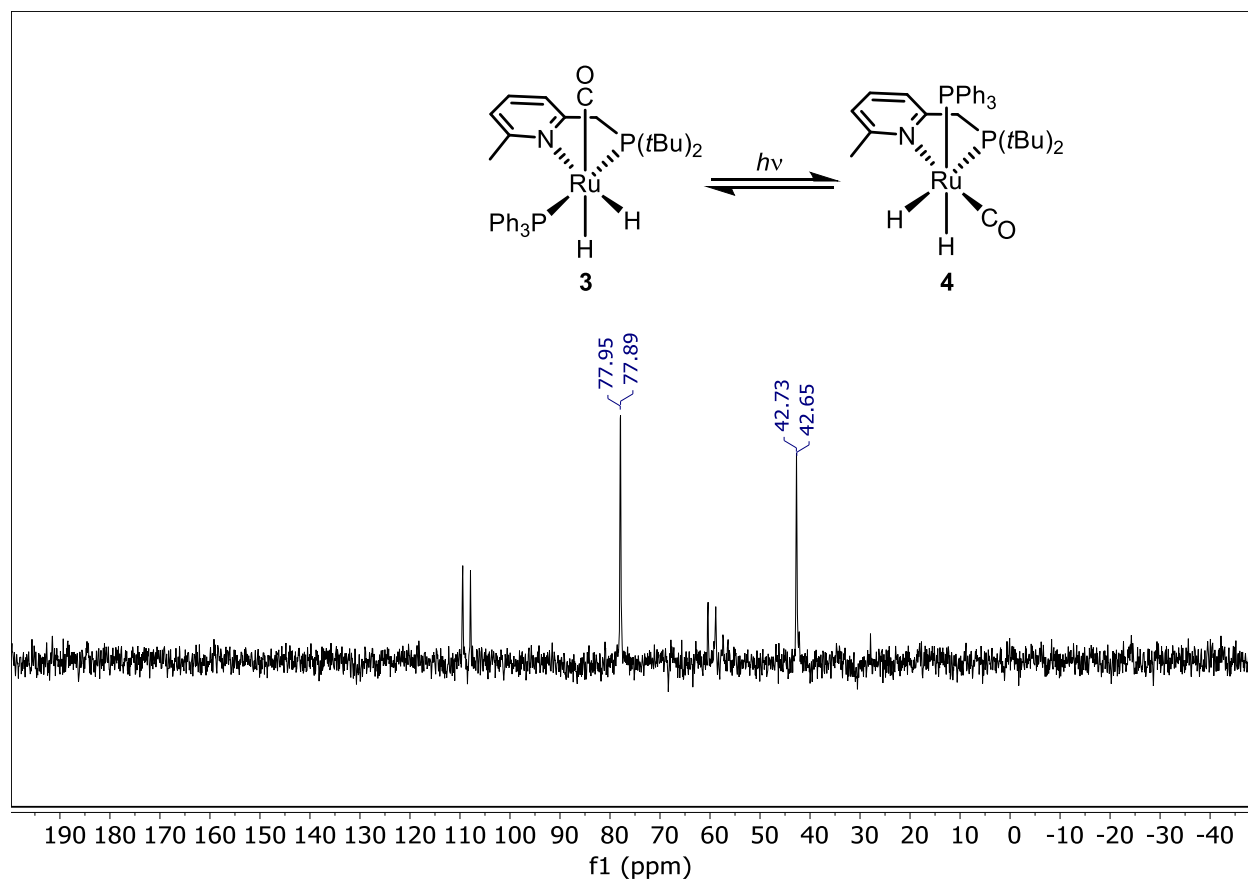


Fig. S26.

121 MHz ^{31}P $\{^1\text{H}\}$ NMR of a solution of **3** in C_6D_6 under H_2 after 1 h of irradiation with no filter at 23 °C. The resonances at ~ 109 ppm and ~ 60 ppm are from complex **3**.

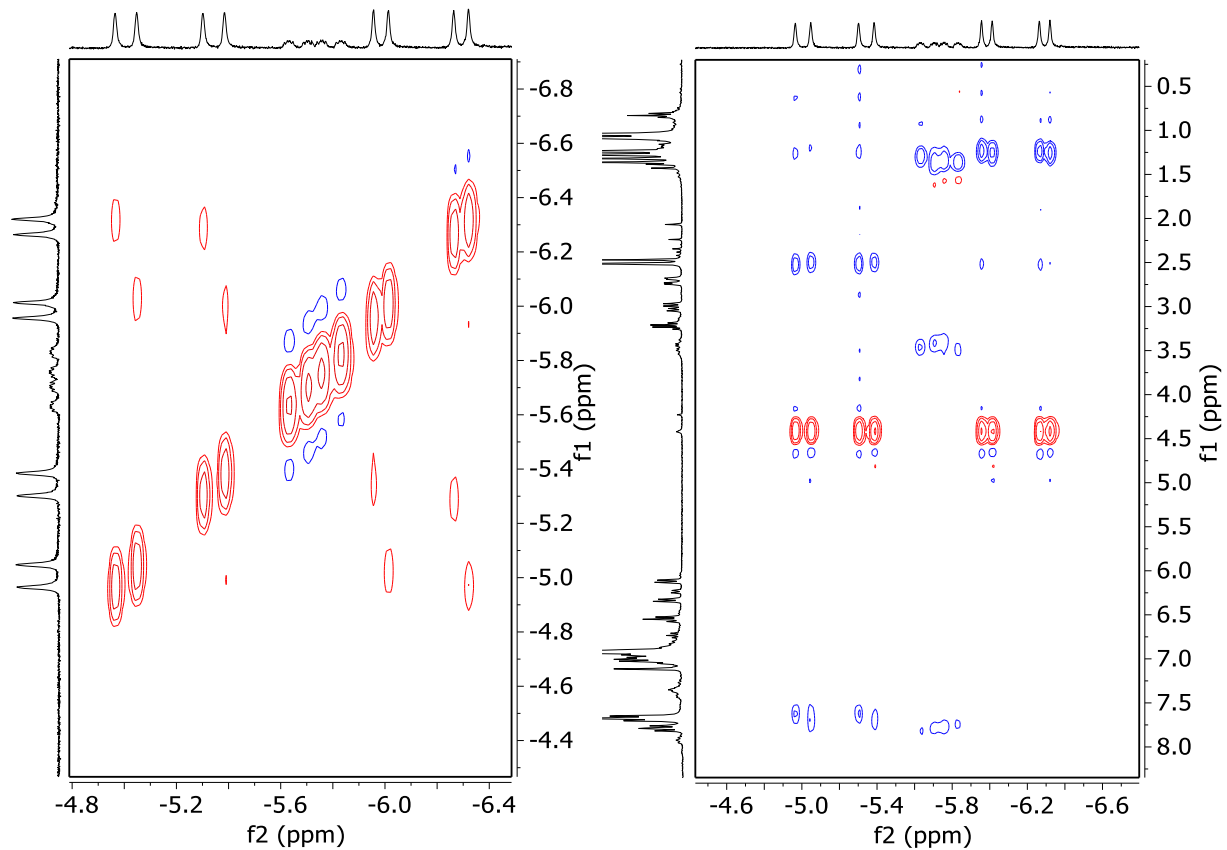


Fig. S27.

300 MHz ¹H-¹H ROESY spectrum of a solution of **3** in C₆D₆ under H₂(g) after 1 h of irradiation with no filter at 23 °C. (left) Zoomed in on the hydride-hydride exchange correlation, (right) other correlations seen with the hydride resonances.

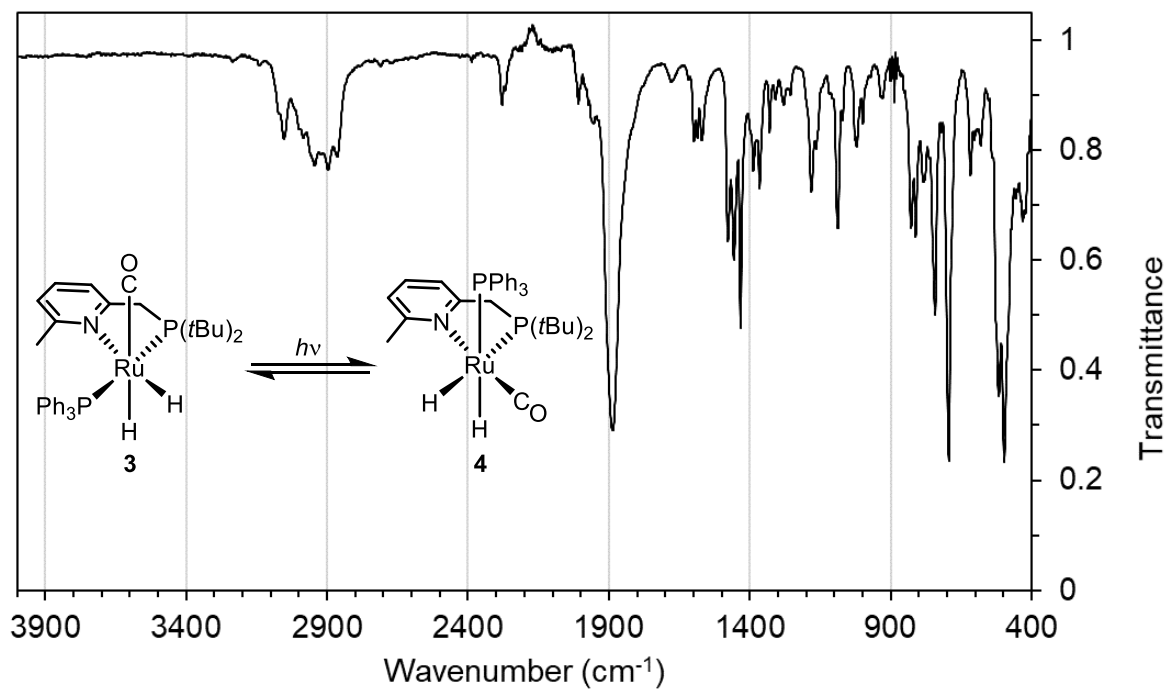


Fig. S28.

FTIR-ATR spectrum of a solution of **3** in C_6D_6 under $\text{H}_2(\text{g})$ after 1 h of irradiation with no filter at 23 °C.

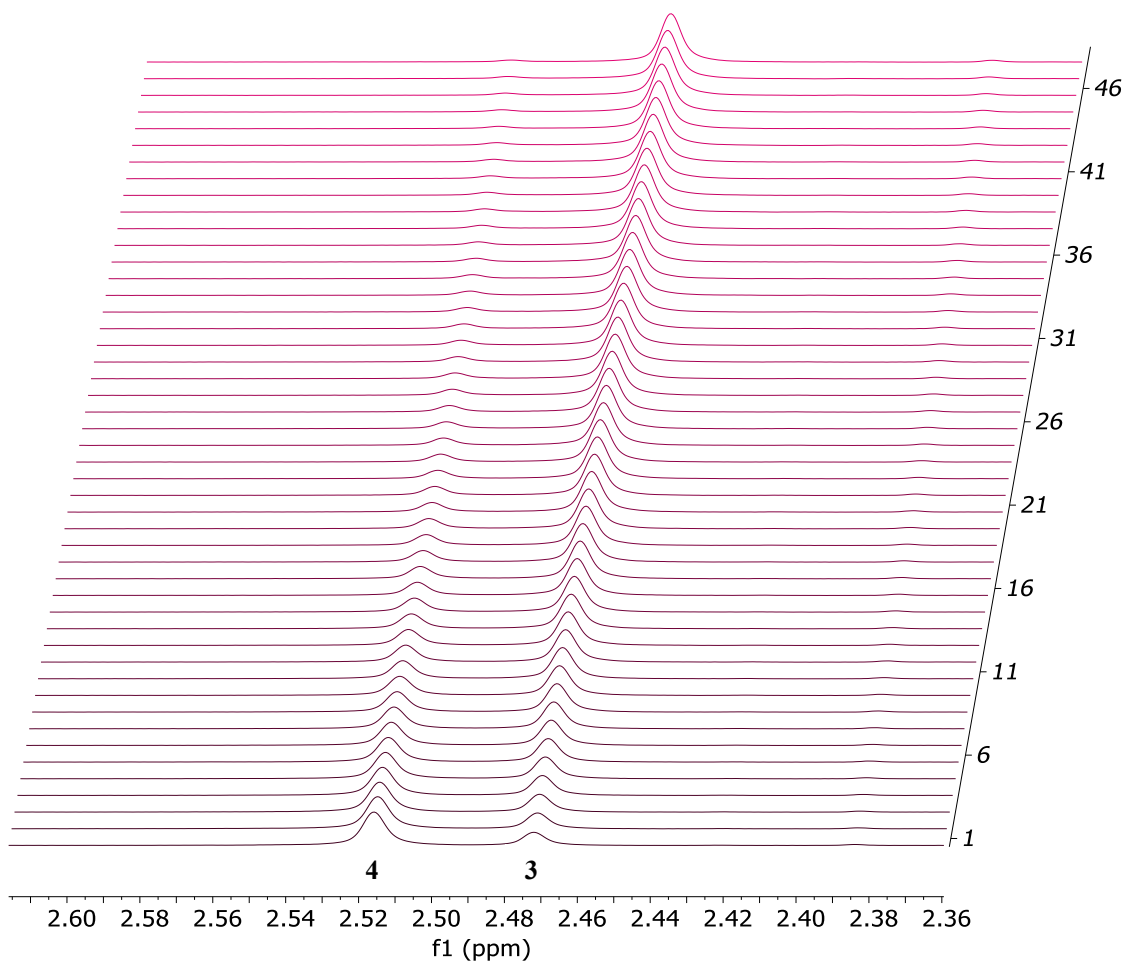


Fig. S29.

300 MHz ¹H NMR spectra of the δ_{CH₃} of **3** and **4** over the course of 2.5 h (bottom to top) after 1 h of irradiation of a solution of **3** in C₆D₆ with no filter at 23 °C under H₂(g).

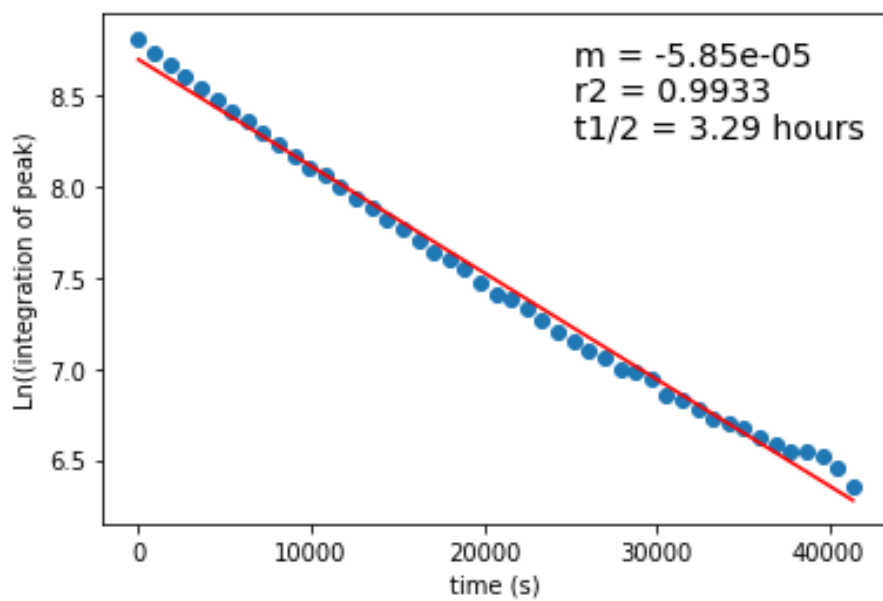


Fig. S30.

Plot of the ln of the peak area of the δ_{CH_3} of **4** versus time (s) under $\text{H}_2(\text{g})$.

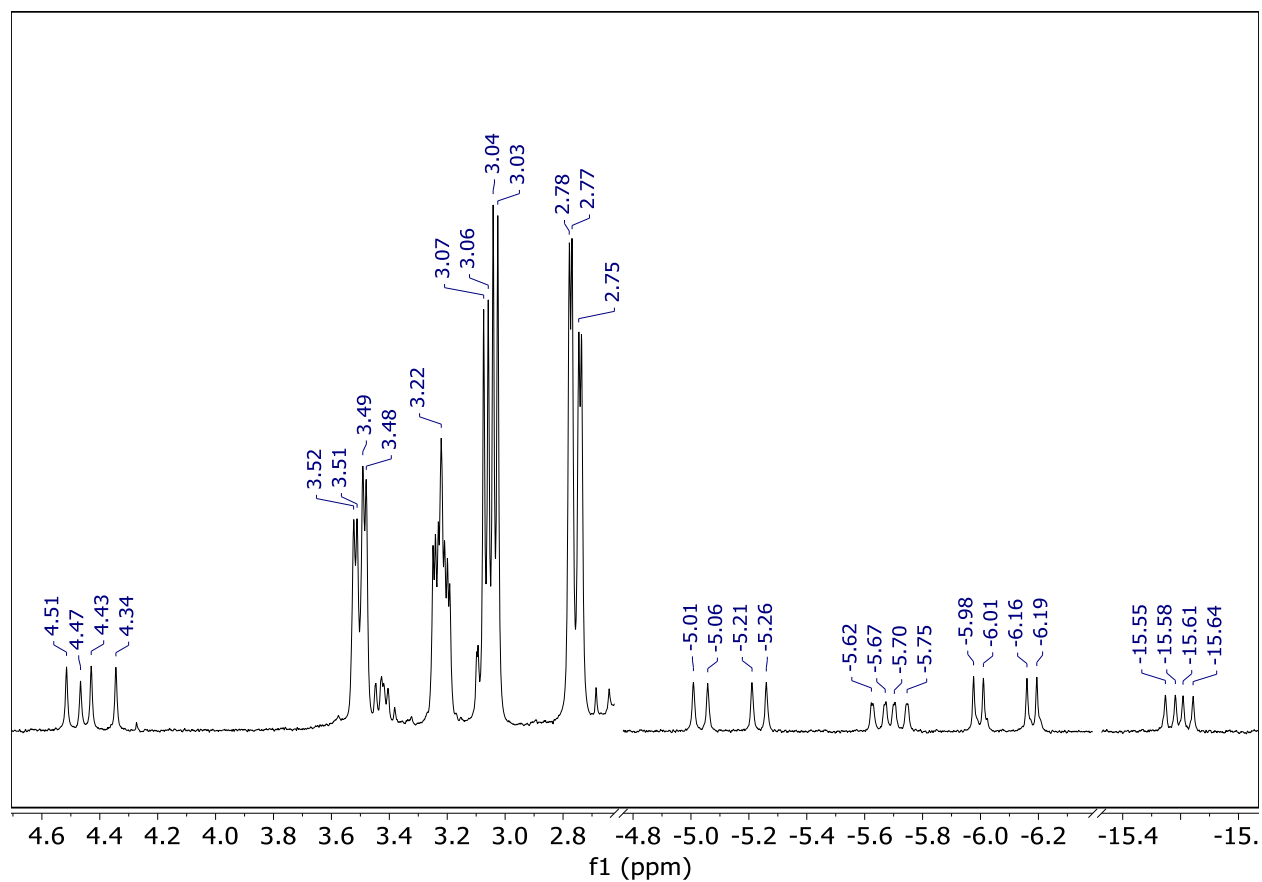


Fig. S31.

500 MHz ^1H NMR spectrum of a solution of **3** in C_6D_6 under D_2 after irradiation with a 345 nm cutoff filter for 1 h at 23 $^\circ\text{C}$. (left) The H_2 (4.47 ppm) and HD (t, 4.43 ppm) resonances observed. (middle) Zoomed in on the δ_{CH_2} of **3** and **4**. (right) Zoomed in on the hydride region.

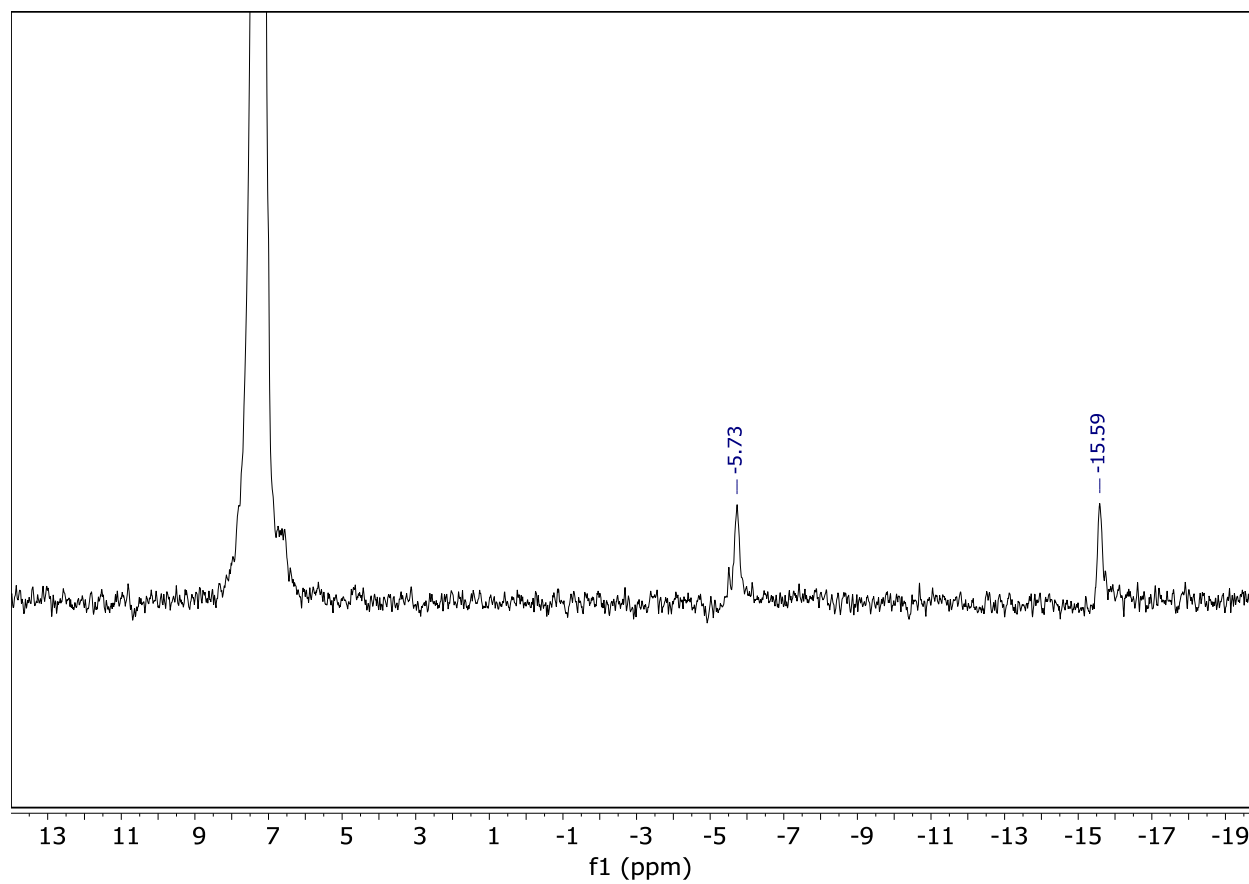


Fig. S32.

500 MHz ^2H NMR spectrum of a solution of **3** in C_6H_6 spiked with C_6D_6 under D_2 after irradiation with a 345 nm cutoff filter for 1 h at 23 °C.

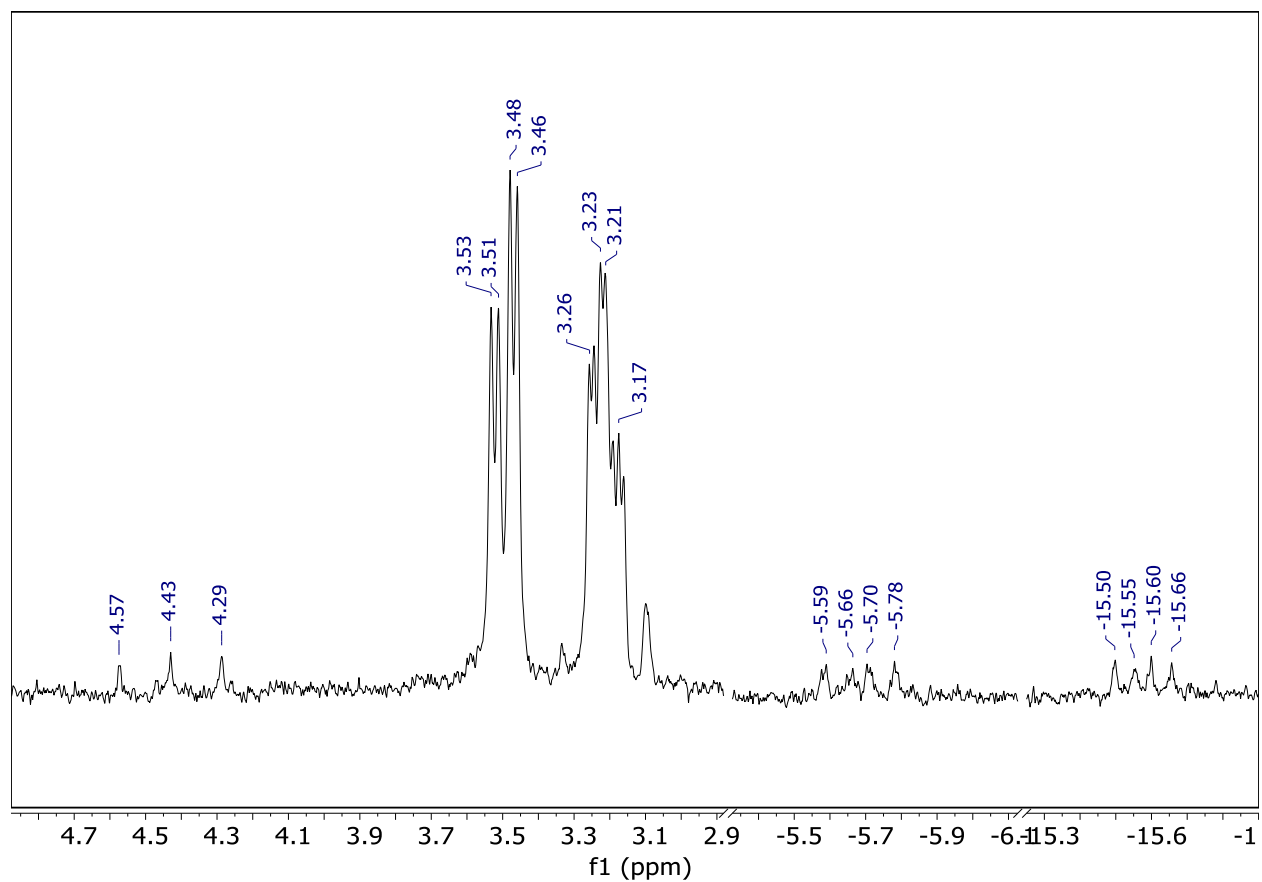


Fig. S33.

300 MHz ^1H NMR spectrum of a solution of **3** in C_6D_6 under D_2 after 4 days in the dark. (left) The trace H_2 (4.47 ppm) and HD (t, 4.43 ppm) resonances observed. (middle) Zoomed in on the δ_{CH_2} of **3**. (right) Zoomed in on the hydride region.

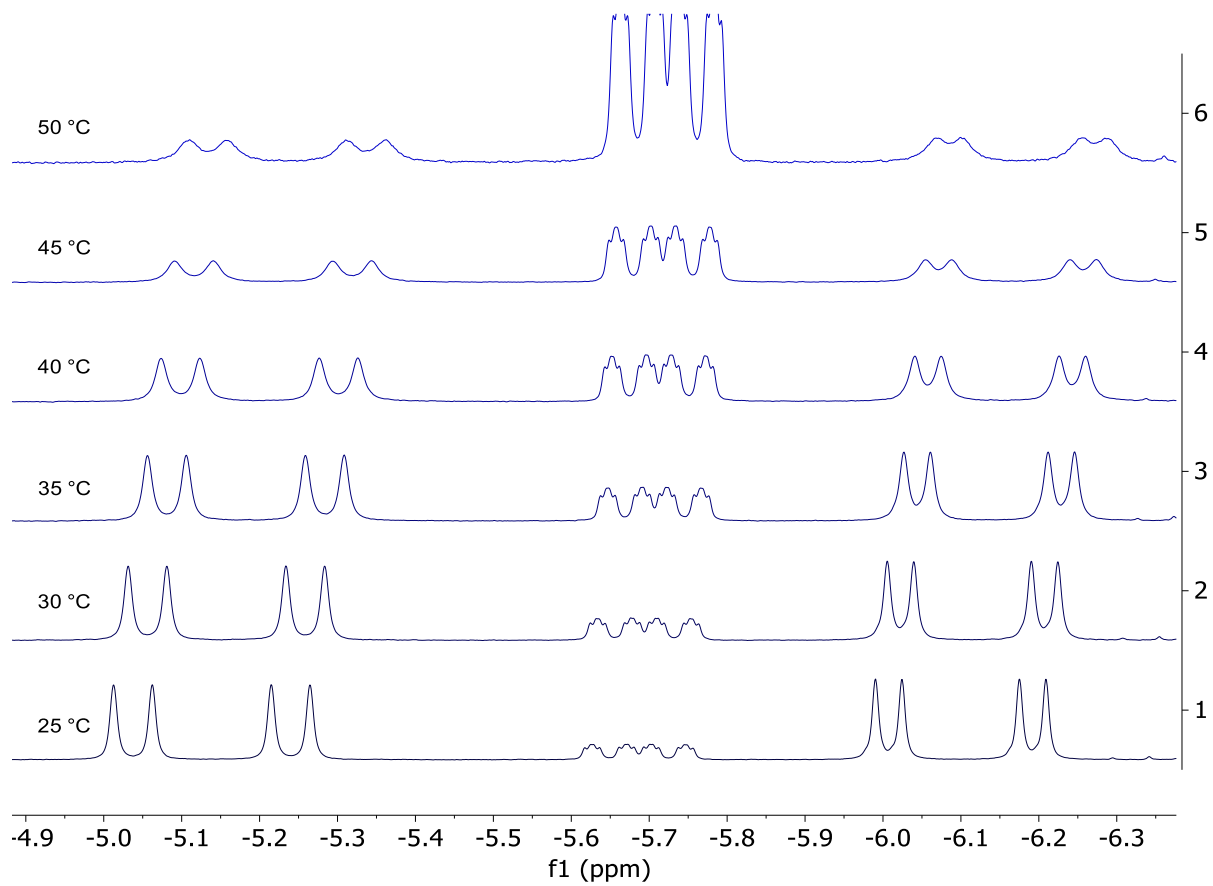


Fig. S34.

A VT 500 MHz ¹H NMR spectra of a solution of **4** in C₆D₆ under H₂(g) at 25–50 °C.

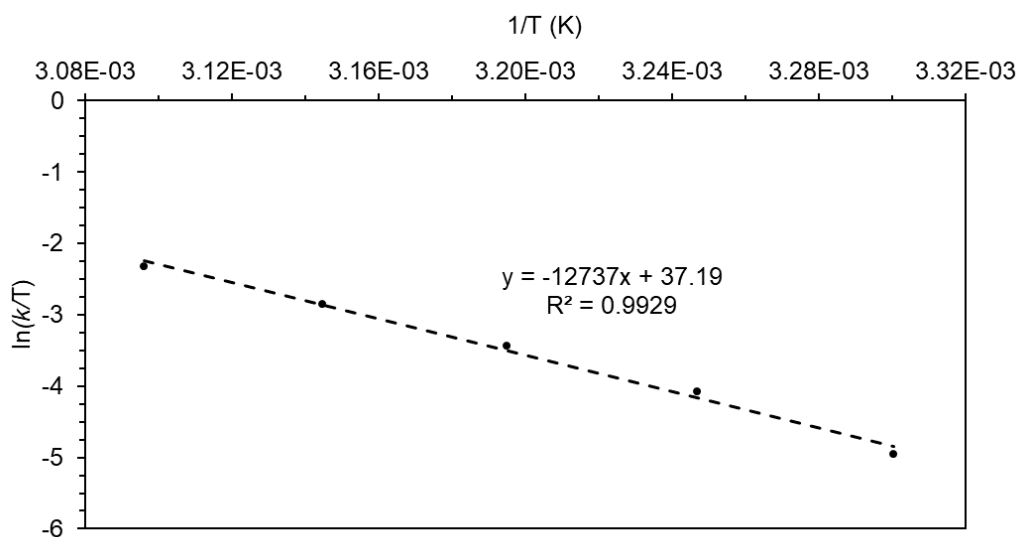


Fig. S35.

Eyring plot of the rates of exchange obtained from line width analysis of the hydride resonances of **4**. The barrier ($\Delta G^\ddagger = 17.4 \text{ kcal}\cdot\text{mol}^{-1}$) was calculated from the slope ($\Delta H^\ddagger = 25.3 \text{ kcal}\cdot\text{mol}^{-1}$) and x-intercept ($\Delta S^\ddagger = 26.7 \text{ cal}\cdot\text{K}^{-1}\cdot\text{mol}^{-1}$). VT studies were carried out between $25 \text{ }^\circ\text{C} - 50 \text{ }^\circ\text{C}$.

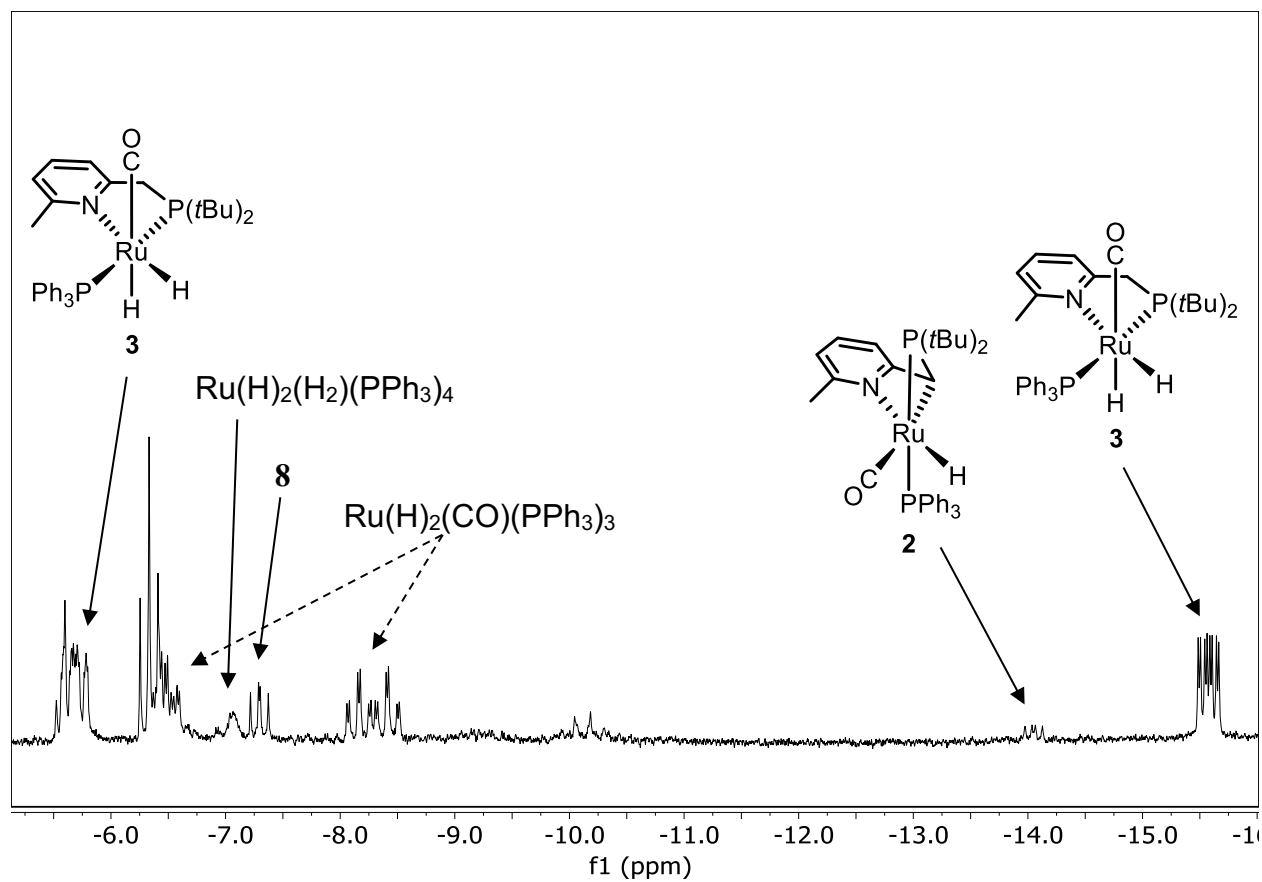


Fig. S36.

300 MHz ^1H NMR of a solution of **3** and 10 equiv. PPh_3 in C_6D_6 after 2 h of irradiation at 23 °C with no filter zoomed in on the hydride region. Unlabeled peaks are unknown products.

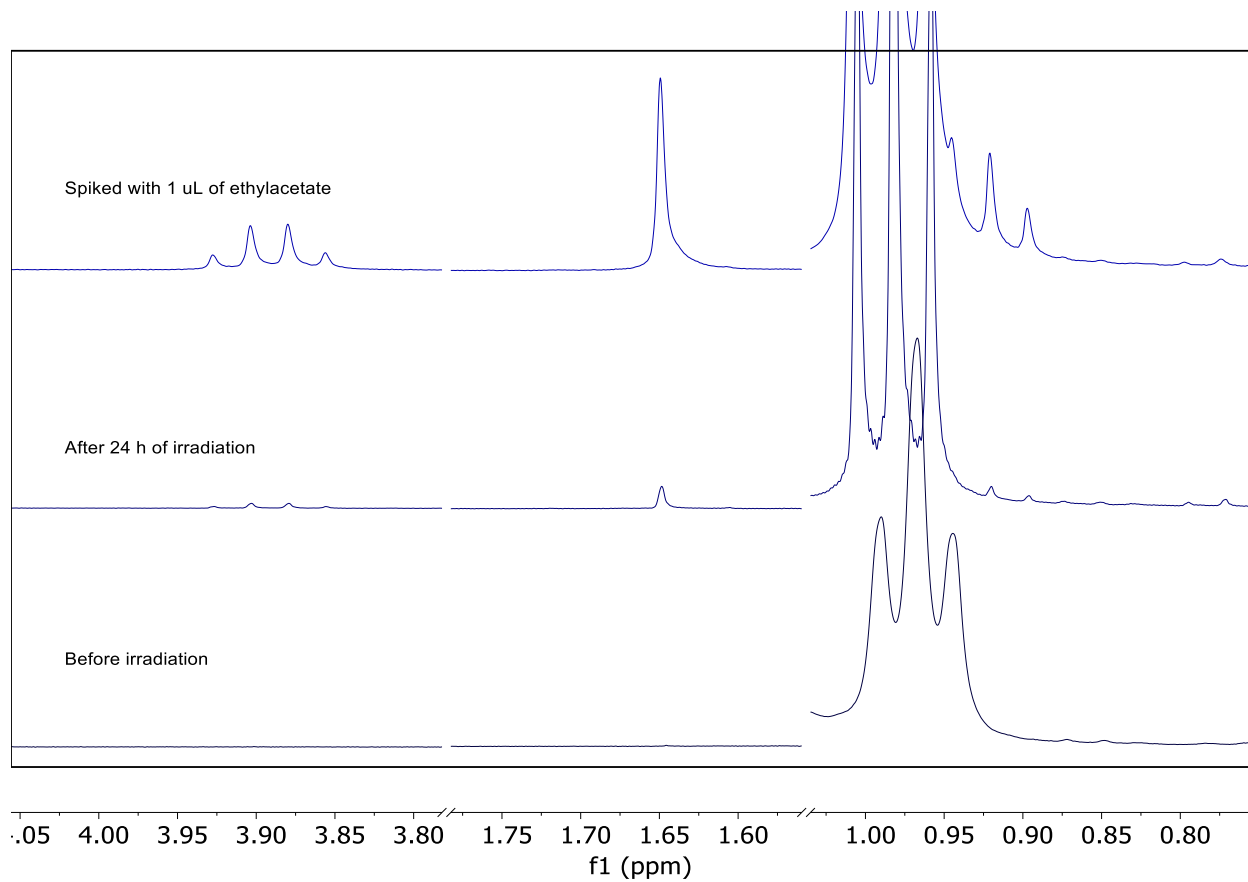


Fig. S37.

300 MHz ^1H NMR spectra of a solution of 0.00310 mmol of **3** in C_6D_6 with 0.155 mmol of ethanol before irradiation (bottom), after 24 h of irradiation with a 345 nm cutoff filter (middle), and after spiking the sample with 1 μL of ethyl acetate.

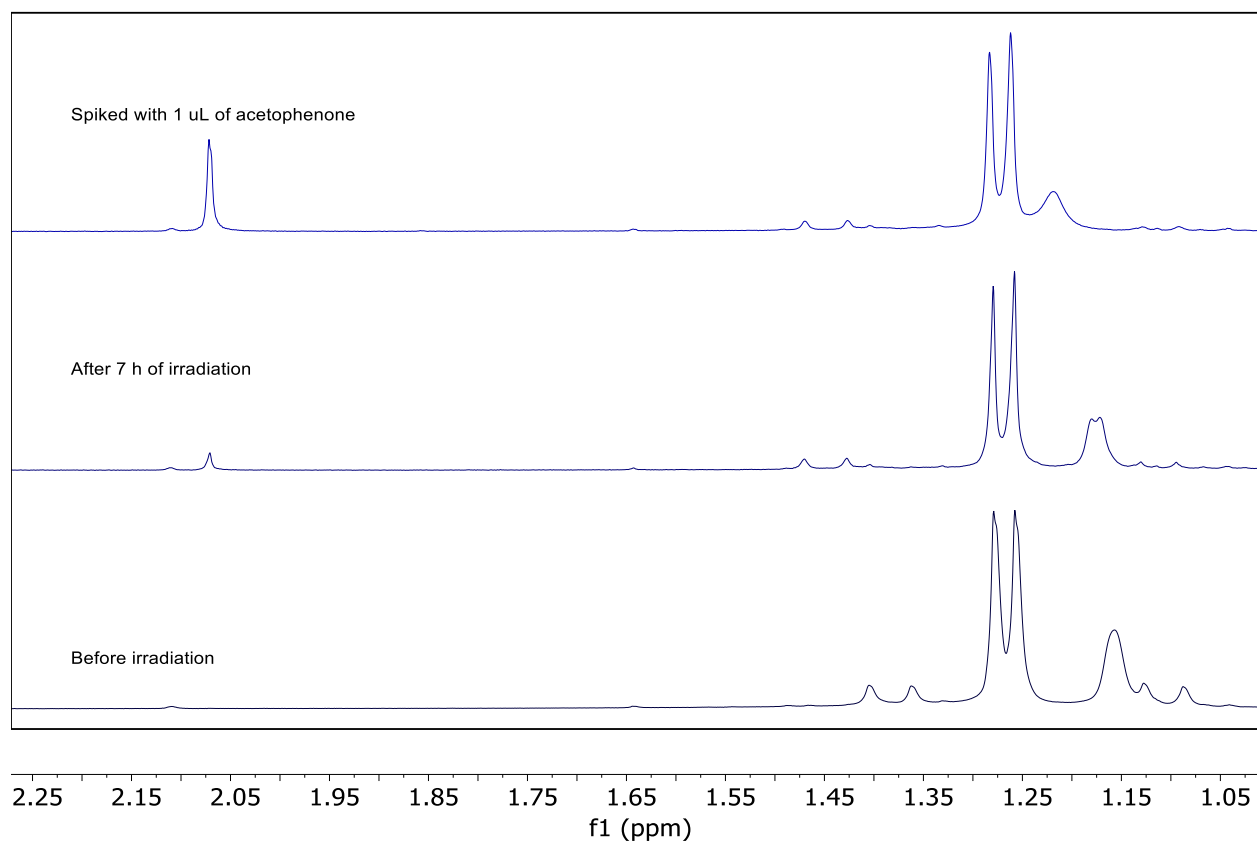


Fig. S38.

300 MHz ^1H NMR spectra of a solution of 0.00310 mmol of **3** in C_6D_6 with 0.0931 mmol of 1-phenylethanol before irradiation (bottom), after 7 h of irradiation with a 345 nm cutoff filter (middle), and after spiking the sample with 1 μL of acetophenone.

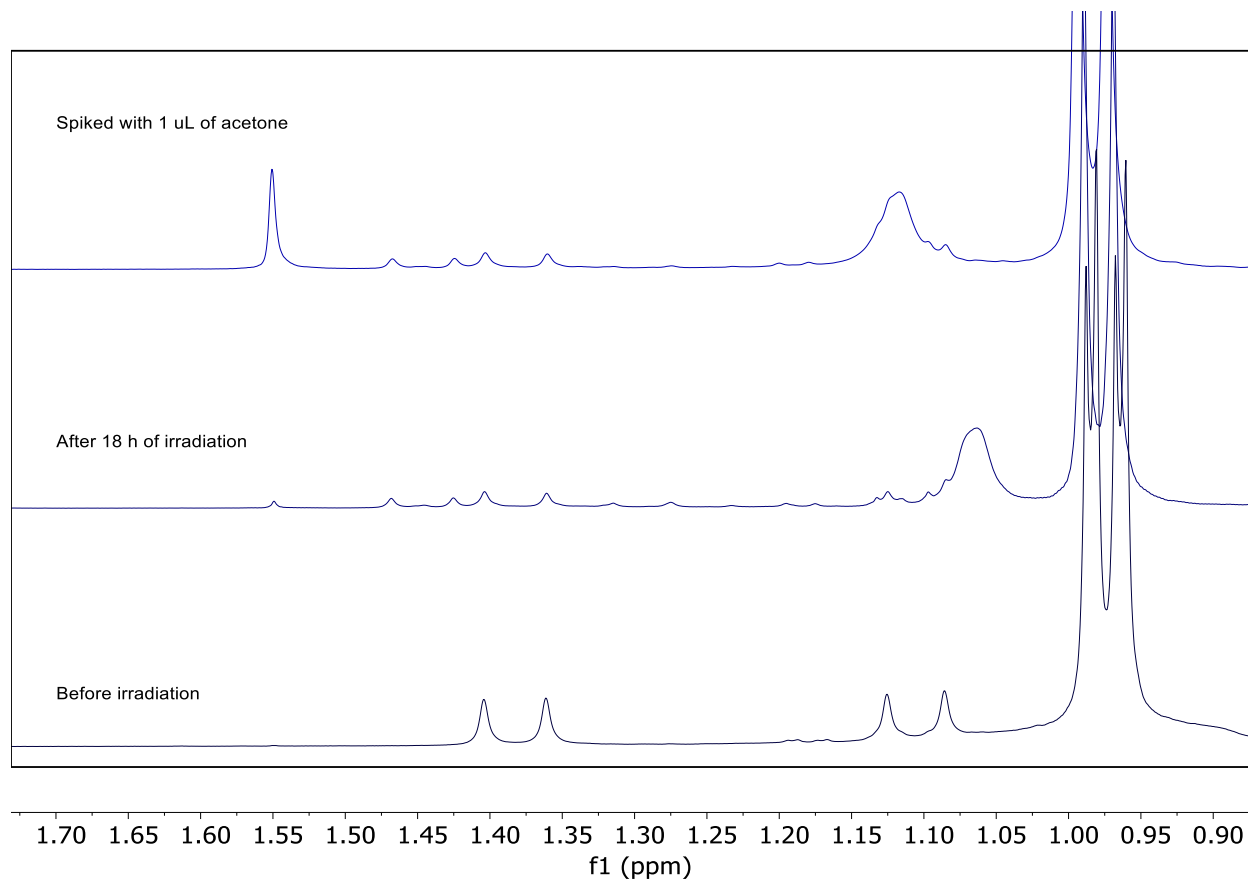


Fig. S39.

300 MHz ^1H NMR spectra of a solution of 0.00480 mmol of **3** in C_6D_6 with 0.0970 mmol of 2-propanol before irradiation (bottom), after 18 h of irradiation with a 345 nm cutoff filter (middle), and after spiking the sample with 1 μL of acetone.

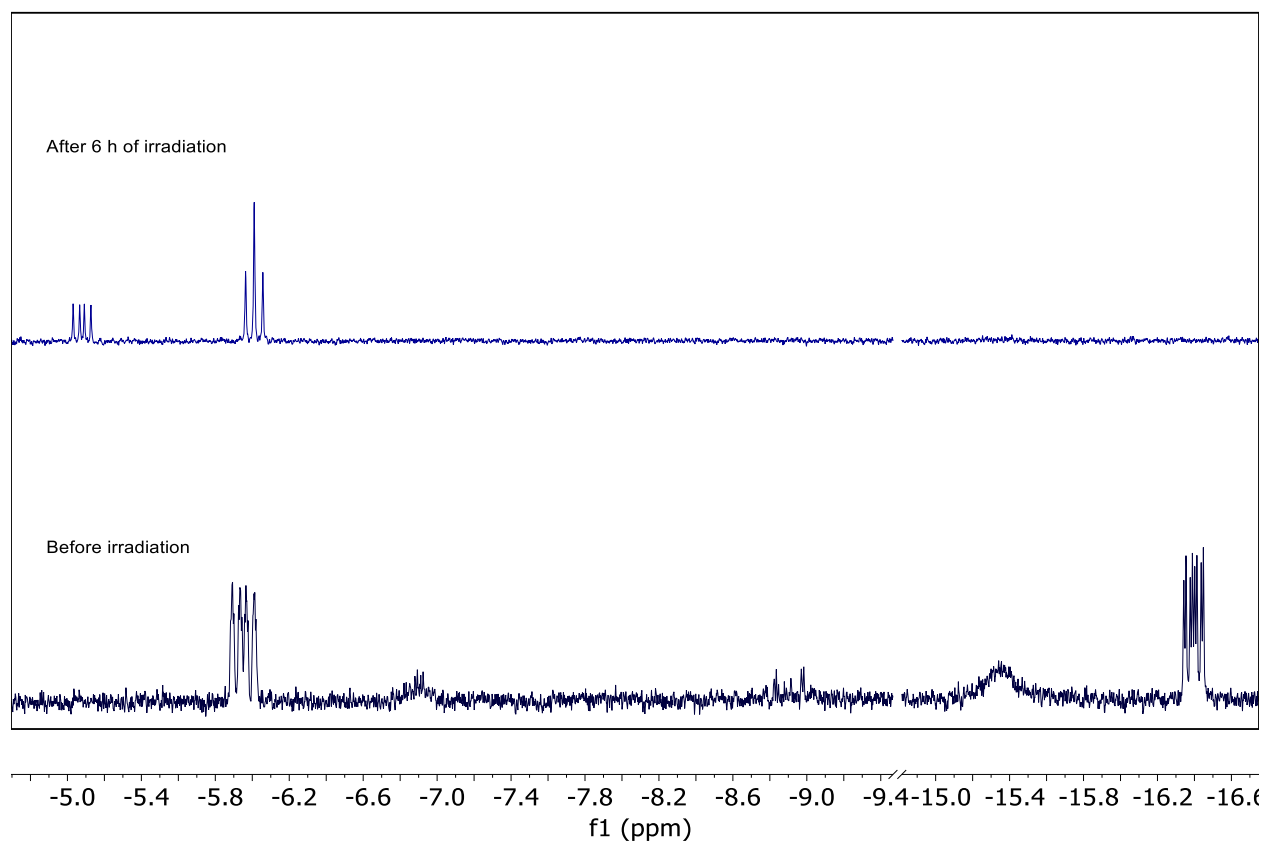
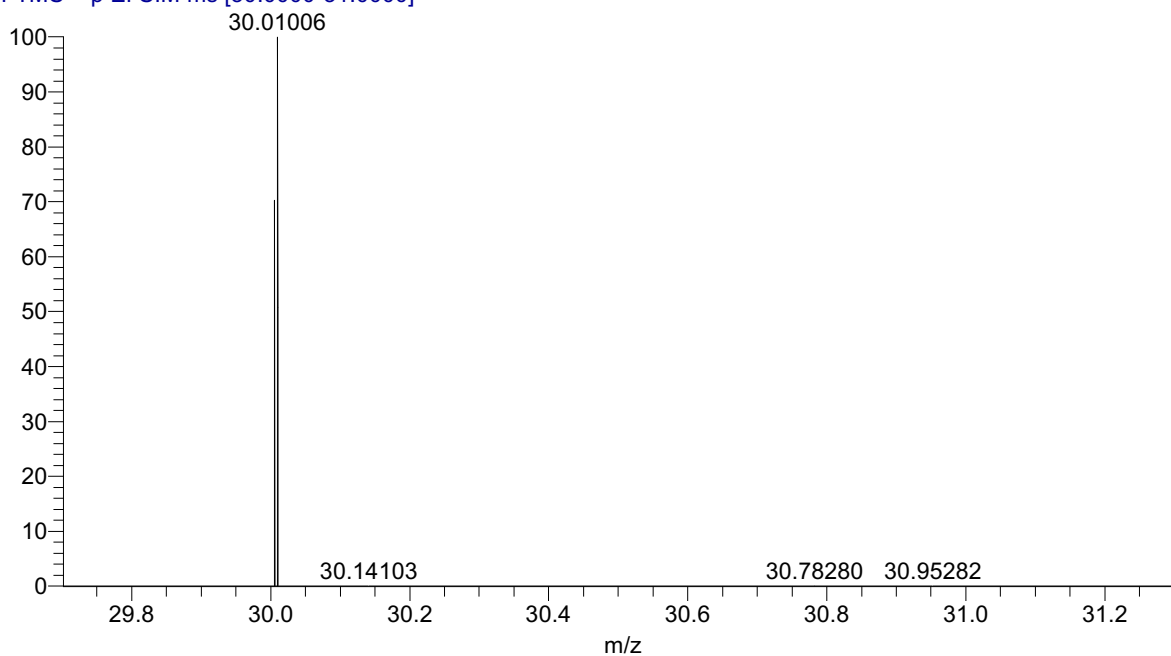


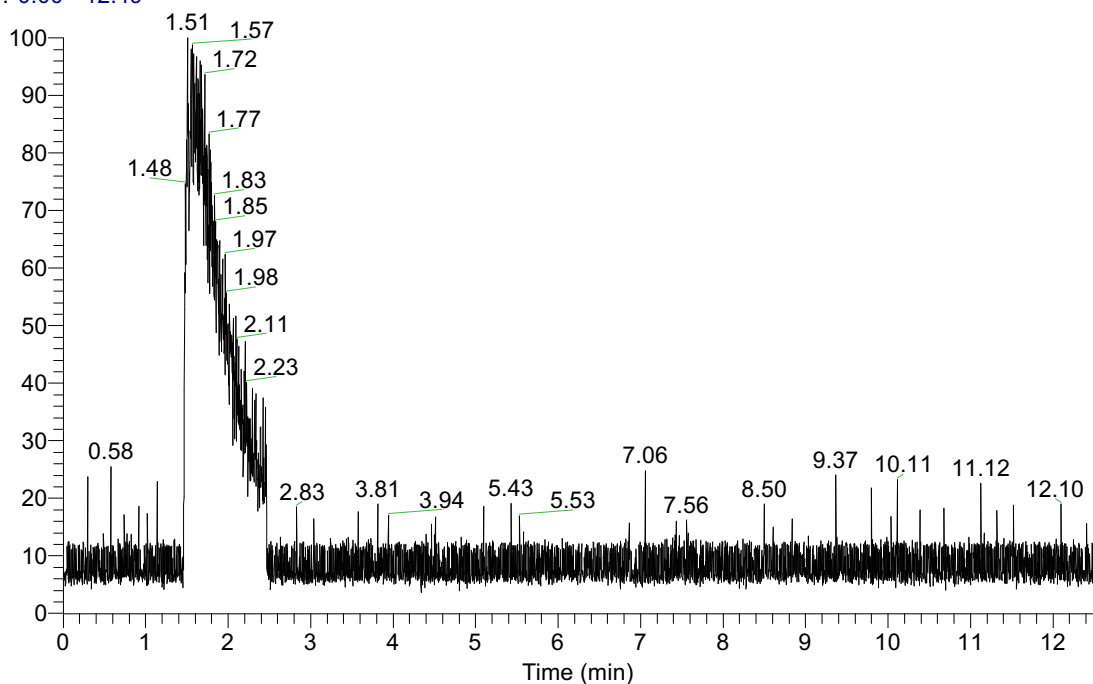
Fig. S40.

500 MHz ^1H NMR spectra of the hydride region of a solution of 0.0030 mmol of **3** in CD_3OD before irradiation (bottom) and after 6 h of irradiation with a 345 nm cutoff filter (top).

05VV078 #576-969 RT: 1.45-2.44 AV: 3 6.49E3
T: FTMS + p EI SIM ms [30.0000-31.0000]



RT: 0.00 - 12.49

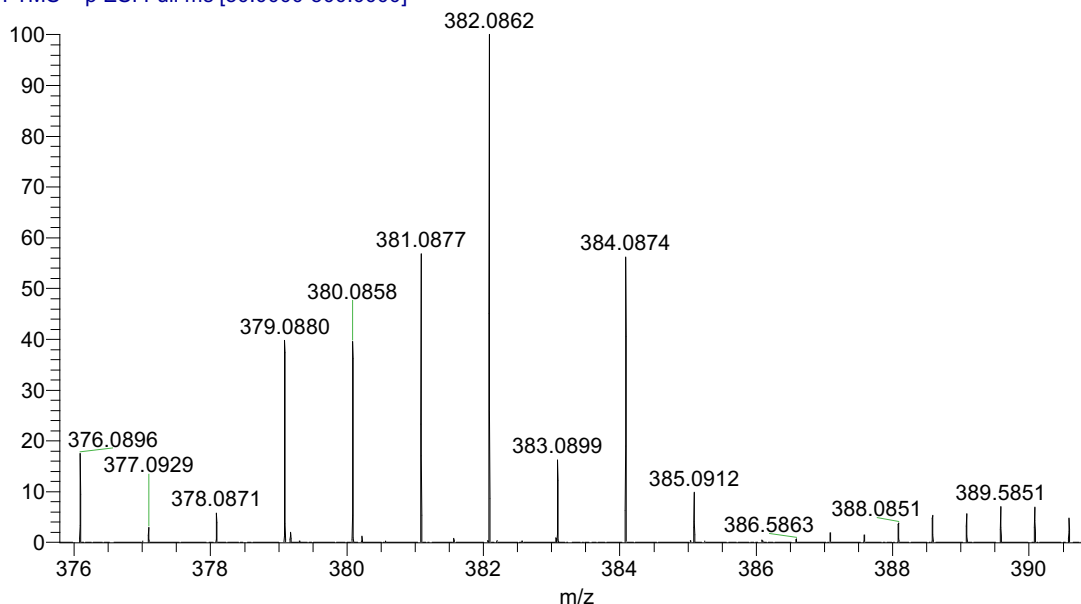


NL:
2.24E4
TIC MS
05VV078

Fig. S41.

QE-GCMSMS headspace mass spectrum (above) and chromatogram (below) of an aliquot (10 μ L) of a solution of **3** in methanol after 5 h of irradiation with a 345 nm cutoff filter at 23 $^{\circ}$ C. A broad peak at 1.50 minutes corresponded to a mass of 30.0101 amu which is in agreement to the formula CH_2O ($M_{\text{calc'd}} = 30.0106$) with a 1.46 ppm error.

05VV078 #108-201 RT: 0.48-0.89 AV: 9 79 1.06-1.41 NL: 2.56E7
T: FTMS + p ESI Full ms [50.0000-500.0000]



RuC16NH27PO: Ru1 C16 N1 H27 P1 O1 f 1

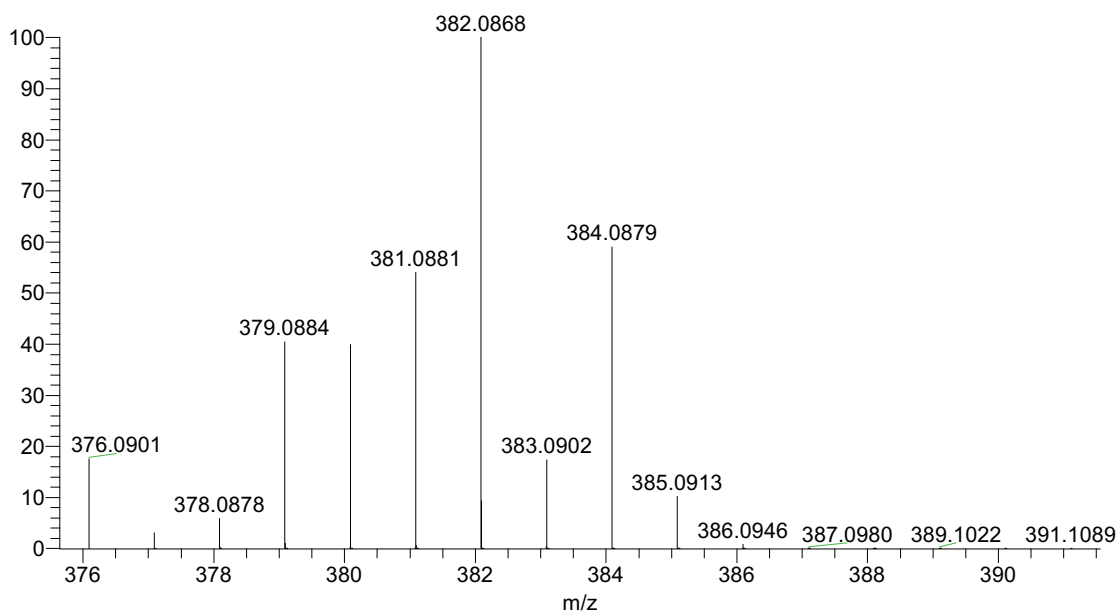


Fig. S42.

Direct injection (10 μ L) of an aliquot of a solution of **3** in methanol after 5 h of irradiation with a 345 nm cutoff filter at 23 $^{\circ}$ C, exposed to ambient atmosphere, into a QE-LCMSMS (above) showed a peak consistent with the formula, Ru(H)(LutP)(CO) ($[M^+]_{\text{calc'd}} = 382.0868$; $[M^+]_{\text{found}} = 382.0862$) and consistent with calculated isotopic distribution (below). A second peak consistent with carbonylation was observed ($[M+\text{CO}]_{\text{calc'd}} = 410.0817$; $[M+\text{CO}]_{\text{found}} = 410.0811$). In addition, peaks with masses consistent with oxidized LutP and triphenylphosphine were observed in the mass spectrum.

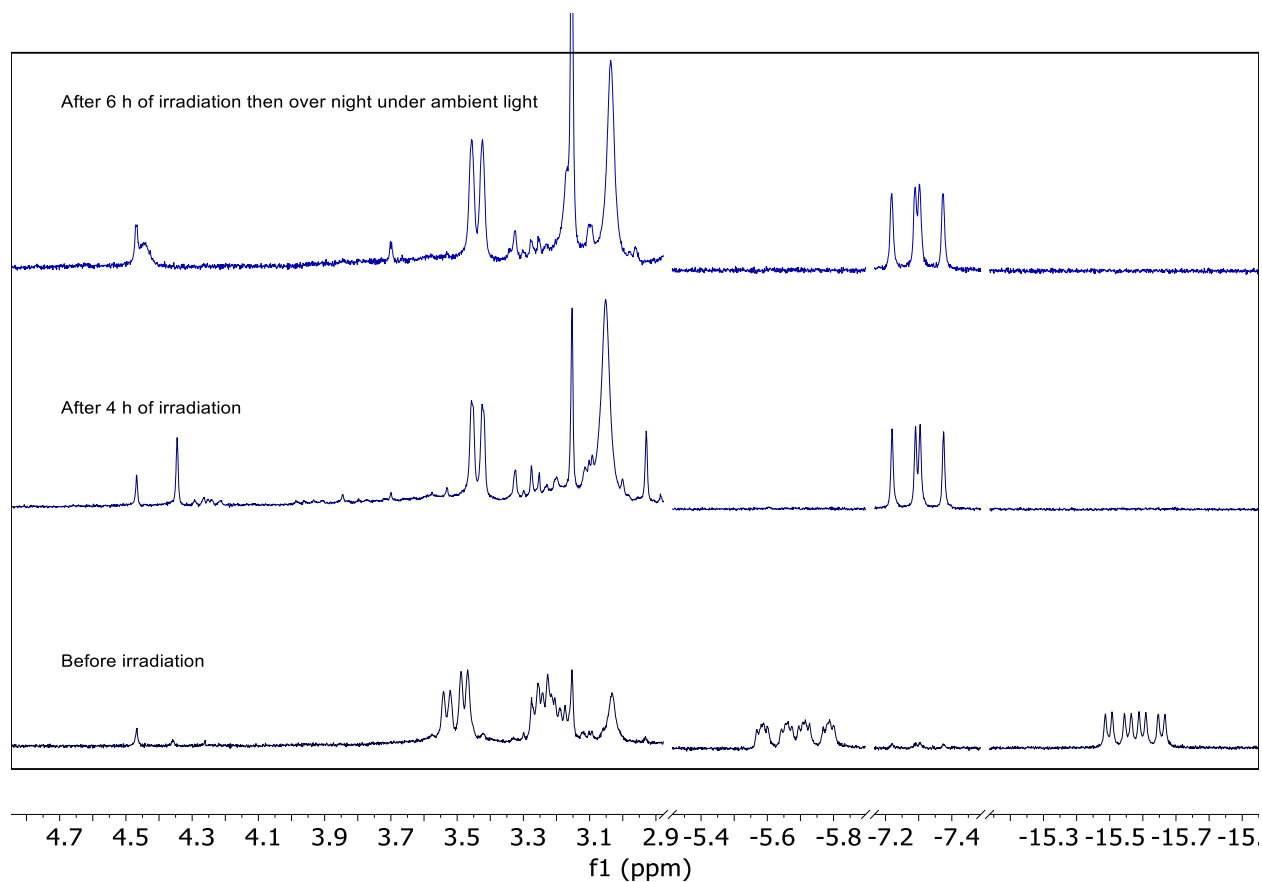


Fig. S43.

300 MHz ^1H NMR spectra of a solution of 0.046 mmol of **3** in C_6D_6 and 0.057 mmol of paraformaldehyde before irradiation (bottom), after 4 h of irradiation with a 345 nm cutoff filter (middle), and after 6 h of irradiation with a 345 nm cutoff filter and left overnight in ambient light (bottom).

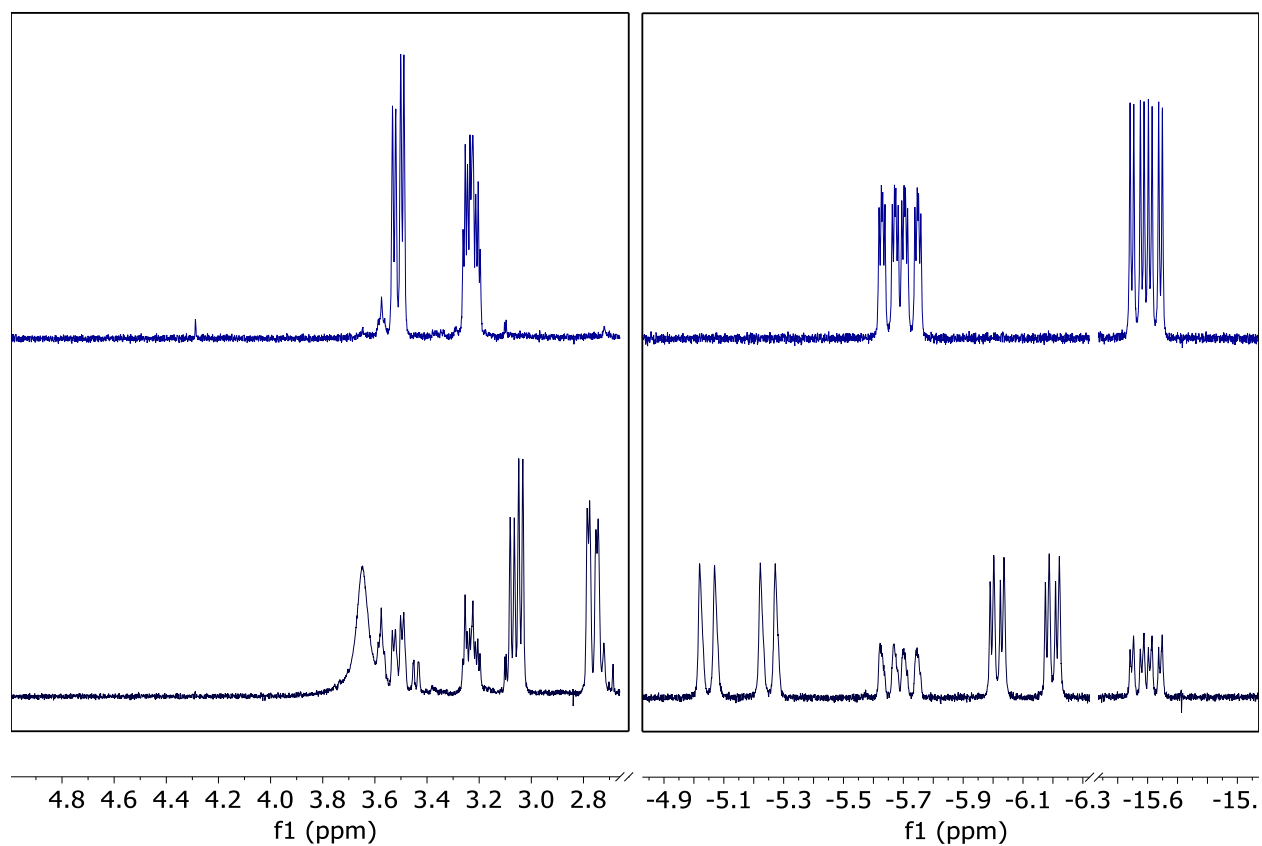


Fig. S44.

(top) 500 MHz ^1H NMR spectrum of a solution of **3** in C_6D_6 and 2-propanol- d_8 . (bottom) The same solution after 1.5 h of irradiation with no filter at 23 $^\circ\text{C}$. (left) Zoomed in on the H_2 , HD, and δ_{CH_2} regions. (right) Zoomed in on the hydride region.

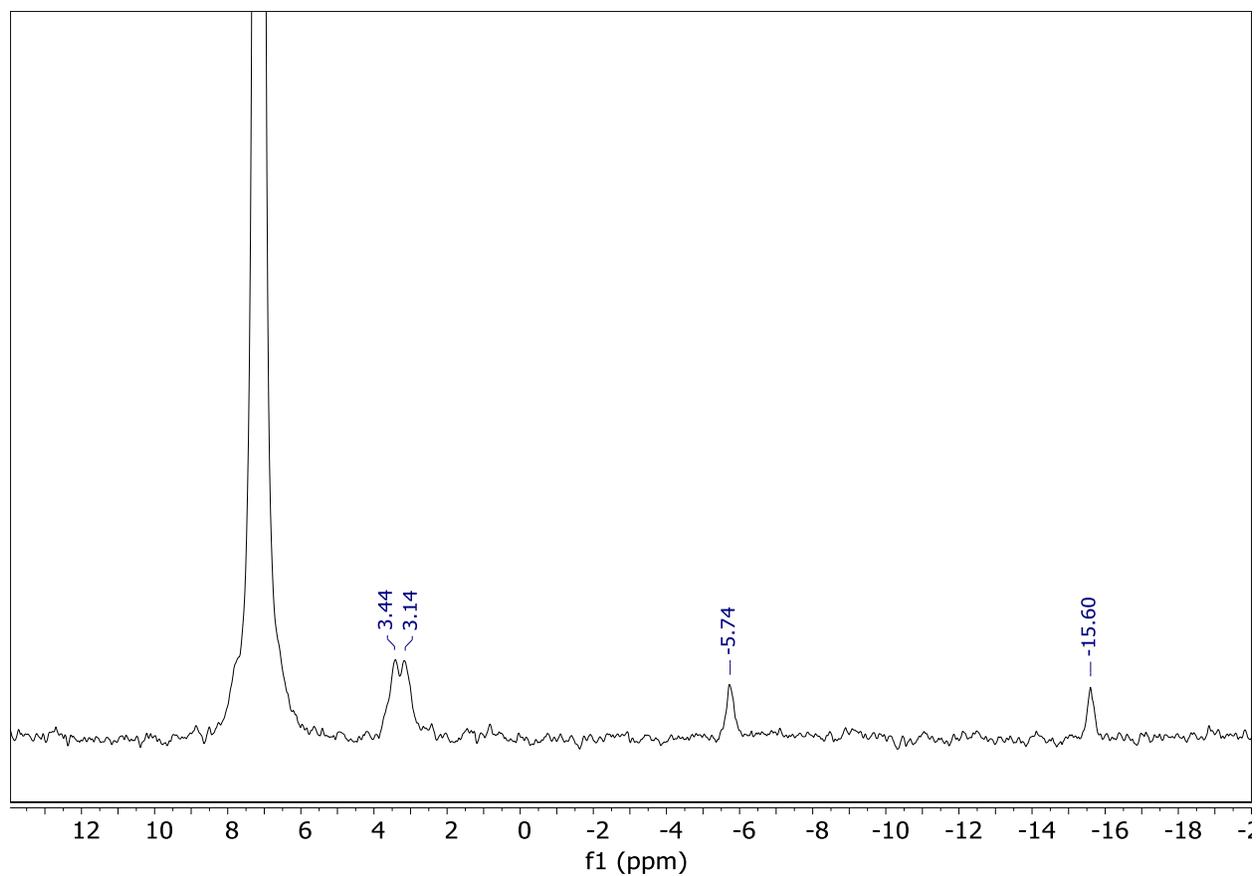


Fig. S45.

500 MHz ^2H NMR spectrum of a solution of **3** in C_6H_6 (spiked with C_6D_6) and 2-propanol- d_8 after 1.5 h of irradiation with no filter at 23 °C.

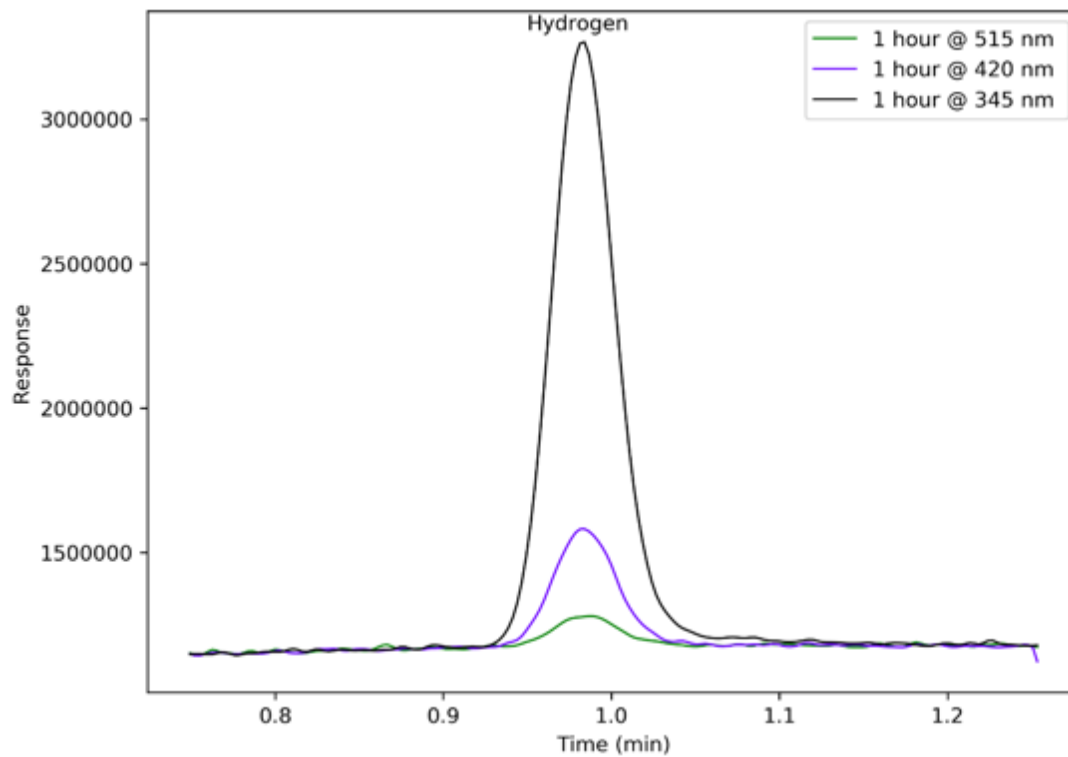


Fig. S46.

GC trace (zoomed in on the H₂ region) of the headspace samplings of a solution of **3** in 2-propanol after 1 h of irradiation at 23 °C with a 315 nm (black), 420 nm (blue), or 515 nm (green) cutoff filter.

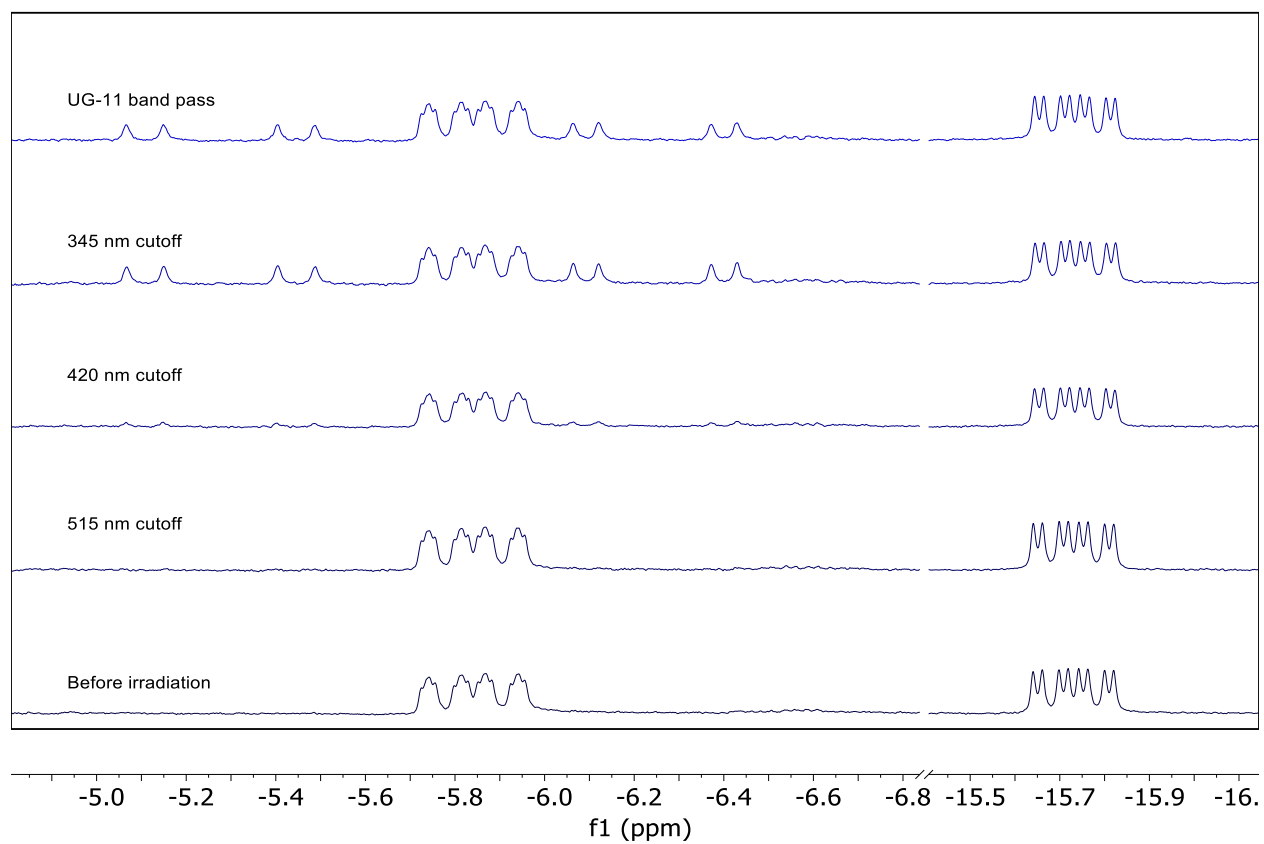


Fig. S47.

300 MHz ¹H NMR of a solution of **3** in C₆D₆ before irradiation (bottom) and after 1 min of irradiation at 23 °C with a 515 nm cutoff, 420 nm cutoff, 345 nm cutoff, and UV band pass filter.

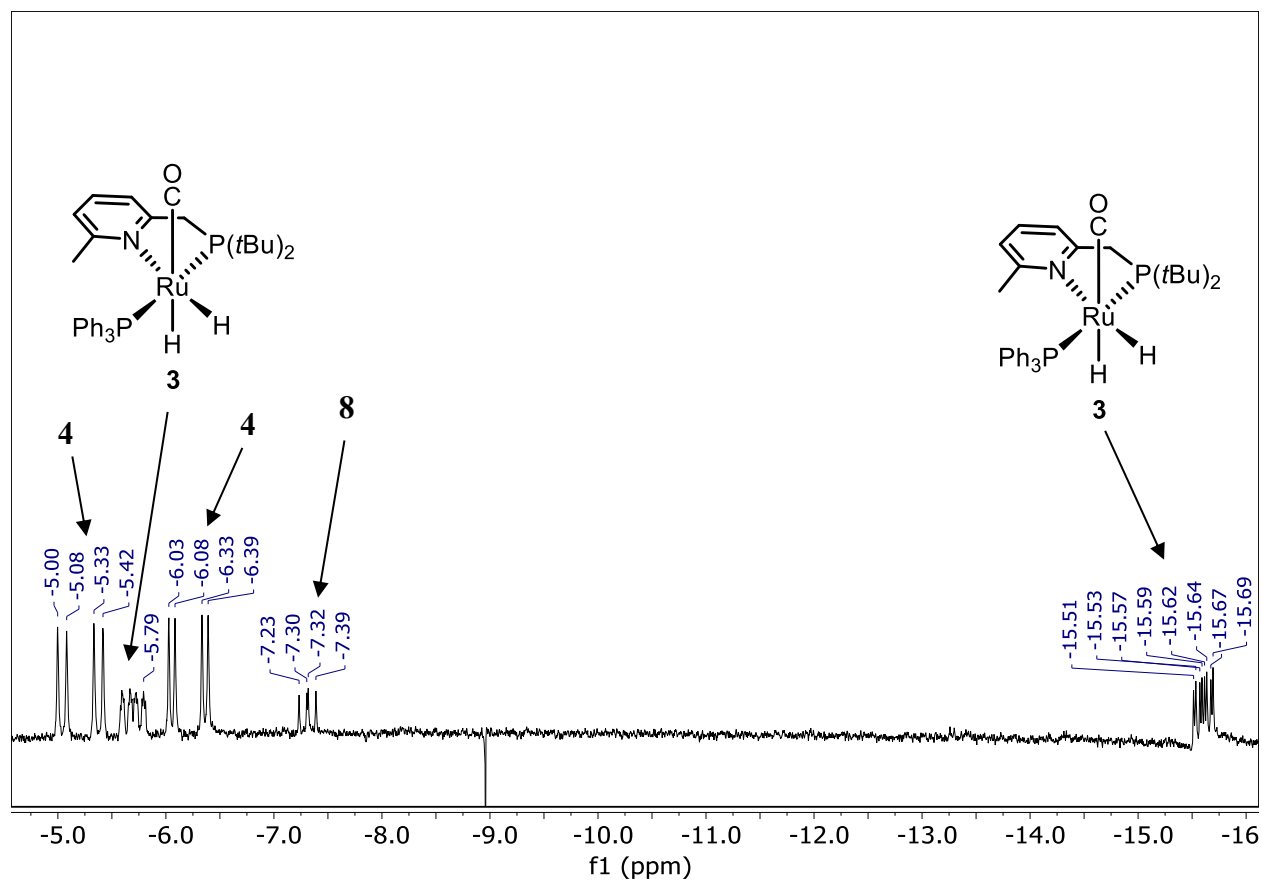


Fig. S48.

300 MHz ^1H NMR spectrum of a solution of **3** and ethanol in C_6D_6 after 4.5 h of irradiation with a 345 nm cutoff filter zoomed in on the hydride region. The same species were observed for 2-propanol and 1-phenylethanol; note for methanol, these species were not observed.

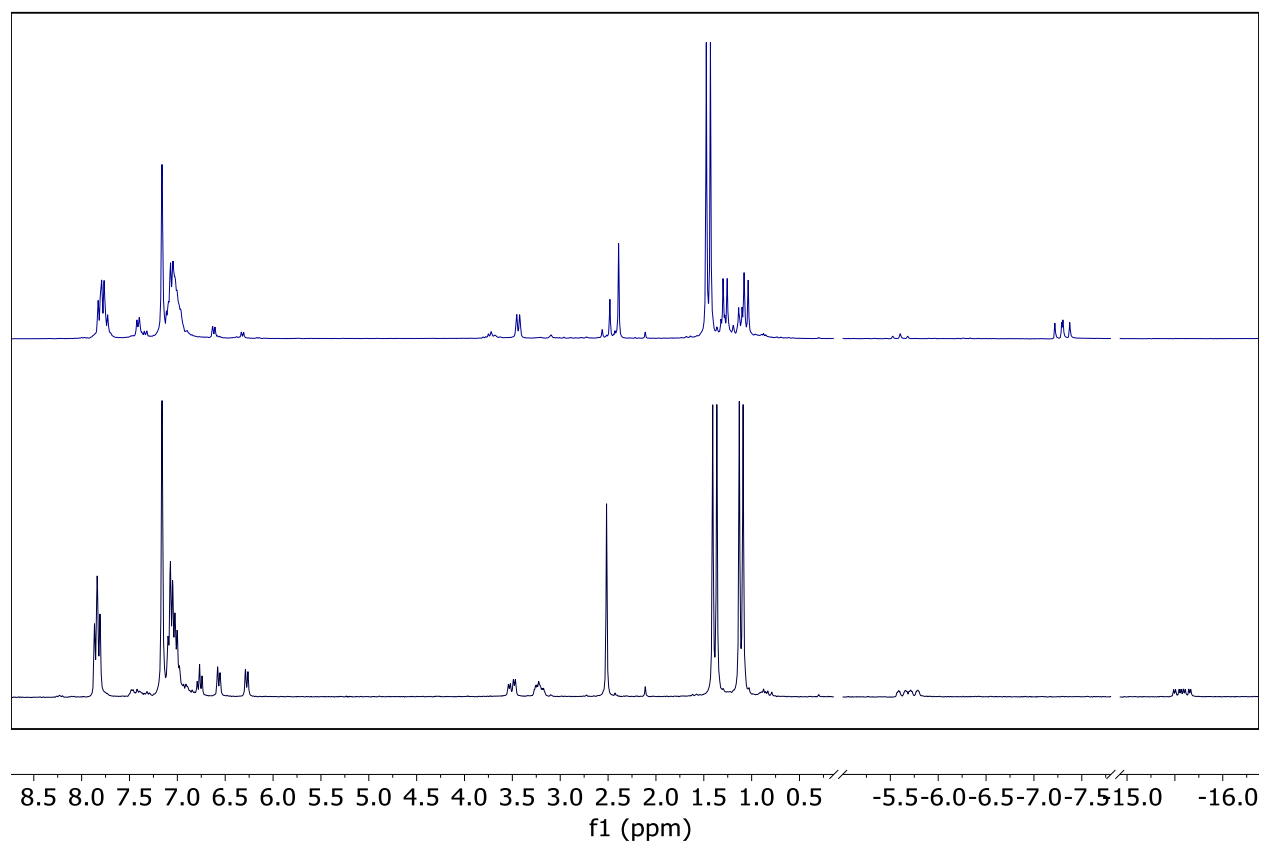


Fig. S49.
300 MHz ^1H NMR spectrum of a solution of **3** under an atmosphere of $\text{N}_2(\text{g})$ (bottom), and $\text{CO}(\text{g})$ (top) in C_6D_6 after 1 h of irradiation with no filter.

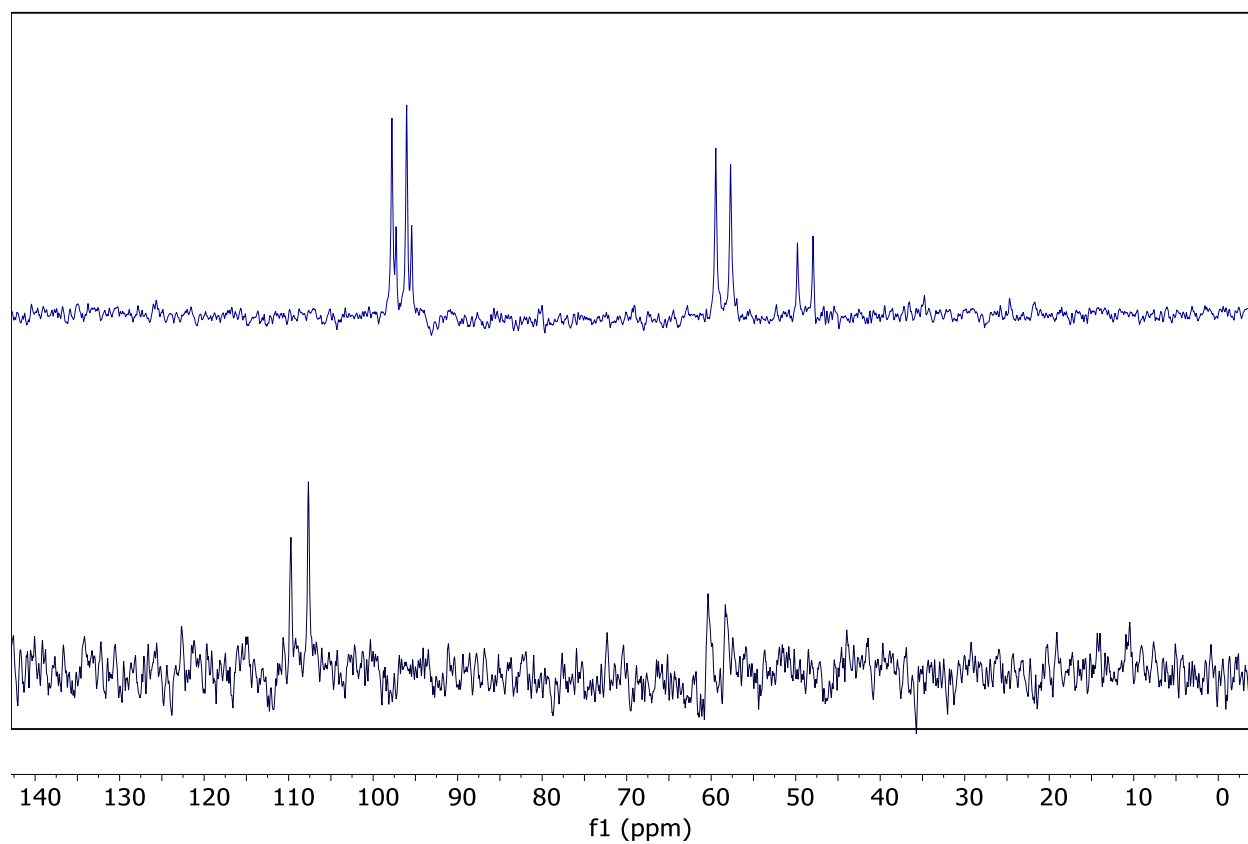


Fig. S50.

121 MHz ^{31}P NMR spectrum of a solution of **3** under an atmosphere of N_2 (bottom), and $\text{CO}(\text{g})$ (top) in C_6D_6 after 1 h of irradiation with no filter.

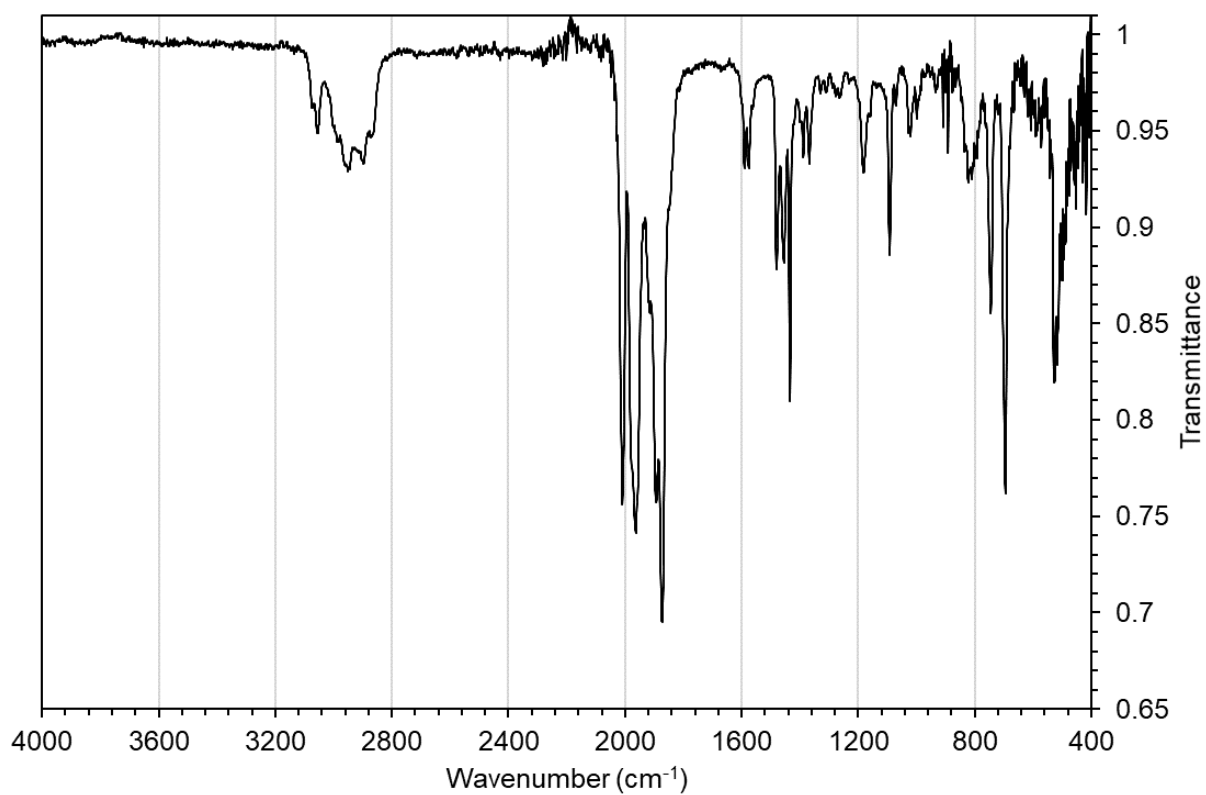


Fig. S51.

Drop-cast FTIR-ATR spectrum of **3** under CO(g) after 1 h of irradiation with no filter.

Table S1.Photochemical H₂ production from alcohol dehydrogenation

Entry	Complex	Alcohol	Other products	%H ₂ (4 h) ^(a)	%H ₂ (12 h)
1	3	iPrOH	acetone	300 ± 24	510
2	3	iPrOH	acetone	27 ^(b)	82 ^(b)
3	3	EtOH	ethyl acetate	640 ± 80	1000
4	3	MeOH	formaldehyde	270 ± 37	400
5	3	1-PhEtOH	acetophenone	640 ± 28	1100
6	1	iPrOH	N/A	78	N/A
7	Ru(H)(Cl)(CO)(PPh ₃) ₃	iPrOH	N/A	28	N/A
8	Ru(H) ₂ (CO)(PPh ₃) ₃	iPrOH	N/A	33	N/A

(a) %H₂ calculated based on the Ru complex, yields with standard deviations are average of three runs. (b) Performed in the dark.

Table S2.
Crystal data and structure refinements for **2** and **3**.

Complex	2	3
Identification code	rlacy87_abs	rlacy86_abs
Empirical Formula	C ₃₄ H ₄₁ NOP ₂ Ru	C ₄₀ H ₄₉ NOP ₂ Ru
Formula weight	642.69	722.81
Temperature	104(7) K	100.0(4) K
Wavelength	1.54184 Å	0.71073 Å
Crystal system	Triclinic	Triclinic
Space group	P -1	P -1
Unit cell dimensions	a = 9.2220(2) Å a = 75.095(2) Å b = 11.9881(3) Å b = 80.973(2) Å c = 15.2279(3) Å c = 74.316(2) Å	a = 10.67863(16) Å α = 86.746(2) Å b = 13.6063(2) Å β = 72.851(2) Å c = 14.2941(2) Å γ = 73.019(2) Å
Volume	1559.37(6) Å ³	1817.97(5) Å ³
Z	2	2
Density (calculated)	1.369 Mg/m ³	1.320 Mg/m ³
Absorption coefficient	5.235 mm ⁻¹	0.550 mm ⁻¹
F(000)	668	756
Crystal size	0.251 x 0.043 x 0.018 mm ³	0.202 x 0.15 x 0.111 mm ³
Theta range for data collection	3.016 to 77.088°	2.864 to 27.101°
Index ranges	-9<=h<=11, -15<=k<=15, -19<=l<=19	-13<=h<=13, -16<=k<=17, -18<=l<=18
Reflections collected	33481	40381
Independent reflections	6554 [R(int) = 0.0585]	8026 [R(int) = 0.0411]
Completeness to theta	99.9% (theta = 67.684°)	99.9% (theta = 25.242°)
Absorption correction	Gaussian	Gaussian
Max. and min. transmission	1.000 and 0.519	1.000 and 0.485
Refinement method	Full-matrix least-square on F ²	Full-matrix least-square on F ²
Data / restraints / parameters	6554 / 0 / 362	8026 / 0 / 419
Goof on F ²	1.076	1.054
Final R indices [I>2sigma(I)]	R1 = 0.0348, wR2 = 0.0918	R1 = 0.0245, wR2 = 0.0604
R indices (all data)	R1 = 0.0373, wR2 = 0.0935	R1 = 0.0309, wR2 = 0.0630
Extinction coefficient	n/a	n/a
Largest diff. peak and hole	0.891 and -1.347 e.Å ⁻³	0.555 and -0.551 e.Å ⁻³

References

27. *CrysAlisPro*; Rigaku OD, The Woodlands, TX, 2015
28. Sheldrick, G. M. *Acta Cryst.* **2015**, A71, 3-8.
29. Sheldrick, G.M. *Acta Cryst.* **2008**, A64, 112-122.
30. Müller, P. *Crystallography Reviews* **2009**, 15, 57-83.